Design and analysis of micro-mirror based tunable optical delay line

S. M. Ali Soleymani

Photonics System Group

Department of Electrical and Computer Engineering

McGill University

Montreal, Canada

December, 2003

Under the supervision of Dr. Andrew Kirk

Canada

Acknowledgments

Firstly, I would like to thank Professor Andrew G. Kirk for the opportunity to do my Master's degree as part of the Photonics System Group. A Combination of his superb teaching ability and his technical and theoretical expertise made this project educative and challenging

I would specially like to thank my colleagues in MEMS group, Xuyen Dai Hoa and James Prentices. Our meetings and discussions have played an important role in writing this thesis. They have been always full of new ideas and encouragements.

I would also thank the students and staff working in PSG who provided a pleasant environment in all aspects during this session: Theodore, Nikolaos, Robert, Dave, Alan, Tang Wei, Johan, Eric, Dominik, Collin, Cibby, Yiying, and Chris. They were at all times so helpful and supportive. I will never forget wonderful time spending with those geniuses.

I also express my gratitude to my supportive parents, Hossein and Giti; my patient sisters, Sanam and Maryam; my caring fiancé, lovely Leili; and all my friends who help me throughout my thesis writing and the whole research work.

Abstract

Optical delay line module is an important building block for advanced communication systems such as OCDMA and OTDMA. The past decade has seen a large research and development activity in this area.

In this thesis, design and performance analysis of a tunable optical delay line which employs pop-up MEMS micro-mirrors have been described. The delay paths which their lengths are in binary fashion are free-space based delay lines. Micro-mirrors operate as a switch to redirect the light through delay paths. One of the main characteristic of this design is to provide constant optical power loss for different delay times. Computer simulations have been shown to evaluate the performance of the system to different sources of misalignments.

The result of simulations suggests using correction mirrors in order to decrease the optical power loss due to misalignment. It has been also concluded that improvement of pop-up micro-mirrors as a main source of misalignment, will alleviate the performance remarkably.

Résumé

Les modules de ligne à retard optique sont un composant important des systèmes de communication avancés comme les OCDMA et OTDMA. Ils furent d'ailleurs le sujet de nombreuses recherches dans la dernière décennie.

Dans cette thèse, le design et l'analyse de performance d'un module de ligne à retard optique accordable qui utilise des micro-miroirs *pop-up* MEMS ont été présentés. Les chemins de retard (*delay paths*) qui ont leur longueur d'une façon binaire sont des chemins de retard sans-fil. Les micro-miroirs fonctionnent comme des interrupteurs qui redirigent la lumière vers des chemins de retard. Une des caractéristiques principales de ce design est de fournir une perte de puissance optique constante pour différents temps de retard. Des simulations par ordinateurs qui évaluent la performance de systèmes avec différents types de mésalignements ont été présentés.

Les résultats des simulations suggèrent d'utiliser des miroirs de correction pour diminuer la perte de puissance optique due au mésalignement. Les simulations montrent aussi que d'améliorer les micro-miroirs *pup-up* améliore la performance de façon remarquable.

TABLE OF CONTENTS

List of figures

List of Tables

1 Introduction

In this chapter, first basic goals of this thesis will be described. Optical Delay Line (ODL) module will be introduced as an important component of many communication systems. In section 1.2, motivations that guide us to propose a new design of tunable ODL will be discussed. To emphasis on importance of ODL in different areas of communications, section 1.3 refers to some applications of this module.

1.1 Objectives

For decades communication systems have been one of the main interest and principle needs for people. The basic purposes of improving communication systems are increasing the speed of data as well as increasing the distance between users. For years electrical communications has employed higher frequency of electromagnetic spectrum in order to increase the data rate. Optical frequency is a portion of electromagnetic spectrum that has been widely used for so many years. With development of optical fibers and new systems such as Time Division Multiplexing (TDM), data rate about order of 10^{12} b/s is achievable [1.1]. The use of Wavelength division multiplexing offers even further improvement in fiber transmission capacity. Many different wavelengths can be sent along the fiber simultaneously by the use of optical multiplexer. However, these strategies do not have the flexibility to satisfy the bandwidth requirements in broadcast with random traffic pattern. When the number of active users increases these systems do not operate well, since the number of active users can not exceed the number of time slots (or wavelengths).

In a Local Area Network (LAN), Optical Code Division Multiple-Access (OCDMA) systems have been examined as an alternative to above mentioned systems [1.2] . This strategy can provide multiple accesses to a network without using wavelength-sensitive components as in WDM and it does not require network protocols with overhead to establish communication between users as in TDM. Additionally, this scheme is well-suited for networks with asynchronous traffic or variable network capacity. Based on the coding approach there are many methods to implement an OCDMA system. One of them is direct-sequence or temporal encoding. In this scheme, optical delay line modules are used to encode an ultra-short optical pulse into a low intensity pulse train. The same modules in receiver with an appropriate delay response are used as a

decoder. Hence, ODLs are an important building block for advanced OCDMA systems. The past decade has seen a large research and development activity in this area, and various ODL technologies and approaches have been proposed.

In this thesis, a design and analysis of a tunable ODL will be studied. This design is based on free space optics as delay path with ability of changing the delay time by the use of micro-electro-mechanical systems (MEMS) mirrors.

1.2 Motivations

At present the search for an ideal ODL continues dynamically. In general the term 'ideal' refers to a low loss, high signal-to- noise ratio, high switching speed, low cross talk level, wide time delay range, and high resolution delay control ODL. Quantifying these ODL parameters depends on the specific application. Over the years, some of the ODL methods proposed include fiber stretching, laser and detector optoelectronic switching, integrated optic switching, polarization switching, fiber Bragg gratings [1.3]-[1.4]. ODLs are being studied to develop a future, wide bandwidth, compact, lightweight and small size and low loss module. In order to obtain a tunable ODL, some methods suggest using MEMS mirrors in order to switch the signal to different delay paths [1.5]-[1.6].

Recent developments in micro-electro-mechanical systems (MEMS) technology are exciting enough to encourage engineers to apply these achievements for different systems. Their fast speed, light weight and small size make them suitable to be used as a sensor and actuator. Because MEMS devices are manufactured using batch fabrication techniques similar to those used for integrated circuits, unprecedented levels of functionality, reliability, and sophistication can be placed on a small silicon chip at a relatively low cost. These advantages of MEMS devices urge us to employ them as a part of our design.

1.3 Other applications

Tunable optical delay lines have important applications in many different areas of communications. As previously said, they are featuring in encoders and decoders in optical code division multiple-access (OCDMA) systems where different codes can be constructed. They are also being used in phased-array antenna to control the direction of main lobe. Optical time division multiple-access (OTDMA) systems use ODL as a part of their transmitter and receiver modules. Such delay lines have also been used in the design of computer interconnects and wavelength switching systems as well as other applications including optical coherent tomography (OCT), ultrasound, astronomy, laser radars, and holography [1.7]-[1.11] . In next chapter some of these applications will be described in detail.

References:

[1.1] Gerd Keiser, "Optical fiber Communication" third edition, McGraw Hill, 2000

[1.2] J. A. Salehi, "Code-division multiple-access techniques in optical fiber networks-Part 1: Fundamental principles," IEEE Trans. Commun., Vol. 37, p 824-833, 1999.

[1.3] Jian Fu, M. Schamschula, H. J. Caufield, "Modular Solid Optic Time Delay System," Opt. Comm. 121, p8-12, 1995.

[1.4] I. Kobayashi, K. Kuroda, " Step-Type Optical Delay Line Using Silica Based Planar Light-Wave Circuit (PLC) Technology," IEEE Transaction on Instrumentation and Measurements, Vol. 49, No. 4, p762-765, 2000.

[1.5] V. K. Kaman, X. Zheng, R. J. Helkey, C. Pusarla, J. E. Bowers,"A 32-Element 8-Bit Photonic True-Time-Delay System Based on a 288x288 3-D MEMS Optical Switch,"IEEE Photonics Technol. Lett., Vol. 15, No.6, p849-851, 2003.

[1.6] K.T.Cornett, J.P. Heritage, and O. Solgaard, "Compact Optical Delay Line Based on Scanning Surface Micromachined Polysilicon Mirrors," IEEE Proceedings of the 2000 IEEE/LEOS International Conference on Optical MEMS (Optical MEMS 2000), pp. 15-16, Kauai, Hawaii, 2000.

[1.7] G.W. Yoffe, J.W. Arkwright, G.E. Town and B.G. Smith, "Tunable optical delay line based on a fibre Bragg grating," Elec. Lett., Vol. 34, No.17, 1688-1690, 1998.

[1.8] Deng K. L ., Kang K.I., S. D. Koehler, I. Glesk, P. R. Prucnal, "Optical fiber stretching technique for precision time delay in ultrahigh speed OTDM systems," CLEO'97.

[1.9] N. Karafolas, "Optical fiber code division multiple-access networks: A review," optical fiber technology 2, p 149-168, 1996.

[1.10] Joseph M. Schmitt, "Optical coherence tomography (OCT): A review," IEEE journal of slected topics in Quantum Electronics, Vol. 5, No. 4, p1205-1215, 1999.

[1.11] P. R. Prucnal, M. F. Krol, J. L. Stacy," Demonstration of a Rapidly Tunable Optical Time-Division Multiple-Access Coder," IEEE Photon. Technol. Lett., Vol. 3, No. 2, p170-172, 1991.

[1.12] W. K. Niblack, J. O. Schenk, B. Liu, M.E. Brezinski, "Dispersion in grating-based optical delay line for optical coherence tomography," Applied optics, Vol. 42, No. 19, p 4115-4118, 2003.

2 Literature review

As has been said in previous chapter there are different technologies of optical delay line. While the main purpose of all technologies is to retard the optical signal, each application requires different method to implement the module. There are also different methods to achieve a variable optical delay line. In this chapter, first different technologies and various methods of variable optical delay line will be introduced briefly. And then several areas of applications will be discussed.

2.1 Different delay line technologies

There are many different methods to implement an optical delay line. Some of these methods will be introduced here:

Delay line based on optical fiber: This is probably the easiest way to make a delay line [2.1]. If we introduce an optical fiber with the physical length of L, the delay time for the retarded light can be obtained as follows:

$$\tau_g = \frac{L}{v_g}$$

Equation 2-1

where v_g is the group velocity in the fiber which is just $\frac{c}{n_g}$,with c is the speed of light in vacuum, and n_g is the refractive index of the fiber medium.

Although optical fiber seems to be ideal photonic delay line due to the low loss and low dispersion, this implementation suffers from three drawbacks: 1) Tunable OPD is difficult to achieve. 2) Long time-delay requires large physical distance, for example, 1 ms delay requires almost 200 meters of optical fiber. 3) For short time-delay, for example, in timing adjusters used for adjusting optical signal propagation delay for synchronization, the unit delay time is usually in order of tens to hundreds of picoseconds corresponding to 2mm to 2 cm length of fiber. Such a short delay times cannot easily be obtained in fiber delay lines because the fiber must be made too short to be set during the fabrication.

In order to achieve an ODL with controllable delay, optical switches are required. Figure 2-1 shows three different architectures to realize six bits of time delay selectivity (providing time delays from 0τ to 63τ) [2.3]. The cascading of six 2x2 switches is the simplest design. Note that the delay time for each segment varies in a binary fashion.

The same system can be designed by cascading of 3 8x8 switches. In this configuration the number of switches has been reduced which will help to reduce the optical loss of system but only with the addition of complexity and many unused ports (fourteen). In this design the delay loops increases to fourteen. Using four 4x4 switches is another configuration which can be considered as a combination of the other two. Here the number of optical switches is reduced compare to the first one, hence experiences lower optical loss. On the other hand the number of unused ports and number of delay loops are reduced to 6 and 9 respectively compared to the second design.
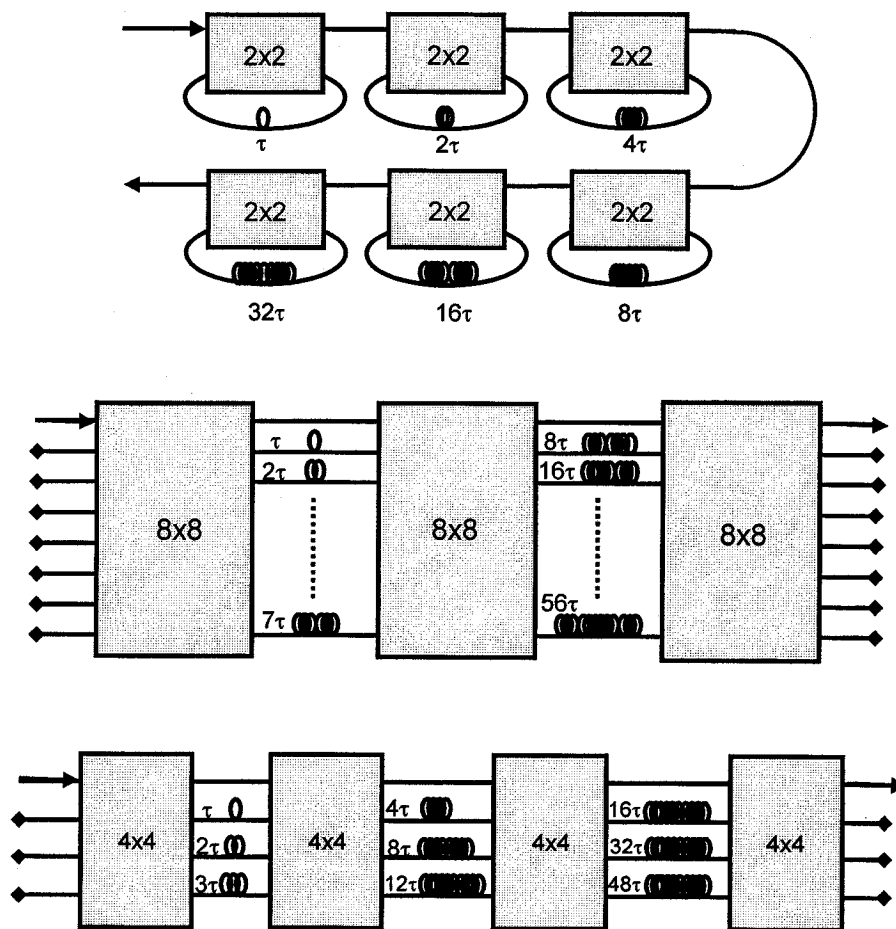
Figure 2-1: Different implementations of controllable optical delay line

E. Ackermen et al. [2.2] implement the third configuration by the use of LiNbO$_3$ waveguide switches at wavelength of 1.3 μm. Total loss of the system varies from 15.5 dB to 16.6 dB depends on the values of delay. This system is able to change the delay from 0 to 30 ns with steps of 470 ps.

The performance of optically switched ODL units based on integrated waveguides is limited by the high fiber to wave guide coupling losses, high polarization dependency losses (PDL's), and a broad loss variation for different paths. Furthermore the relatively small sizes of waveguide-based optical switches (up to 8 x 8) require a cascade system which increases optical loss and overall cost. To avoid these matters optical switches based on MEMS mirrors have been suggested as an alternative [2.3]. As a result of recent development of 2-dimentional micro-electromechanical-system (2-D MEMS) using this switches causes lower optical losses (maximum 3.1 dB) with size up to 16 x 16. Additionally, with the developments of 3-D MEMS the demonstration of much larger switches can be seen. For example 288x288 optical switch using 3D-MEMS has a median loss of 1.4 dB at 1.31μm and for all paths is less than 2.3 dB.

The schematic of two different realizations of 8-bit ODL which provides delay in range from 0τ to 255τ can be seen in Figure 2-2.
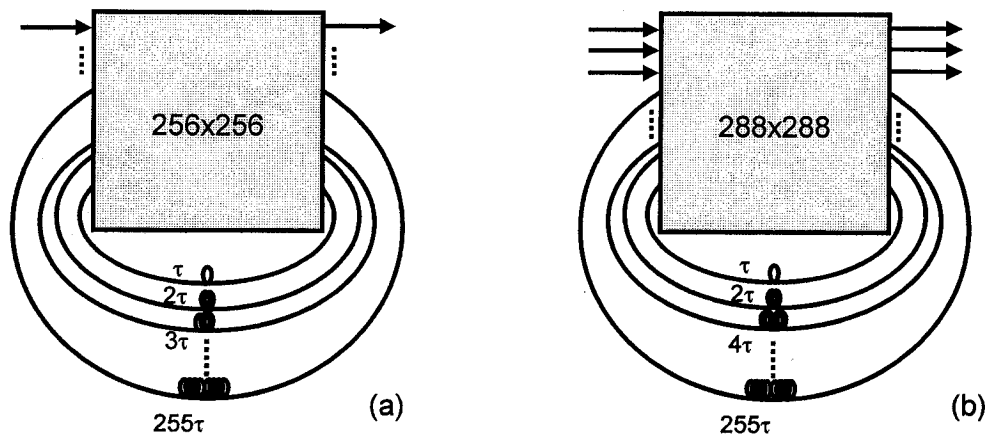
Figure 2-2: Realization of a variable optical delay line of with (a) large switch and linear delays, (b) large switch and binary delays.

One uses 256x256 3-D MEMS switch with linear combination of delays. The other uses 288x288 3-D MEMS switch where fiber delays are combining in the binary way. Linear configuration would support a single input elements for 8-bit resolution with a maximum loss of 2.8 dB (power loss of the optical switch is 1.4 dB per path.) However, this low loss is achieved at the expense of many unused ports. For second architecture, the loss would be 12.6 dB in the worse case as a trade of number of fiber delays for 32 elements ODL. A major drawback for using these switches is misalignment of the micro-mirrors, which imposes the quality of a switch.

Delay line based on Free-space propagation: This is another easily achievable method. The other method to establish a tunable ODL is using free-space as a medium that light travels in. As it is shown in Figure 2-3, ODL module is based on adjustment of an air gap (optical path length in free space) between the fiber collimators. Reflectors in this configuration can move forward and backward mechanically. These systems, however, suffer from the low switching speed as well as precision of delay due to the mechanical part. [2.4]
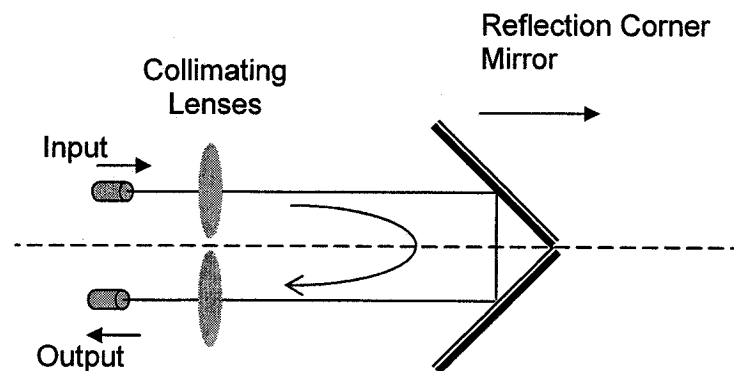
Figure 2-3: A simple draw of an ODL based on free-space optics.

In order to obtain variable delay line which is auto-aligned with lateral displacement, Klovekorn and Much [2.5] have suggested a configuration as shown in Figure 2-4 . The

polarizing beam splitter (PBS) passes the beam through M1 and then Corner cube reflector (CCR) and M2. The polarization of light would change 90° when it passes through the quarter wave plane (QWP) twice. Therefore at the PBS it goes directly towards output. The delay distance is approximately 4L, where L is the distance between M1 and CCR. Because the mirror M2 always retro-reflects the beam back through the CCR, the same lateral shift will be experienced. This results in an auto-aligning delay line that is independent of the lateral displacement of the corner cube. Although angular alignment would still be an issue.
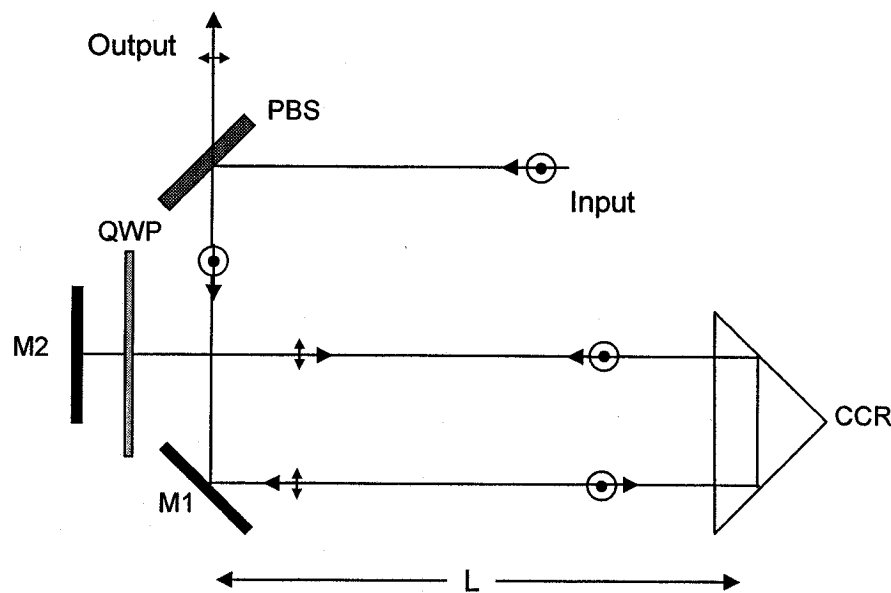
Figure 2-4: Configuration of an ODL with auto-aligning property

Delay line based on optical Waveguides: Another technology offered for ODL is integrated optics. One advantage that they have over fiber delay lines is they are compact and their length can be controlled with submicron precision. A number of groups have demonstrated optical delay lines using various integrated waveguide technologies, including silica, III-V semiconductors, and polymers [2.6]-[2.12]. While III-V semiconductor waveguides have the high refractive index (n = 3.5 -4compared to n=1.46 for silica) and, thus provide largest delay per length ratio, they suffer from higher cost of

substrate and also high waveguide losses. Silica, on the other hand, has been the most promising technology since it costs lower and has low losses. Some of these different methods are represented as follows:

Takakura H. and Kuroda K. [2.8] designed and evaluated the waveguide type ODL using thermo–optic effect. The optical waveguide material is SiO_2, and the length is about 1m which is calculated in order to get a displacement of ΔL= 100 µm using TO effect.

One of the most important factors in forming a long waveguide is bending loss. It is function of core size as well as bending radius and difference of waveguide materials refractive index. For this case n_{core}=1.454, n_{clad}=1.444 (Δ= (n_{core} -n_{clad})/n_{core} =0.69%) , and size of the core is: 6 µmx6µm, a 90° bend with the bend radius of 5 mm results a loss of 0.0003 dB. Using this bend radius, a 1m waveguide on the substrate of 70 mm x 41.2 mm, requires approximately about twenty six-90° bends.

The optical path length change can be calculated from Equation 2-2:

$$\Delta L = n_{core} \alpha L \Delta T$$

Equation 2-2

where α is the coefficient of linear expansion of silica, L is waveguide length and ΔT is temperature change.

The main problem with waveguide-based optical delay line is polarization dependency and the loss due to the interconnection of fiber and waveguide which for wavelength of 1.31 µm has been experienced around 8.12 dB.

Long delay line structures, in integrated optical materials with small Δ's are limited in the practical size reductions and bend radii that can be fabricated. By using a technology which provides a large Δ, small guide dimensions can be made. Arsenosilicate glass (AsG) is used by Beaumont et al. [2.7]. In this materials Δ=1.7%, consequently this reduces the bend radii significantly so delay line can be densely packed than possible by

other process. Single mode guides operating at 1550 nm with diameter of 3 μm can be fabricated. The delay time achieved by this method is 100 ps and the insertion loss for entire system (fiber to fiber) is 11.27 dB.

Silicon-on-Insulator waveguide technology first is demonstrated by Yegnanarayanan et al. [2.10]. It combines the advantages of silica substrate with semiconductor high refractive index (n=3.46). The SOI waveguides show low losses of 0.1 -0.2 dB/cm. Another advantage of SOI, is its compatibility with silicon integrated circuit technology which implies low cost and high yield manufacturing. Despite the large refractive index step, single mode propagation can easily be obtained in a large section of waveguide with mode size comparable to single mode optical fiber. The micrograph of the ODL waveguide is shown in Figure 2-5. This chip has been designed for 3-b (8 channels) time delay network. The dimensions are 2 cm x 0.9 cm. the minimum bend radius is 5000 μm and the incremental path length difference is 1 mm corresponding to the delay resolution of 12.3 ps. In order to select a particular time-delay, the most obvious choice is a switch, which in its turn can be costly. The total insertion loss of the chip was dominated by the fiber to waveguide coupling efficiency and is estimated to be 6.5 dB.
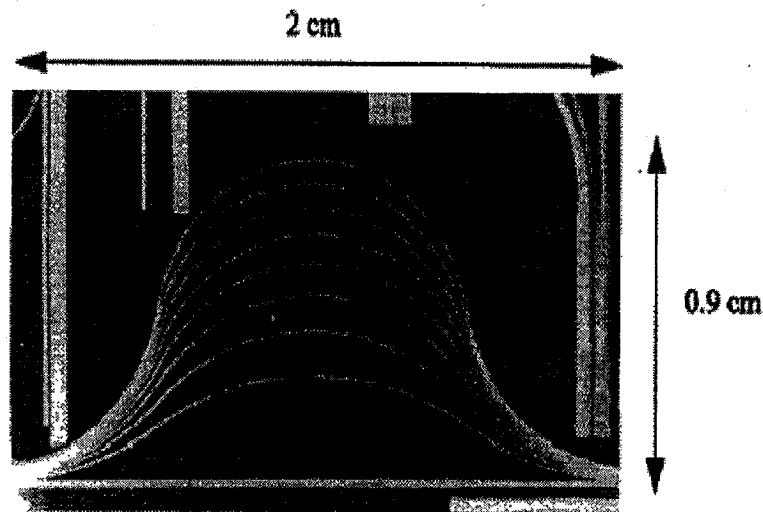
Figure 2-5: Micrograph of a waveguide based ODL. [2.10]

Step-type ODL using Silica-based Planar Light-wave Circuit (PLC) technology has been designed and analyzed by Kobayashi I. and Kuroda K. [2.6]. Figure 2-6(a) shows the circuit layout of the step-type ODL. It is composed of eight delay units (U1-U8) connected in series, which can delay lights in the 1.55 μm band by 0.2, 0.4, 0.8, 1.6, 3.2, 6.4, 12.8, and 25.6 mm. Figure 2-6 (b) shows the structure the delay unit, which consists
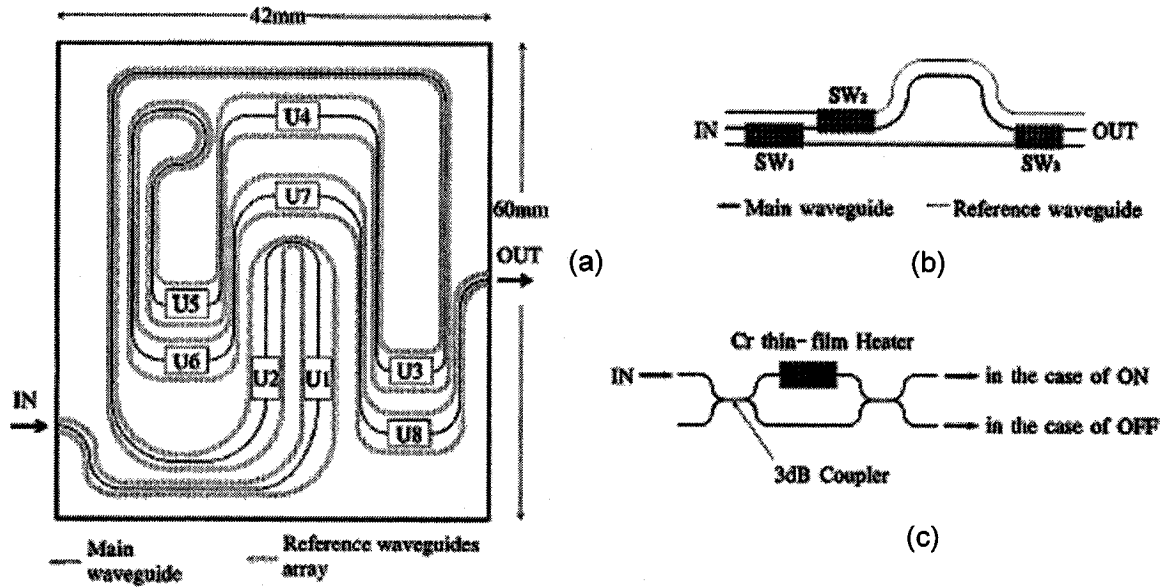
Figure 2-6: (a)Circuit layout of a step-type ODL designed by Kobayashi I. et al. [2.6],(b) structure of each delay units, (c) structure of TO switches.

of three thermo-optical(TO) switches(SW1-SW3) and two waveguides whose optical path length difference is equal to the optical delay. Figure 2-6(c) shows the structure of TO switch, which consists of Mach-Zehnder interferometer composed of two waveguide with the same length, two 3-dB couplers and a Cr thin film heater build into one waveguide as a phase shifter. When current passes in the Cr thin-film heater (ON), incident light is radiated from through port. Whilst Cr thin-film heater has no current (OFF), light comes out from the cross port. When SW1-SW3 are all ON, the incident light will be delayed, and when they are all OFF, the incident light do not experience any delay.

Si has been used for substrate and SiO_2-GeO_2 for the core and SiO_2 for cladding. The core size is 7 μm x 7 μm. The refractive index difference is 0.75%. The dimension of the device is 42 mm x 60 mm. Insertion losses under various delay condition slightly changes and it is smaller than 5.2 dB. The error for each delay unit will not exceed of 0.47 %.

Although silica-based waveguide have been demonstrated with low optical insertion loss, thermo-optic switches used for waveguide routing are slow and have high electrical power consumption even for a fixed routing statue. Wenshen Wang et al. [2.9] suggest using polymer non-linear optical (NLO) material for on-wafer delay line applications. They can be easily spin-cast on a large piece of wafer. Long waveguide delay lines can be achieved on a single wafer, and these delay lines can be integrated with E-O (electro-optical) switches, all made of NLO polymer. Large delays over tens of centimeters can be obtained. The switching response is in order of nanoseconds with low electrical power consumption. The total insertion loss of the system is less that 20 dB and the whole unit can be fabricated on 4" Si wafer, making it very compact.

Delay line based on a birefringent material: Yamaguchi M. et al. [2.14] proposed a variable OPD based on a birefringent planar optical platform and a liquid-crystal (LC) cell. It is compact and can vary delays within 1 ms to 100 μs. It applies the fact that the two indices of refractions in birefringent materials for different light polarizations are different. The basic structure of the birefringent planar optical platform (one-way type) is shown in Figure 2-7. It consists of a birefringent plate sandwiched between two λ/4 plates and two highly reflective dielectric mirrors. In each rectangular λ/4 plate, the angle between the optical axis and the side is 45°. A linearly input light beam (ordinary beam) enters from point *A* and propagates straightly through birefringent material to point *B*,

passes by the λ/4 plate and reflects by the highly reflective mirror. The direction of reflected beam's polarization is rotated by 90° because the light goes through the lower λ/4 plate twice. The reflected light goes from *B* to *C* because the light is now extraordinary beam for the birefringent material. At *C* and after reflections light becomes an ordinary and travels towards *D* and continue in the same manner as at point *B*. The light beam thus propagates in a zigzag way to the right of the plat form by such reflections and goes out of the platform at point *G*. Each zigzag path of light beam similar to one from point *A* to point *C* is called hop. The delay of each hop can be determined by accurately setting the thickness of the birefringent plate. Figure 2-7(b) shows another structure with a round trip zigzags. By partially replacing the λ/4 plate with an isotropic material (e.g., glass) at point *G*, the polarization direction remains the same at this point , therefore the light comes back in the same path and goes out from the platform at point *A*. By the moving the position of the isotropic material inside the λ/4 plate, a variable optical path can be obtained. Also in zero other structures to control the optical path have been proposed.

Delay time with resolution of 239 ps can be achieved. Insertion loss in this system from fiber to fiber is experienced 6 dB. The transition time for switching delay is estimated at from 10 to 100 ms. The physical size of delay line with 7 steps of delay (7 hops) is approximately 5 mm ×12.4 mm ×22 mm.

(a)   (b)
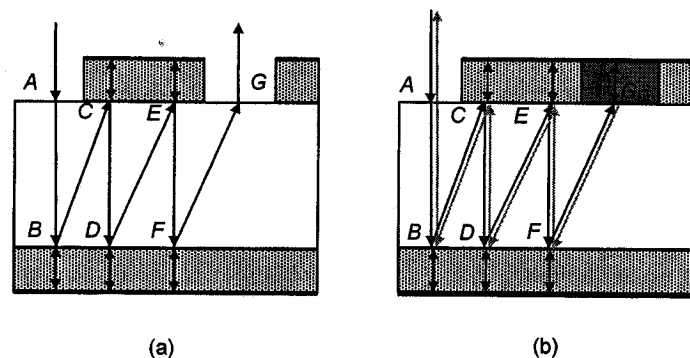
Figure 2-7: Variable ODL based on birefringent material

Tunable optical delay line based on Fiber Bragg Grating (FBG): Some methods suggest use of FBG in order to delay optical signal. A variable ODL based on a long, strong, apodised, unchirped FBG is proposed in [2.15]. The optical signal to be delayed has a wavelength just outside the stop-band of grating. A short segment of the grating is perturbed by temperature or strain so that it reflects light. The delay time of reflected signal depends on the position of the perturbation.

A schematic of the system is shown in Figure 2-8. The optical signal is directed by a coupler into FBG, which should be strong enough to reflect the signal over a length of a few millimeters and be apodised to remove any side-lobs from reflection spectrum. The signal wavelength is then selected so that it is just above the stop-band of the grating so in normal operation the signal passes the grating with little or no reflection. The grating is then locally perturbed, either by heating or stretching the fiber, such that the period of the grating is increased over a short length. This causes a strong reflection close to the perturbation position. By varying the position of the heater, hence, the delay observed at port 2 of the coupler, can be changed. Results of experiments for this system shows that changing the position of the heater from 0 to 7 cm can vary the delay linearly from 0 too 700 ps.
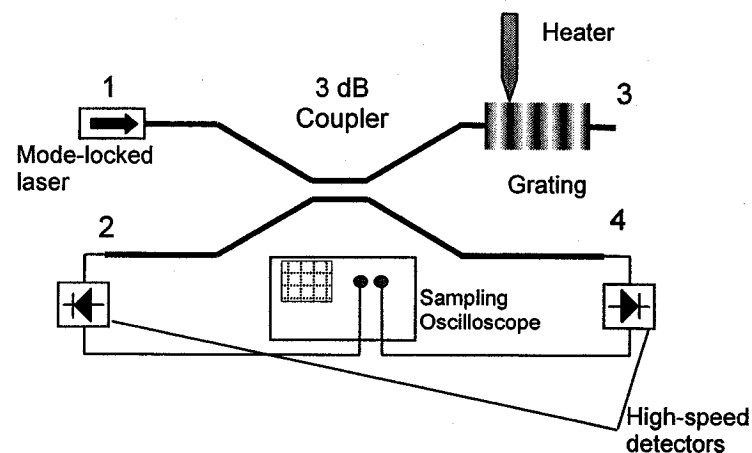
Figure 2-8: Schematic of a variable ODL based on FBG

Optical delay line based on scanning mirror: In this method, a variable ODL can be achieved by changing the optical signal path using a scanning mirror. This approach of rapid-scanning optical delay (RSOD) can be useful for femtosecond and picosecond delay times. In [2.17] a configuration of RSOD has been described. It is capable of scanning at speed of 500 Hz with low vibration. The operation of the RSOD is based on the technique of femtosecond Fourier-transform pulse shaping [2.17]-[2.19]. A well-known property of Fourier transforms is utilized: The addition of a linear phase ramp in the frequency domain results time delays.

The configuration is schematically illustrated in Figure 2-9. It consists of a grating with the period of Λ and a lens with focal length of f and a mirror which can be tilted.

One can calculate the delay time as a function of RSOD geometry by evaluating the frequency dependence of the impressed phase. The grating diffracts the spectral component $\Delta\omega=\omega-\omega_0$ into the angle $\Delta\theta = \dfrac{\Delta\lambda}{\Lambda\cos\theta_0}$, where $\Delta\theta=\theta-\theta_0$ is the difference between the diffraction angle of the frequency components ω and ω_0. The mirror, tilted
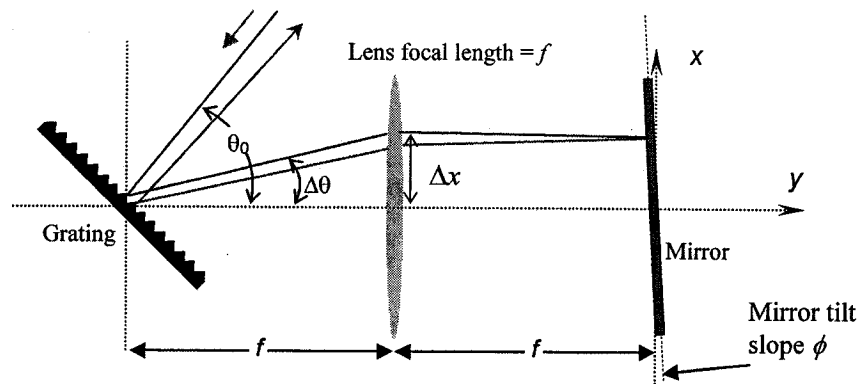
Figure 2-9: Schematic of ODL with micro scanning mirror

from normal incidence with a slope ϕ, causes a delay time as follows:

$$\tau_g = \frac{2f\lambda_0}{c\Lambda\cos\theta_0}\phi$$

Equation 2-3 is the essential equation for design of an RSOD at wavelength λ_0. Note the delay is linearly proportional to the mirror slope ϕ which in this system is mechanically varied so that a useful scanning time delay is produced.

By the use of this method, an variable ODL can be implemented which is compact and the speed of switching between different delay states is fast due to the small size of micro-mirror. This method seems to be useful for delay times in order of femtoseconds.

Optical delay line based on polarization property: Jian Fu and al. [2.20] introduce a modular solid optic time delay system which is based on polarization switches and polarizing beam splitters. This method uses polarization switches such as liquid crystal (LC) or electro-optical switches to select one of a number of fixed delay paths. No complex fiber-switch interface alignment procedures are required per switch as in some integrated-optic planar systems.

The modular solid optical delay system is composed of polarizing beam-splitter (PBSs); Polarization switches (PSs) and time insertion units. The basic cell consists of two PSs and two PBSs as shown in Figure 2-10.
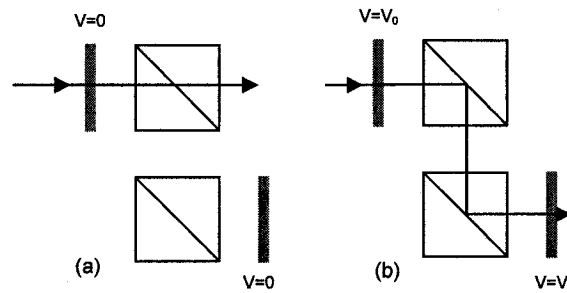
Figure 2-10: Basic cell, (a) both PSs are off, light will transmits from the PBS, (b) both PSs are on, light is reflected by PBS.

The PBS is such that light in p-polarized state is transmitted, while light in the orthogonal s-polarized state is reflected. When the voltage applied to the PS is zero, the polarization state of transmitted light is unchanged and light propagates through the PBS and when voltage is V_0, the polarization state switches from p to s, so it reflects twice by the PBSs and travels towards the second PS. A totally solid system can be built in space between two PBSs. As it can be seen in Figure 2-11 there are two transparent materials P and G, with refractive indexes n_1 and n_2, respectively. A total thickness L is k percent occupied by G and (1-k) percent is build by P. The optical path length (OPL) is:

$$OPL = n_1(1-k)L + n_2kL = n_1L + \Delta nkL \qquad (\Delta n = n_2 - n_1)$$

Equation 2-4

and the time delay is:

$$\tau = OPL/c = (n_1L + \Delta nkL)/c$$

Equation 2-5
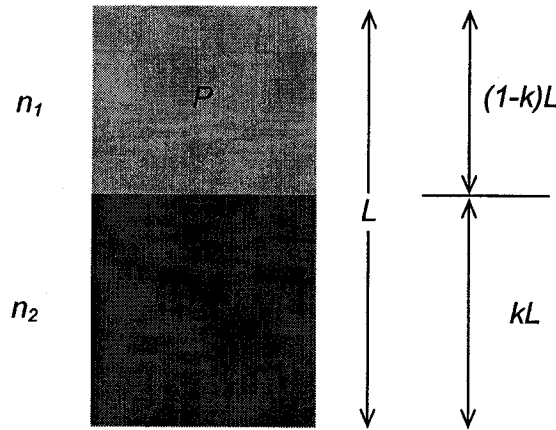
Figure 2-11: Combination of two materials with refractive index n_1 and n_2

The base delay is n_1L/c. When k is changing from 0 to 1, the additional delay can be made continuous from 0 to $\Delta nkL/c$. As it is shown in Figure 2-12 the schematic of system consists of number of basic cells with different values of k.
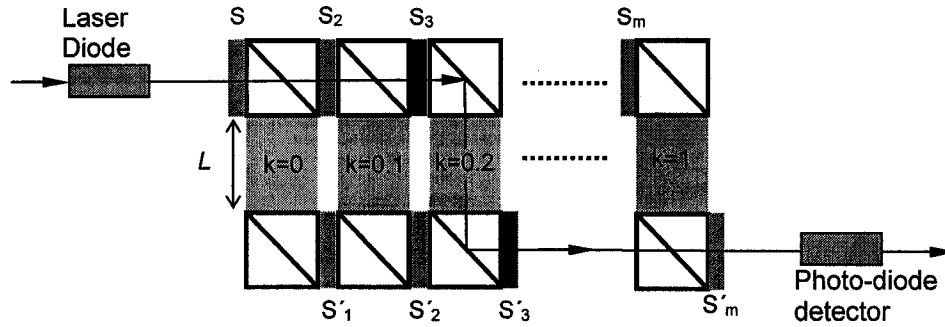
Figure 2-12: Solid optical delay system

This module can provide the delay in order of picoseconds 10 ps to 900 ps depending on design values of L, n_1, n_2 and number of stages, m. Optical loss is less than 0.5 dB per switch and optical cross talk is about -50 dB.

Numerous techniques of implementing an ODL have been suggested. These techniques mostly differ from methods of switching of light through different delay paths. Some of these techniques can be seen as references at the end of this chapter. [2.21]-[2.34]

2.2 Different application of variable optical delay line

The ability to change the arrival time or phase of optical signals is a crucial function in many optical systems. Various applications of ODL in different systems such as broad band wireless access network, optical coherence tomography, broad-band filters, radar phase noise measurements, and computer interconnects can be seen prominently[2.32]-[2.47]. In this section the application of ODL in some of these systems such as optical time division multiple-access (OTDMA), optical code division multiple-access (OCDMA) and phased-array radar will be described.

2.2.1 Application of delay line in OTDMA system

Fast tunable optical delay lines, capable of rapidly changing the delay time of optical pulses, have important applications in OTDMA and OCDMA systems. They are

expected to be utilized in the encoders/decoders in OCDMA systems, where different codes can be constructed, by using pulses in different temporal positions (as will be discussed in the following section). In OTDMA systems, since different time slots correspond to different channel addresses, they can be used at the transmitter/receiver ends obtain fast channel assignment/access respectively.

OTDMA has become an important means for different communications systems applications, such as broad band networks, switching, and computer interconnects.

It carries simultaneously many data channels on single fiber [2.40]. If N data channels, each with a bit rate 1/T b/S, are to share the fiber, then each bit interval is divided into N time slots j= 0,..., N-1 of duration τ within a time frame of T. The time slots correspond to addresses, either of source (as in fixed-transmitter assignment OTDMA) or destination (as in fixed-receiver assignment OTDMA).

An OTDMA coder selects the desired address by delaying the data to the appropriate time slot. By the help of mode locked lasers, extremely short pulses and correspondingly short time slot τ (in order of femto-seconds) can be generated. For high speed access to a large network, the OTDMA coder must rapidly select one of a large number of optical delays. A feasible design of coder has been demonstrated in Figure 2-13 It allows rapid tuning among a large number of delays. It consists of $\log_2 N$ delay stages; each of them consists of a 2x2 optical switch, a connection to the next stage at one output, and a fixed optical delay. The value of this fixed delay for the kth stage is $T/2^k$. Each optical switch can rapidly be set in either the bar or the cross state. The state of each switch can be controlled electronically, where 0 at the control sets the switch in the cross state, whereas a 1 sets it in the bar state.
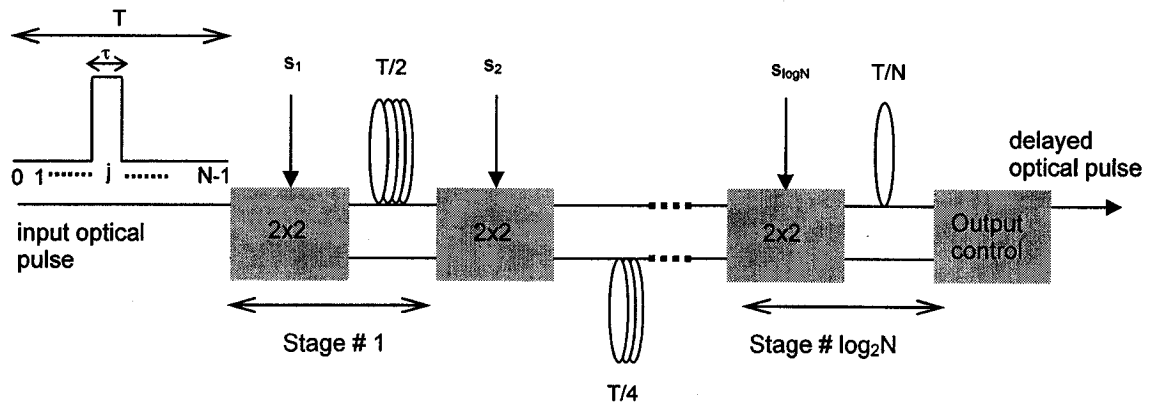
Figure 2-13: Schematic of an optical time division system with tunable delay line

The state of coder is set by a control sequence (s_1, s_2,..., s_k,...) where control bit s_k sets the state of the *k*th stage. The output stage is set to be 0 if the parity of the control sequence is odd or 1 if the parity of the control sequence is even. There are different versions of implementing delay lines in OTDMA system but the basic idea is the same.

2.2.2 Application of delay line in OCDMA system

Optical Code Division Multiple-Access (OCDMA) has been investigating over a decade for application in optical fiber networks. This scheme can provide multiple accesses to network without using wavelength-sensitive components, as in Wavelength Division Multiplexing (WDM), and without employing high speed electronic data processing devices as are needed in Time Division Multiplexing (TDM) networks [2.41]. The main reason which has motivated the communications industry to use this method is the asynchronous access capability in transmission offered by OCDMA. Additionally the fact that all the components can be realized all optically, and therefore achieving a truly transparent network, could potentially lead to network throughput of the rate of TB/s. In the simplest configuration, OCDMA achieves multiple-access by assigning a unique code to each user. Two users can communicate with imprinting the agreed-upon code. The receiver can decode the bit stream by locking into the same code sequence. The

Schematic diagram of an OCDMA communication system is shown in Figure 2-14 [2.43]. This system should be able to extract the specific pulse sequence in the presence all other users' pulse sequences. Therefore different methods of coding such as prime coding or orthogonal coding have been suggested to satisfy this operation.
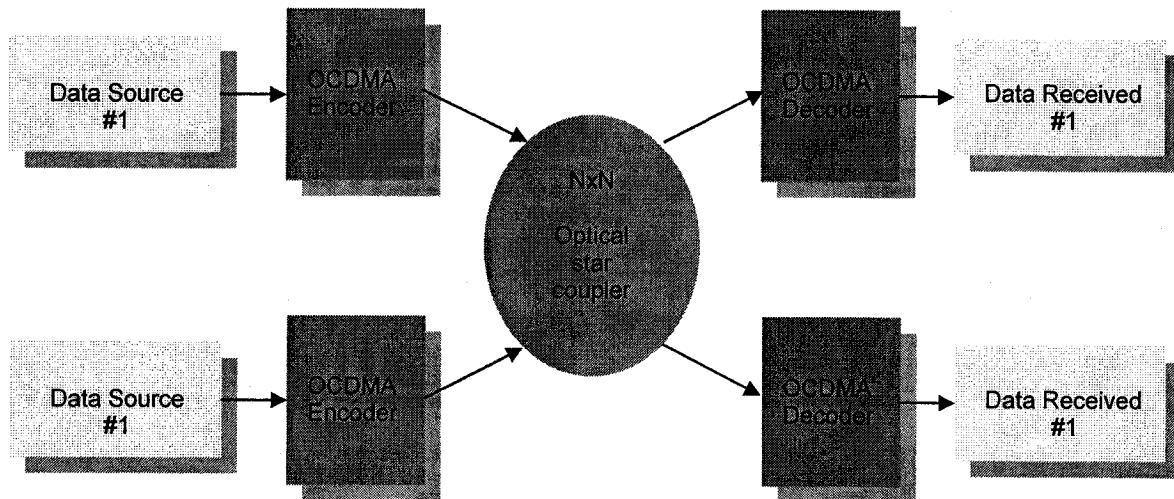
Figure 2-14: A schematic diagram of an OCDMA communication system

One of the common OCDMA systems is called incoherent OCDMA. This method is using direct optical detection. Optical delay lines can be applied in encoders and decoders for construction of a code. The encoder (decoder) consists of a splitter, tunable optical delay line and a combiner as shown in Figure 2-15. The input pulse splits, producing a train of pulses which are properly delayed within the data bit period according to the delay time. The decoder has the reverse impulse response from the encoder, therefore recovers the data pulse. To send information from node j to node k, the address code for node k is impressed upon the data by the encoder at node j. At destination, the receiver correlates its own address with the received signal. [2.39]
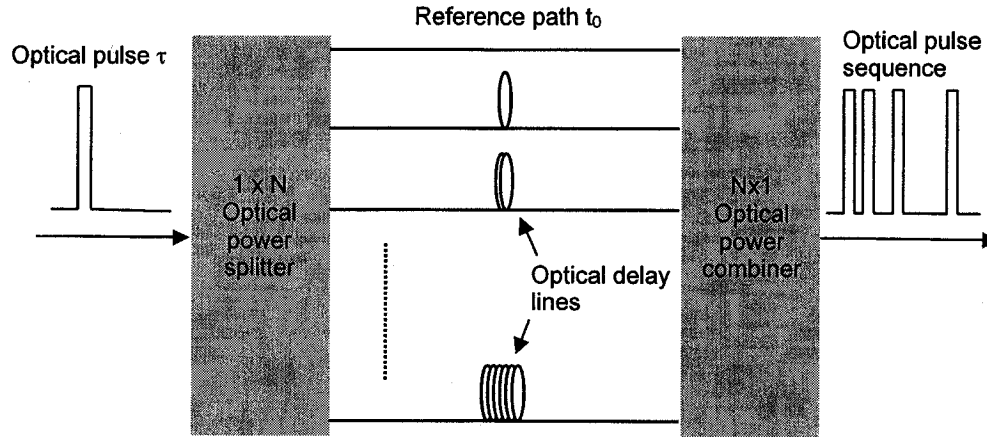
Figure 2-15: Block diagram of an OCDMA encoder using parallel architecture.

2.2.3 Application in phased-array antenna

The antenna of a phase-array radar system is actually a group of many radiating antennas that generate a transmitting signal pattern called a beam, whose direction and shape is determined by the relative phases and amplitudes of the currents in all the individual antennas, or elements of the array; thus, by properly varying the relative phases, it is possible to steer the direction of the beam. The array is usually arranged as a one-dimensional linear array, where the elements of antenna are placed in a straight line, or as a two-dimensional array, where the elements are placed on a surface.

The schematic of a microwave phased array antenna consisting of (N+1) elements are shown in Figure 2-16. To steer the radiated beam, the microwave signal (of frequency ω_m) exciting each radiating element is first routed a RF phasing unit. If the ratio of RF output to RF input of each of these units is given by $a_n e^{j\psi_n}$, the far field of the antenna beam at the angle θ is given by following expression:

$$E(\theta,t) = \sum_{n=0}^{N} a_n e^{j(\psi_n + nk_m \Lambda \sin \theta)} e^{j\omega_m t}$$

Equation 2-6

where Λ is the distance between the elements and k_m is the wave number (= ω_m/c) of the radiated beam. The time independent part of E is proportional to the array factor of the antenna. The phase front, and therefore beam's direction can be controlled by variation of relative phase between successive radiating elements of the array. For example, to direct the radiated beam at the angle of θ_0, the value for ψ_n can be obtained as following:

$$\psi_n = -nk_m\Lambda\sin\theta_0$$

Equation 2-7
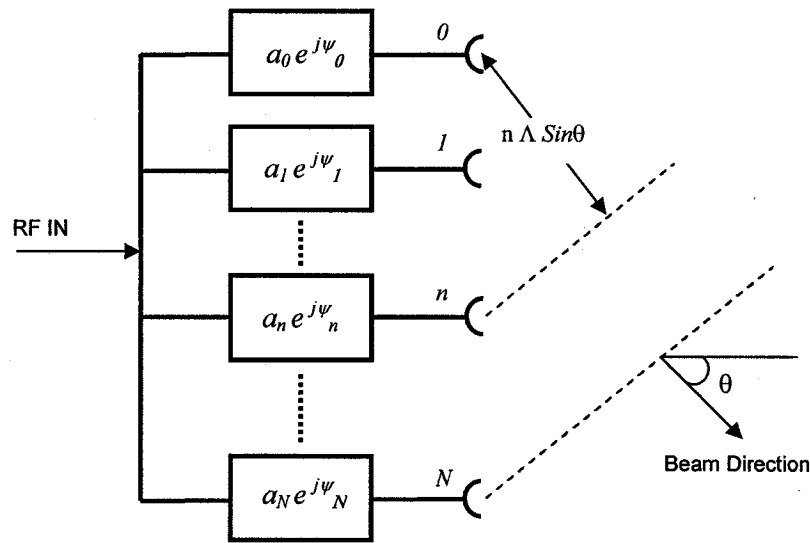
Figure 2-16: Schematic of phased-array antenna

If we take the differential of Equation 2-7, we can see for the fixed value of ψ_n's, the directed beam will change by an amount of $\Delta\theta_0$, which is given by:

$$\Delta\theta_0 = -\tan\theta_0(\frac{\Delta\omega_m}{\omega_m})$$

Equation 2-8

for an instantaneous change of the microwave frequency equal to $\Delta\omega_m$. This undesirable change of direction can drop the gain in the main direction, and cause the phenomenon called "beam squint".

To achieve a wide instantaneous bandwidth, "time shifter", as distinguished from the "phase shifter" described above, can be used to create relative phase shift between the elements. In this method by the use of time delay line, the path difference between two radiators will be controlled by varying the path from the microwave feed to the radiating elements. The length of delay for the (n+1)th antenna element is designed to provide a delay time $t_n(\theta_0)$ given by:

$$t_n(\theta_0) = \frac{n\Lambda\sin\theta_0}{c}$$

Equation 2-9

for the (n+1)th delay element. For all frequencies ω_m, ψ_n is now obtained by:

$$\psi_n = -\omega_m t_n(\theta_0)$$

Equation 2-10

Substituting Equation 2-7 into Equation 2-9, it is clear that Equation 2-10 enables constructive interference to be obtained in the direction of θ_0 at all frequencies. Even if ω_m is changed instantaneously, the radiated beam will not drift from its main direction.

Using electrical delay lines is not easy to be implemented because it requires the use of heavy, bulky coaxial cables/waveguides serving as a RF delay lines. Optical delay lines offer light and compact solution to accomplish time delay module. In addition to these, the bandwidth of optical delay module is large and electromagnetic interference is negligible comparing to its microwave equivalent. Figure 2-17 shows the schematic of the phased array antenna using optical delay line module.

Optical delay module   Photo-detector

RF input

τ_0

$2\tau_0$

$3\tau_0$

Switching and laser diodes

Optical coupler 8 to 1

RF output
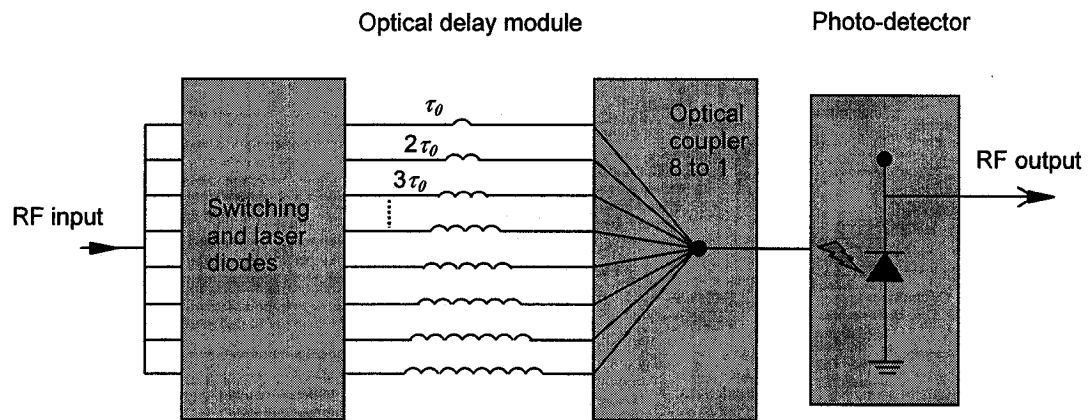
Figure 2-17: Schematic of 3- bit phased-array antenna using delay line module

Various configurations have been used a true-time-delay module for phased array antenna. [2.42]

In the next chapter our design of tunable ODL will be described. It consists of free space delay paths and micro-mirrors to change trajectory of light through the delay path.

References:

[2.1] G. Lenz, B. J. Eggleton, C. K. Madsen, and R.E. Slusher, "Optical delay lines based on optical filters," IEEE Journal of Quantum Electronics, Vol. 37, No.4, p525-532 , 2001.

[2.2] E. Ackermen, S. Wanuga, and D. Kasemet, "Integrated 6-Bit Photonic True-Time-Delay Unit for Lightweight 3-6 GHz Radar Beam-former," in IEEE MTT-S Symposium Digest, Vol.3, p1111-1114, 1995.

[2.3] V. K. Kaman, X. Zheng, R. J. Helkey, C. Pusarla, J. E. Bowers,"A 32-Element 8-Bit Photonic True-Time-Delay System Based on a 288x288 3-D MEMS Optical Switch,"IEEE Photonics Technol. Lett., Vol. 15, No.6, p849-851, 2003.

[2.4] Wencai Jing, Yimo Zhang, Ge Zhou, " Design of MOEMS Adjustable Optical Delay Line to Reduce Link Set-up Time in a Tera-bit/s Optical Interconnection Network," Optics Express, Vol. 10, No. 14, p591-596, 2002.

[2.5] P. Klovekorn and J. Munch, "Variable Optical Delay Line with Diffraction-Limited Autoalignment," Appl. Opt., Vol. 37, No. 10, p1903-1904, 1998

[2.6] I. Kobayashi, K. Kuroda, " Step-Type Optical Delay Line Using Silica Based Planar Light-Wave Circuit (PLC) Technology," IEEE Transaction on Instrumentation and Measurements, Vol. 49, No. 4, p762-765, 2000.

[2.7] C. J. Beaumont, S. A. Cassidy, Dr. D. Welbourn, Dr. M. Nield, A. Thurlow, " Integrated Silica Optical Delay Line," TuB5-6, p241-244, IOOC-ECOC 1991.

[2.8] H. Takakura, K. Kuroda, "Optical Delay Line Using Waveguide," 21st Proc. Australian Conference on Optical Fiber Technology(ACOFT'96), p317-320, 1996

[2.9] Wenshen Wang; Yongqiang Shi; Weiping Lin; Bechtel, J.H., Waveguide Binary Photonic True-Time-Delay Lines Using Polymer Integrated Switches and Waveguide Delays," Proceedings of the SPIE - The International Society for Optical Engineering, Vol. 2844, p200-211, 1996

[2.10] S.Yegnanarayanan, P. D. Trinh, F. Coppinger, and B. Jalali, "Compact Silicon-Based Integrated Optic Time Delays," IEEE Photonics Technology Lett., Vol. 9, No. 5, p643-635, 1997.

[2.11] C. T. Sullivan, S. D. Mukherjee, M. K. Hibbs-Brenner, A. Gopinath, E. Kalweit, T. Marta, W. Goldberg and R. Walterson, "Switched Time Delay Elements Based on AlGaAs/GaAs Optical Waveguide Technology at 1.32 μm for Optically Controlled Phased Array Antennas," in Proc. SPIE, Vol. 1703, p264-271, 1992.

[2.12] K. Horikawa, I. Ogawa, T. Kitoh, H. Ogawa,"Silica-Based Integrated Planar Lightwave True-Time-Delay Network for Microwave Antenna Applications," OFC'96 Technical Digest,p100-101, 1996.

[2.13] E. J. Murphy, T. F. Adda, W. J. Minford, R. W. Irvin, E. I. Ackerman, and S. B. Adams, "Giuded-Wave Optical Time Delay Network," IEEE Photonics Technol. Lett., Vol. 8, No.4, p545-547, 1996.

[2.14] Masayasu Yamaguchi and Hirabayashi K., "Variable optical delay line based on a birefringent planar optical platform," Opt. Lett., Vol. 20, No.6, p644-646, 1995.

[2.15] G.W. Yoffe, J.W. Arkwright, G.E. Town and B.G. Smith, " Tunable optical delay line based on a fibre Bragg grating," Elec. Lett., Vol. 34, No.17, 1688-1690, 1998.

[2.16] J.W. Arkwright, G.W. Yoffe, G.E. Town, B.G. Smith, "All-fiber tunable optical delay line based on a uniform Bragg reflection grating," ACOFT'98 Proceedintg, 23rd Australian conference on optical fiber technology, p117-120, 1998.

[2.17] K.T.Cornett, J.P. Heritage, and O. Solgaard, "Compact Optical Delay Line Based on Scanning Surface Micromachined Polysilicon Mirrors," IEEE Proceedings of the 2000 IEEE/LEOS International Conference on Optical MEMS (Optical MEMS 2000), pp. 15-16, Kauai, Hawaii, 2000.

[2.18] K.T. Cornett, P.M. Hagelin, J.P. Heritage, O. Solgaard, and M. Everett, "Miniature Variable Optical Delay Using Silicon Micromachined Scanning Mirrors," Conference on Lasers and Electro-Optics (CLEO), Technical Digest, pp. 383-384, San Francisco, California, 2000.

[2.19] K.F. Kwong, D. Yankelevich, K. C. Chu, J. P. Heritage, and A. Dienes, "400-Hz Mechanical Scanning Optical Delay Line," Opt. Lett. Vol. 18, No. 7, p558-560, 1993.

[2.20] Jian Fu, M. Schamschula, H. J. Caufield, "Modular Solid Optic Time Delay System," Opt. Comm. 121, p8-12, 1995.

[2.21] B. C. Wang, Ivan Glesk, R. J. Runser, P. R. Prucnal, " A Fast Tunable Parallel Optical Delay Line," Optics Express, Vol. 8, No. 11, p599-600, 2001

[2.22] P . Goutzoulis, D.K.Davies, J.M. Zomp, "Prototype Binary Fiber Optic Delay Line," Optical Eng., Vol. 28, No. 11, p1193-1202, 1989.

[2.23] S. T. Johns, D. A. Norton, C. W. Keefer, R. Erdmann, R. A. Soref, "Variable Time Delay of Microwave Signals Using High Dispersion Fiber," Elec. Lett., Vol. 29, No. 6, p555-556, 1993.

[2.24] N. Madamopoulos, N. A. Riza, "Adaptable-Delay Balanced-Loss Binary Photonic Delay Line Architecture Using Polarization Switching," Optics Communications, 152, p135-143, 1998.

[2.25] B. L. Anderson and R. Mital, "Polynomial-Based Optical True-Time-Delay Devices with Microelectromechanical mirror arrays," App. Opt. Vo. 41, No. 26, p5449-5461, 2002.

[2.26] K. L. Hall, D. T. Moriaty, H. Hakimi, B. S. Robinson, K. A. Rauschenbach, "An Ultrafast Variable Optical Delay Technique," IEEE Photonics Technol. Lett., Vol. 12, No. 2, p208-210, 2000.

[2.27] N. A. Riza, "Acousto-Optically Switched Optical Delay Lines," Optics Communications, 145, p15-20, 1998.

[2.28] N. A. Riza, "Liquid Crystal-Based Optical Time Delay Units for Phased Array Antennas," J. Light. Technol., Vol. 12, No. 8, p1440-1447, 1994.

[2.29] N. A. Riza, N. Madamopoulos, "Characterization of a Ferroelectric Liquid Crystal-Based Time Delay Unit for Phased Array Antenna Applications," J. Light. Technol., Vol. 15, No. 7, p-1088-1094, 1997.

[2.30] N. A. Riza , "Polarization-Based fiber optic delay lines," SPIE Proc., Vol. 2560, p120-129, 1995.

[2.31] N. Madamopoulos, N. A. Riza,"Polarization Selective Hologram-Based Photonic Delay Lines," Optics Communications, 157, p225-237, 1998.

[2.32] Nikos Karafolas, D. Uttamchandani, "Optical Fiber Code Division Multiple Access Networks: A Review," Optical Fiber Technology 2, 0017, p 149-168, 1996.

[2.33] V. Baby, B. C. Wang, L. Xu, I. Glesk, P. R. Prucnal, "Highly Scalable Serial-Parallel Optical Delay Line," Optics Communications, 218, p235-242, 2003.

[2.34] N. A. Riza, S. Sumriddetchkajorn, "Fault-Tolerant Polarization-Intensive Photonic Delay Line Architectures Using Two-Dimensional Digital Micro-mirror Devices," Optics Communications, 160, p311-320, 1999.

[2.35] K. P. Jackson et al., "Optical Fiber Delay-Line Signal Processing," IEEE Transactions on microwave theory and techniques, Vol. MTT-33, No. 3, p-193-210, 1985.

[2.36] D. B. Sarrazin, H. F. Jordan, V. P. Heuring, " Fiber Optic Delay Line Memory," App. Opt., Vol. 29, No. 5, p627-637, 1990.

[2.37] W. Ng, A. A. Walston, G. L. Tangonan, J. J. Lee, I. L. Newberg, and N. Bernstein, " The First Demonstration of an Optically Steered Microwave Phased Array Antenna Using True-Time-Delay," J. Lightwave Technol., Vol. 9, p1124-1131, 1991.

[2.38] Deng, K.-L., Runser, R.J. Toliver, P. Coldwell, C. Zhou, D., Glesk, I. Prucnal, P.R., "Demonstration of a highly scalable 100-Gbps OTDM computer interconnect with rapid inter-channel switching capability,"Optical Fiber Communication Conference, 1999, and the International Conference on Integrated Optics and Optical Fiber Communication. OFC/IOOC '99. Technical Digest ,Volume: 3 , p165-167, 1999

[2.39] J.-G Zhang, G. Picchi, "Tunable Prime-Code Enmcoder/Decoder for All-Optical CDMA Applications," Elec. Lett., Vol. 29, No. 13, p 1211-1212, 1993.

[2.40] P. R. Prucnal, M. F. Krol, J. L. Stacy," Demonstration of a Rapidly Tunable Optical Time-Division Multiple-Access Coder," IEEE Photon. Technol. Lett., Vol. 3, No. 2, p170-172, 1991.

[2.41] Gerd Keiser, "Optical fiber Communication" third edition, McGraw Hill, 2000,p514-515.

[2.42] M. Fisk, M. M. Prcic, G.Rzyski, R. Stevens, " Application of fiber optic delay lines in radar phase noise measurement," AUTOTESTCON '94. IEEE Systems Readiness Technology Conference, Conference Proceedings. , 20-22 ,p179 – 182, 1994

[2.43] N. Karafolas, " Optical fiber code division multiple-access networks: A review," optical fiber technology 2, p 149-168, 1996

[2.44] K. L Deng et al. ,"Optical fiber stretching technique for the precision time delay in ultrahigh speed OTDM system," CLEO' 97, p 416 -418 , 1997

[2.45] Vidal, B., Madrid, D., Corral, J.L., Polo, V., Martinez, A., den Besten, J.H., Soares, F., Marti, J., Smit, M.K., "Photonic true-time delay beam-former for broadband wireless access networks at 40 Ghz band," Microwave Symposium Digest, 2002 IEEE MTT-S International , Volume: 3 , 2-7 ,p1949 - 1952, June 2002

[2.46] Joseph M . Schmitt, "Optical coherence tomography (OCT): A review," IEEE journal of slected topics in Quantum Electronics, Vol. 5, No. 4, p1205-1215, 1999

[2.47] W. K. Niblack, J. O. Schenk, B. Liu, M.E. Brezinski, " Dispersion in grating-based optical delay line for optical coherence tomopgraphy," Applied optics, Vol. 42, No. 19, p 4115-4118 , 2003

3 Design Description

In this chapter we study the design process of an optical delay module that uses MEMS technology. Section 3.1 outlines the general targets and specifications of the module. Section 3.2 presents the features of our design and its advantages. Different parts of the module are described separately in section 3.3. The overall system design is shown in section 3.4.

3.1 General Description and Design Targets

Our objective is to design and analyze a tunable optical delay line using MEMS pop-up micro-mirrors, a device which would allow us to redirect the incident light in different paths to obtain the desirable delay time. The basic configuration of the free-space optical delay line is shown in Figure 3-1.

One option is made of up to m delay stages, each consisting of a pair of micro-mirrors and a stationary corner reflector (or pair of perpendicular mirrors). Each of these stages provides a constant delay time, which can be defined as the *delay time resolution* of the module, τ_{res}. As implied by their name, the pop-up mirrors could either be in the down (off) state, in which case the delay segment of stage m is bypassed, or in the up(on) state in which case the delay segment of stage m becomes part of the signal trajectory.
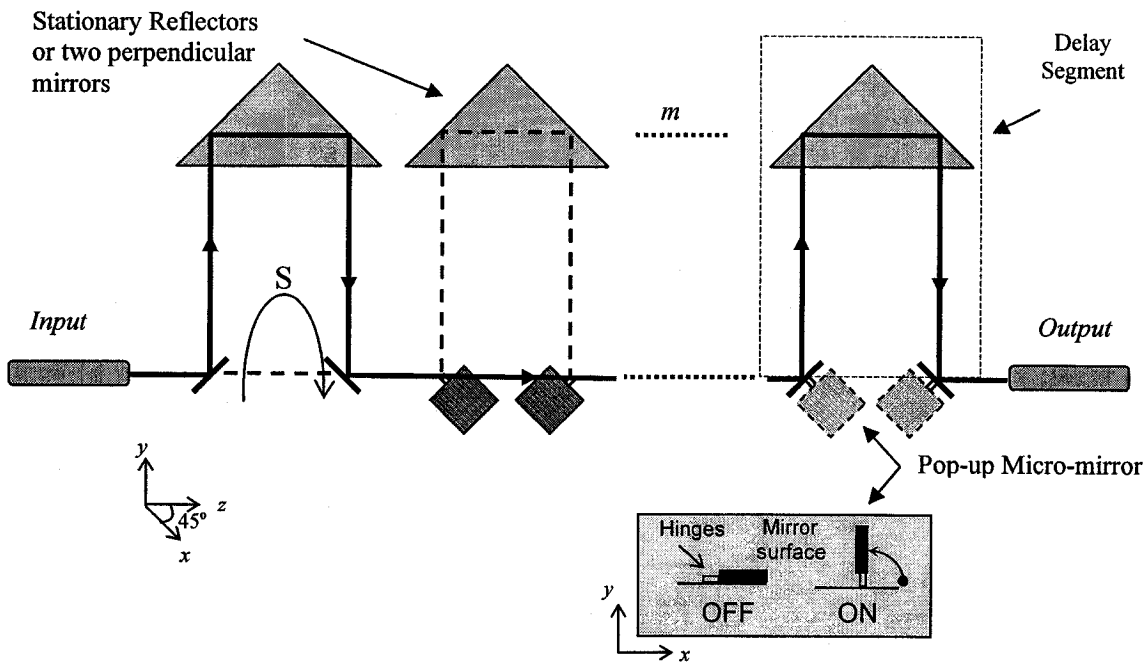
Figure 3-1: Schematic of a delay line using controllable MEMS

Assuming that the length of each delay path is S and that the light propagates in free space then, the delay in each section is:

$$\tau_{res} = cS$$

where, $c = 3 \times 10^8$ m/s is the speed of light in free space.

Thus in order to achieve a given maximum delay of τ_{delay}, m delay paths are needed, where m is defined as follows:

$$m = \frac{\tau_{delay}}{\tau_{res}}$$

Note the device will consist of $2m$ micro-mirrors and m corner reflectors (or m pairs of perpendicular mirrors). However, as we will show, it is possible to conceive a design with fewer mirrors.

Our target is to design a system similar to the one presented in Figure 3-1 The specifications of the delay module discussed in this thesis are summarized in Table 3-1. The delay range from 100 ps to 6300 ps with the resolution of 100 ps is required. Such a module can be envisioned as part of an OCDMA system to form the pulses. In such a case, 63 states are needed for a system as depicted in Figure 3-1. This system will be operating in a wavelength with low dispersion of fiber.

Table 3-1: Primary specification of the system

Parameter	Symbol	Value
Beam-waist at fiber	ω_{SMF}	4.77 μm
Wavelength	λ	1.31 μm
Maximum delay	τ_{max}	6300 ps
Delay Increments	τ_{res}	100 ps

There are some key constraints which will affect the performance of this system:

- *Optical loss due to imperfect mirror and corner cube reflectance:*

Loss of the optical power in the MEMS micro-mirrors is mainly due to reflection loss, which can be expressed as follows:

$$L_{max} = -10(2m)\log(1-\alpha) \quad (dB) \quad m = 1,2,3,...$$

Equation 3-3

where α is the reflection loss of each mirror.

Equation 3-3 shows that in order to minimize L_{max}, the reflection of each mirror should be increased while the number of mirrors should be reduced. The former can be achieved by the use of high reflectivity gold coating or dielectric coating which improves the reflectivity. Issues related to the number of mirrors are discussed in the next section. Note that, this is only for MEMS micro-mirrors and loss of reflection for corner cube reflectors have not been considered yet.

- *Optical loss due to beam spreading (diffraction) in the delay loops:*

This is one of the basic constraints of free-space optics. It is well known that light coming out of the Single Mode Fiber (SMF) follows a Gaussian profile. This problem can be alleviated by locating collimating lenses at the entrance and exit ports and wherever else necessary. In section 3.2.2 and 3.2.3 we attempt to design an appropriate collimating system. More materials about diffraction and Gaussian beam profile can be found in [3.1].

- *Optical loss due to misalignments throughout the system:*

This problem as well as its effects is discussed in detail in Chapter 4. Remedies shall also be presented.

3.2 Design principles

The constraints outlined in the previous section, namely the effect of number of mirrors and of beam spreading, can have a very important impact on the system performance. These two important constraints, and how their effects can be minimized, are considered in the next two sub-sections.

3.2.1 Binary Scaling:

As shown in chapter 2 many designs of tunable ODL consist of several delay paths, which their lengths are in binary fashion. This way reduces the number of mirrors in our design. In other words, we can have delay loops of different lengths, each of which provides twice the delay time of the previous one. For m delay segments, the k th loop time delay is defined:

$$\tau_k = 2\tau_{k-1} \quad , \qquad \tau_1 = \tau_{res}, \qquad k = 2,..,m$$

Equation 3-4

, and the maximum possible delay is:

$$\tau_{max} = (2^0 + 2^1 + 2^2 + ... + 2^{(m-1)})\tau_{res} = (2^m - 1)\tau_{res}$$

Equation 3-5

To obtain a given maximum delay, the required number of segments is:

$$m = 1 + \left\lfloor \log_2\left(\frac{\tau_{max}}{\tau_{res}}\right) \right\rfloor$$

Equation 3-6

Comparing Equation 3-2 and Equation 3-6 it can be seen that the binary case reduces the required number of segments, as a result the number of micro-mirrors. This is shown in Figure 3-2.
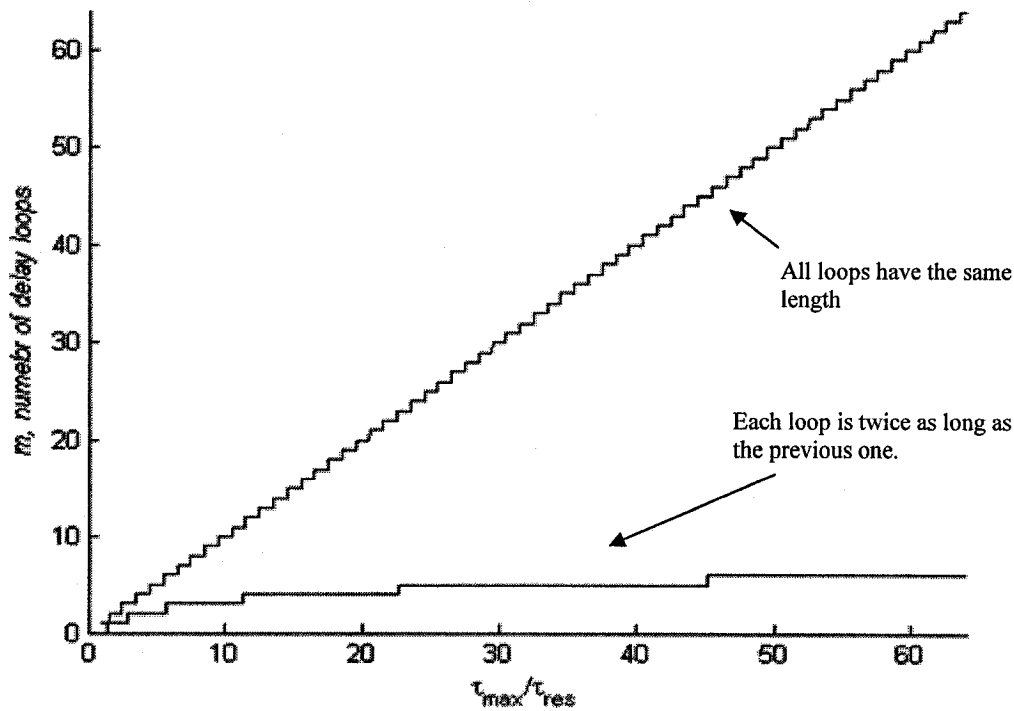
Figure 3-2: Comparison of the number of loops for equal and binary path lengths

For the desired system in Table 3-1, we would require six loops with delays of 100 ps, 200 ps, 400 ps, 800 ps, 1600 ps, 3200 ps, compared to 64 equal-delays of 100 ps. In Figure 3-3 the new system is shown. Note that the same resolution can be obtained in both designs.

Some parameters which are important for the design are:

L_{min} is the distance between input and output of the overall system, when all mirrors are off, so it is the minimum distance that light travels from input to output.

d is the separation distance between a set of two mirrors in the same delay segment.

d' is the thickness of the corner reflector, as shown in Figure 3-3.

Equation 3-7 relates these three parameters:

$$L_{\min} = md' + (m+1)d$$

Equation 3-7

For *m*=6;

$$L_{min} = 6d' + 7d$$

d and d' need not be equal within each segment, but this assumption can simplify calculations, therefore $d=d'$: $L_{min}=13d$.

The total length of each loop can be calculated from:

$$s_k = 2^{k-1} c \tau_{res}$$

Assuming that light always propagates in free-space, the full length of the delay paths are then: 2 cm, 4 cm, 8 cm, 16 cm, 32 cm, 64 cm successively.
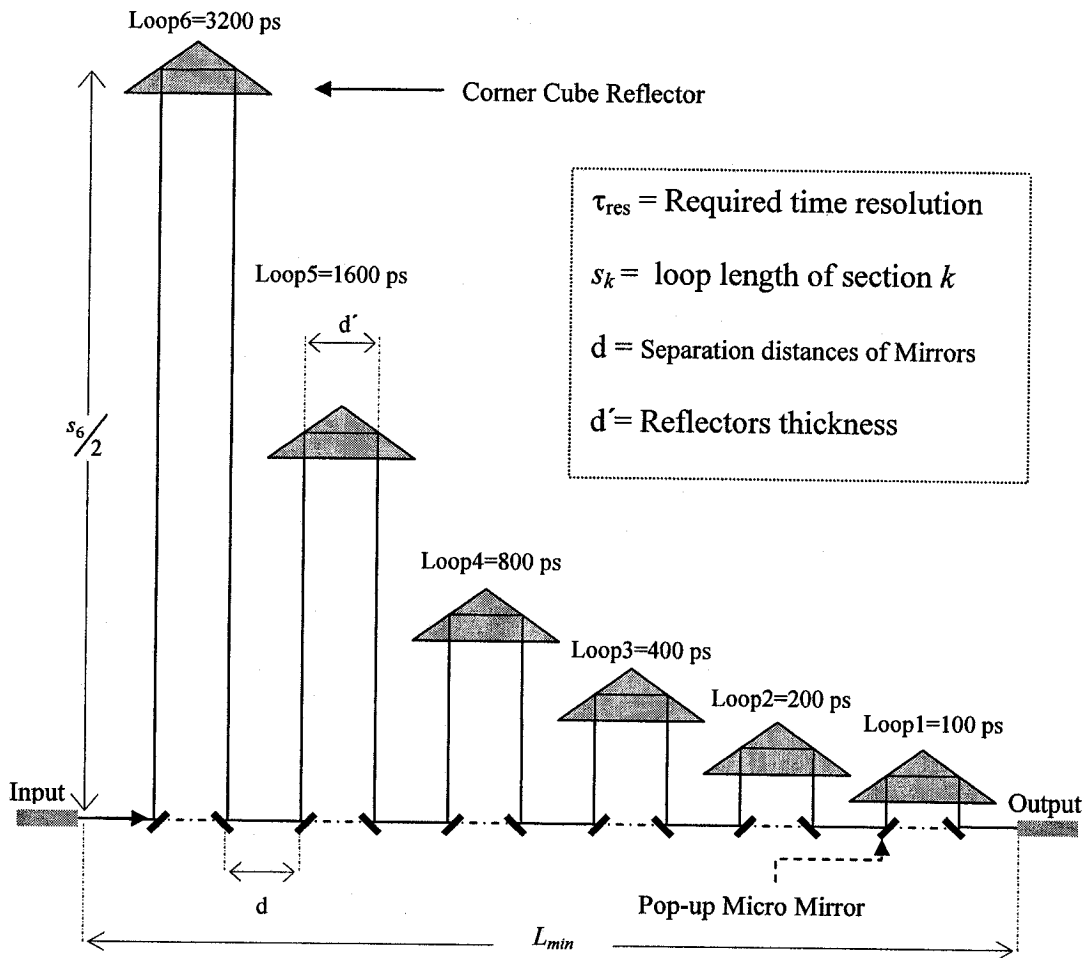
Figure 3-3: Schematic of an optical delay line with binary loops

3.2.2 Invariant Beam-size:

A Gaussian beam profile suffers from beam-spreading, which severely reduces the coupling efficiency, if not corrected. As such, collimating lenses may be located following the input fiber and prior to output fiber and also within each delay segments as shown in Figure 3-4. The challenge is to design the fiber and segment collimating lenses, in order to avoid a non-uniform insertion loss, as the optical path length varies (as mirrors are switched on or off). In Appendix A, a system which uses only fiber collimating lenses is simulated. These lenses are chosen such that when all mirrors are on, i.e. all delay segments are activated, the system has optimal performance. However, when all the mirrors are off and the light travels the shortest path, the insertion loss climbs beyond an acceptable level. Collimating lenses are therefore required in each segment in order to compensate for the beam spreading corresponding to the specific distance in segment.

f_L: Focal length of the lens referred to as fiber collimating lens
f_m: Focal length of the lens referred to as segment collimating lens
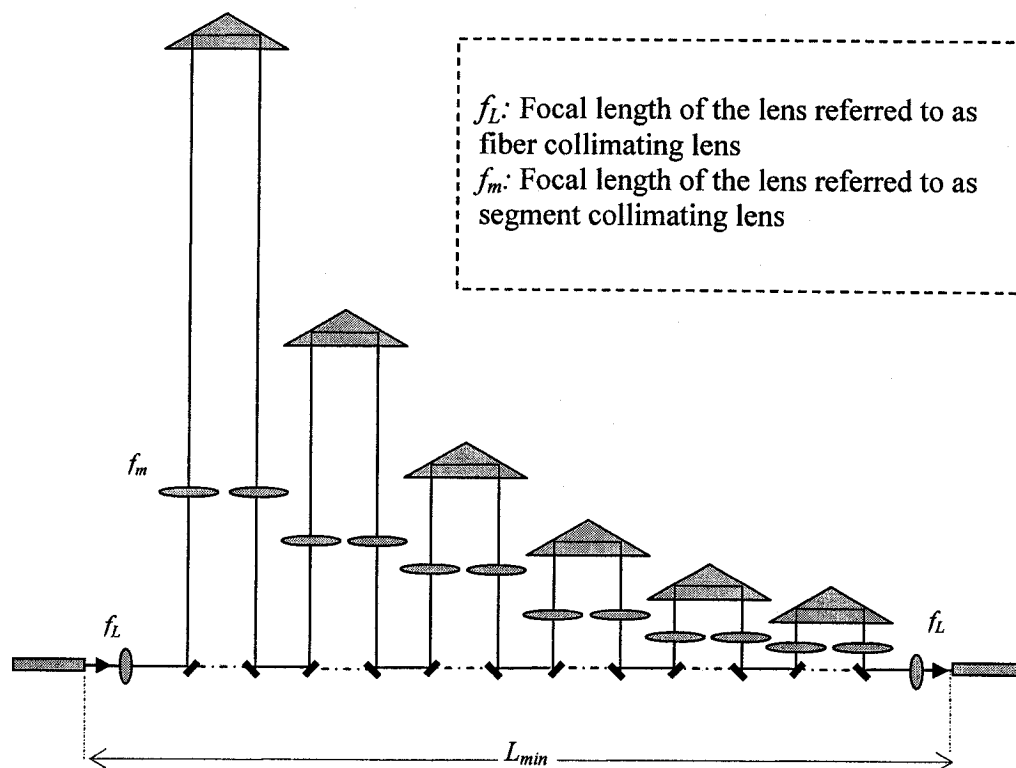
Figure 3-4: Schematic of the system including collimation lenses

In particular, *the segment collimating lenses should be designed such that the beam-waist following the second mirror of the segment is maintained at the value if would have been had the light not traveled through the segment.* This is depicted in Figure 3-5.
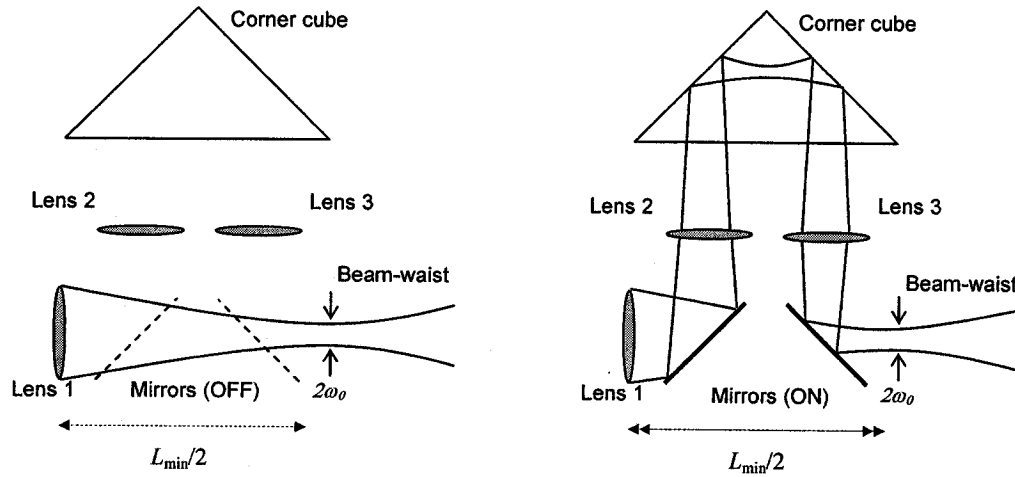
Figure 3-5: Segment collimating lenses result in invariant beam-waist size and location.

Although it is possible to design segment collimating lenses, but the implementation of these lenses can be an important issue. To prevent this using a solid material in delay segments is suggested.

3.2.3 Using solid material in delay segments:

The overall design that will be analyzed in this thesis is presented in Figure 3-6. A single block of solid material, with refractive index of n_g, is located above the MEMS mirrors. Within each delay segment, two surfaces, having equal curvature of R_m, are molded into the bulk, however at a different distances (σ_m and δ_m) from MEMS mirrors. These distances and curvatures should be calculated in a way that light be collimated in the delay path, and also as is mentioned in previous section, maintain the beam size at the end of each segment as if there is no delay line (equivalent functionality as the two

segment collimating lenses in the previous section). However, having a single block reduces implementation complexity considerably.

Note that part of the delay path $(\delta_m + \sigma_m)$, is located in the air while the rest $(2y_m)$ is through material with refractive index n_g.

$\tau_1 = 3200$ ps

n_g: Refractive index of the block
f_L: Focal length of the collimating lenses
σ_m: Distance from mirror to the lens vertex
δ_m: Distance from the lens vertex to mirror
y_m: Half length of propagation inside the block
R_m: Radius of curvature

$\tau_2 = 1600$ ps

$\tau_3 = 800$ ps

$\tau_4 = 400$ ps

$\tau_5 = 200$ ps

$\tau_6 = 100$ ps

R_m

σ_m δ_m

Input fiber

M_1 M'_1 M_2 M'_2 M_3 M'_3 M_4 M'_4 M_5 M'_5 M_6 M'_6

f_L

Output fiber

f_L

Figure 3-6: Illustration of the design

3.3 Design of Different Components

In previous section, the main components of the system and the design parameters were introduced. In this section the implementation details will be addressed.

3.3.1 Design and Characteristics of the MEMS Mirrors
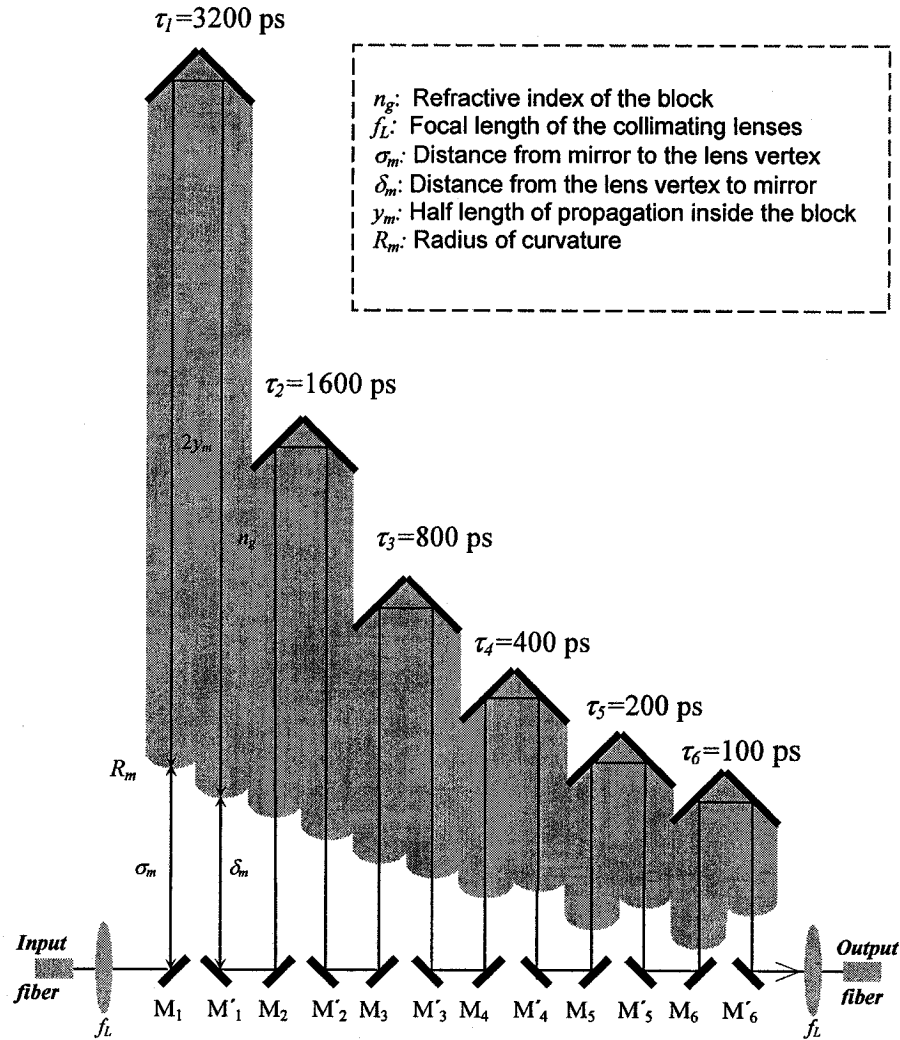
Interest in MEMS has grown in the past decade due to the vast number of potential applications, and also due to improved methods of manufacturing. This section begins with a brief background of MEMS mirror theory, followed by design of the mirror used in this system.

3.3.1.1 MEMS Theory

MEMS mirror are very attractive technology to use, since their small size makes them appropriate to integrate with other optical components. Their response time is fast, and their power consumption is low. Of the various fabrication techniques for MEMS, the two most important ones are bulk micromachining and surface micromachining. Bulk micromachining technology is based on single crystal silicon etching. In other words, a single silicon substrate is etched according to set patterns leaving the desired structure on the substrate. A characteristic of this technique is that it removes significant amount of silicon from a substrate, therefore, it can produce thicker structure, allowing larger and flatter surfaces. On the other hand, in surface micromachining the wafer remains intact. All constituent materials (usually Polysilicon) are deposited onto the wafer in the form of layers, which are then patterned and partially removed to create a MEMS device. Surface micromachining can involve multiple layers, depending on the foundry and technique used. The MEMS foundry service offered at Sandia National Laboratories offers a four-layer polysilicon called SUMMiT (Sandia Ultra-planar, Multi-level MEMS Technology)[3.3] or a five-layer polysilicon process called SUMMiT-V. Another service called Multi User MEMS Processes (MUMPs) [3.4] offers the same kind of process, but with only 3 layers. Less complex systems can be realized with MUMPS, but it offers increased reliability and lower cost. This is the technique which was made available at

McGill University, for this and other work, through the assistance of CMC (Canadian Microelectronics Corporation) [3.2].

One of the main advantages of surface micromachining technique is that it is compatible to today's IC circuit design and manufacturing. However, due to the two dimensional nature of the process, most devices will remain flat on the wafer, unless they are pushed to the desired angle. This tends to limit the degree of vertical motion that can be achieved. The use of scratch drives can be a solution to this limitation [3.5],[3.8]: as shown in Figure 3-7, this device can move parallel to the surface of the wafer, and therefore can move other parts of the MEMS device. When a pulse voltage is applied to the Scratch Drive Array (SDA) the actuator plate moves toward the fixed hinge, causing the micro-hinge between the support plate and MEMS surface to elevate from the substrate. When the support plates moves to its furthest point, the MEMS surface makes a 90° angle with substrate.
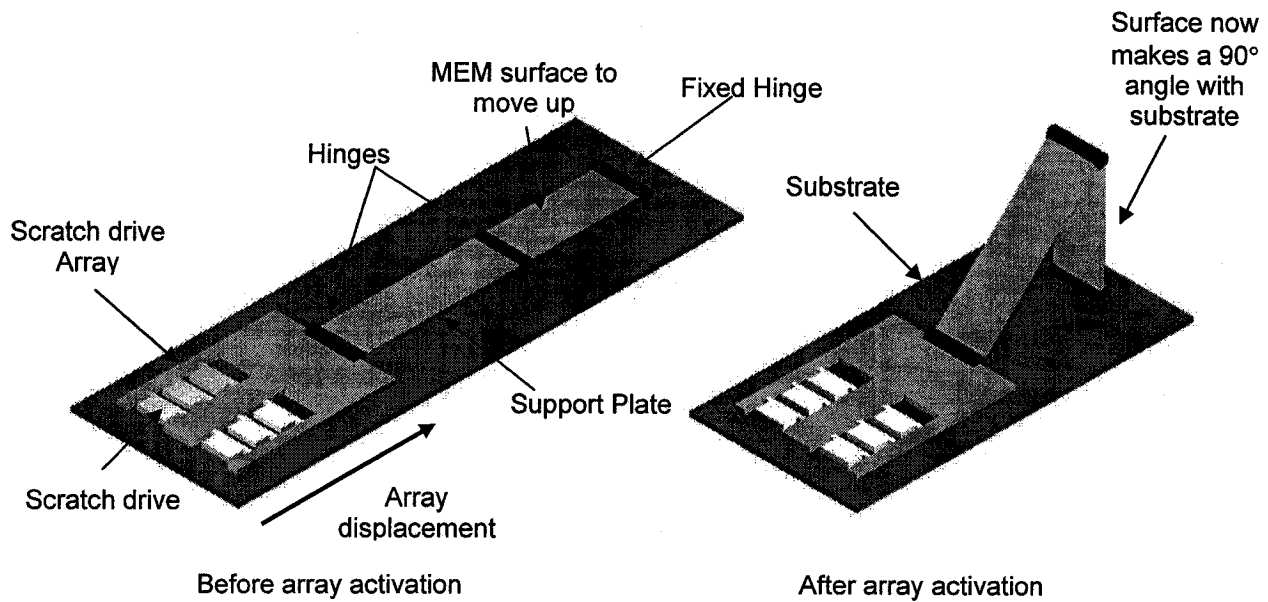
Figure 3-7: Schematic of an automated mounting system using a scratch drive array to mount a MEMS surface.[3.5]

The optical switch, shown in Figure 3-8, uses this concept [3.7]: an electrode can be mounted vertically by the SDA. This electrode makes a 45° angle with a torsion mirror which in turn makes a 45° angle to the input fiber. The torsion mirror is hinged to the side of electrode surface. As shown in Figure 3-8, when no voltage is applied, the vertical mirror redirects the incident light to the first output (reflection mode). When the electrode is activated, it makes the mirror tilt; allowing light travels directly to a second output (transmission mode). The mirror is 200 μm wide, 160 μm tall and 1.5 μm thick. The surface of the mirror is coated with 0.1 μm-thick gold to improve the reflectivity. These switches usually have a slow response time.

Figure 3-8: SEM of a vertical torsion mirror and the scratch drive arrays used to mount the back electrode. The mirror itself is kept in place using latches [3.7]
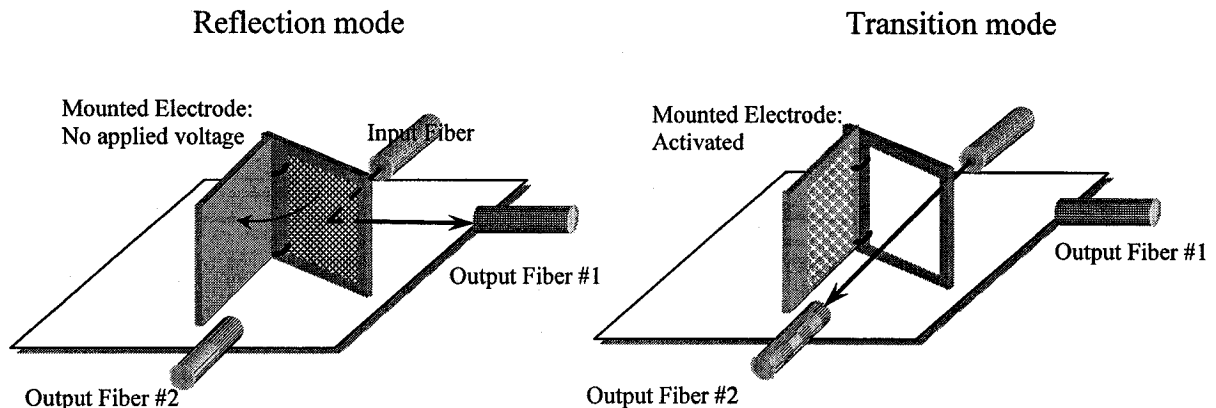
Figure 3-9: Optical switching by using of torsion mirror

Another method, similar to the previous, has also been used for optical switching, and shown in Figure 3-10:
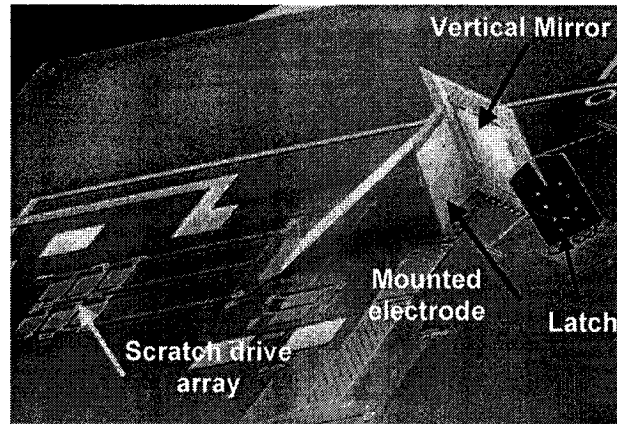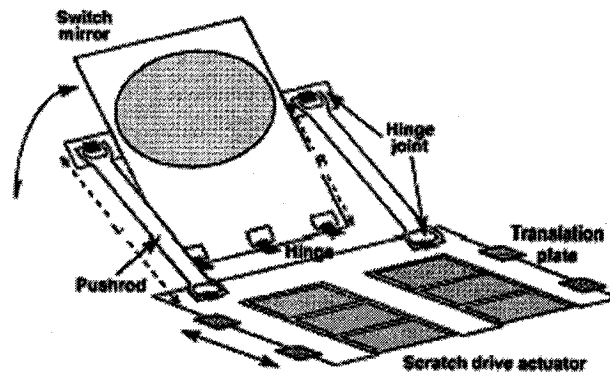

Figure 3-10: Schematic of the micro-machined free- rotating switch mirror.[3.8]

Micro-fabricated hinges hold the mirror plate to the substrate. The mirror is connected to the translation plate by the mean of pushrods. The translation plate is actuated forward by SDAs, such that the mirror is raised (or popped-up) about the hinges.

A detailed discussion over properties of Polysilicon such as roughness and reflectivity can be found in [3.7].

3.3.1.2 Design Specification

This section discusses the design characteristics of the MEMS mirrors designed by Mr. Xuyen Hoa of McGill University Photonics group. The principle of operation is as follows: Two micro-motors, each able to rotate in clock-wise and counter clock-wise directions, are located next to each other, as shown in Figure 3-11. Each motor has a jagged section which allows it to grip on to a pull-bar. The mirror is anchored by hinges, which allow it to be pulled up as the motors are turned in the indicated directions.

The pull-bar is connected to the mirror slightly off- axis in order to create torque, as shown in Figure 3-12.

The micro-motors are actuated by successively applying voltage around the stator. Typically voltage is around 100V, with switch-time in the micro-seconds. Once the micro-motors are actuated [3.5], they begin rotating. The teeth of the micro-motor and of the pull bar become engaged, which moves the pull-bar laterally and causes the mirror surface to pop-up perpendicular to the surface of the substrate [3.5].

In order to have a high reflectivity, a gold coating can be used for mirrors, as has been discussed in [3.7]. The characteristics and dimensions of the mirror and micro-motors are shown in Table 3-2.

This is a compact system with the digital controllability. The motors were designed to rotate in precise steps. The pop-up angle is determined by the amount of motor rotation, which in turn is determined by the applied voltage. Thus, the mirror can have a 45° degree angle with the substrate by applying required voltage.

Figure 3-11:.Top view of the design of micro-mirror
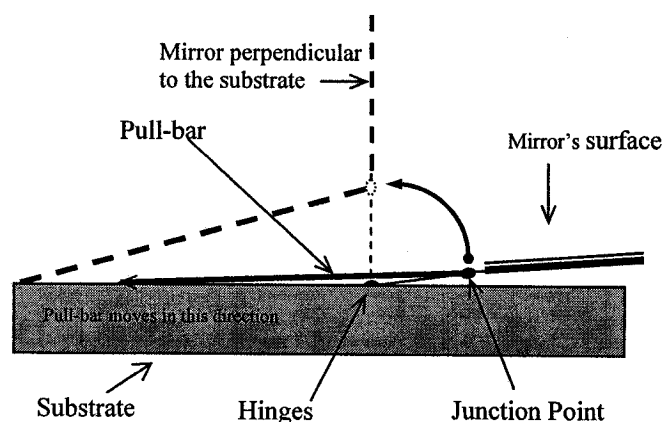
Figure 3-12: Side view of the design

Therefore, we have two options; either implements the mirror in a way that makes a 45° angle with the input fiber and it pops-up to 90° or it stops at 45°angle relative to the substrate and is located parallel to the fiber.

Table 3-2: The important parameters of MEMS mirrors

Parameter	Value
Effective Reflective Area (Mirror)	250 µm x 250 µm
Surface Reflectivity	0.5-0.7 dB
Curvature/F:#	Typically R = 20 mm and F:# = 40-50
Micro-mirror Diameter	600 µm
Operating Voltage	70-100 V
Overall Dimension (Mirror & Motor)	1.4 mm x 1.2 mm
Device Separation (Mirror center to mirror center)	45° configuration: 0.7 mm 90° configuration: 0.9 mm and 1.3 mm

The layout of the chip has been drawn in Figure 3-13:
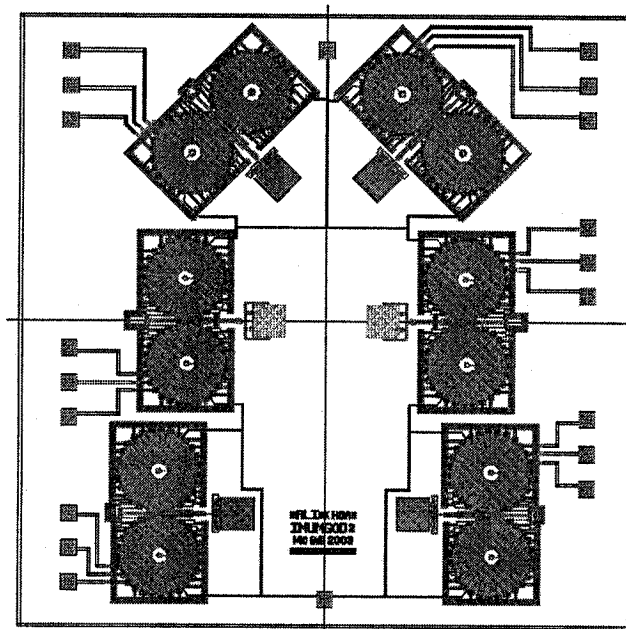
Figure 3-13: Layout of the micro-mirror chip (Courtesy of Mr. Xuyen Hoa)

3.3.2 Design of the Collimating System

As discussed previously, collimation system is an essential part for a practical free-space interconnected fiber-optic module. The loss in coupling efficiency between the input and output fiber due to beam spreading (diffraction) would otherwise be significant. While several alternative solutions to this problem have been studied [3.13], Gradient Index (GRIN) lenses have been established as the standard collimation lens. Micro aspheric lenses are often used lens type as well. We begin this section with a brief background of collimation lenses and will seek design which minimizes system dimensions and path dependent loss.

3.3.2.1 Collimating System Theory

According to Gaussian beam propagation, the basic equations for calculating the location of beam waist as the beam travels through a thin lens with focal length of f_L is as follows: [3.1]

$$z - f_L = \frac{z'-f_L}{(z'-f_L)^2 + z_{SMF}^2}$$

Equation 3-10

where z_{SMF} is the Raleigh range for single mode fiber Gaussian beam and z' is the distance from the input fiber to the lens.

$$z_{SMF} = \frac{\pi \omega_{SMF}^2}{\lambda}$$

Equation 3-11

The beam is collimated by making the location of the new waist, z, as distant as possible from the lens. The maximum of z occurs when:

$$z' = z_{SMF} + f_L$$

Equation 3-12

and the value of this maximum would be:

$$z = f_L + \frac{f_L^2}{2z_{SMF}}$$

Equation 3-13

L_{min} is defined as twice as this maximum z:
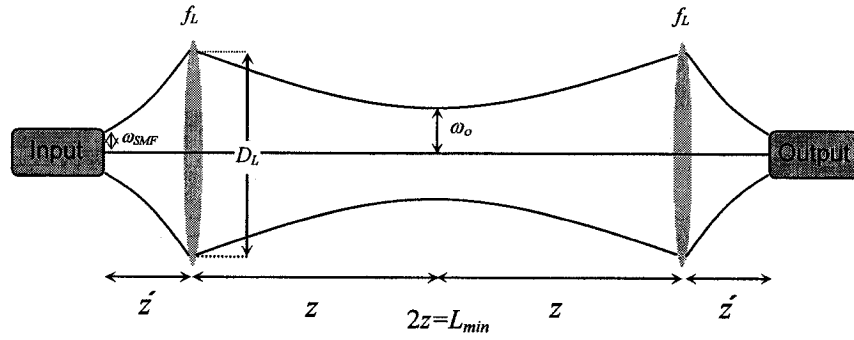
Figure 3-14: Collimation lenses

Given the input fiber and incident light parameters, namely the wavelength, λ, and the beam waist of the incident beam, ω_{SMF}, and the lens separation distance L_{min} the value of f_L can be determined from:

$$f_L^2 + 2z_{SMF}f_L - z_{SMF}L_{min} = 0$$

Equation 3-14

Solving for f_L,

$$f_L = -z_{SMF} + \sqrt{z_{SMF}^2 + z_{SMF}L_{min}}$$

Equation 3-15

Combining Equation 3-12 and Equation 3-15:

$$z' = \sqrt{z_{SMF}^2 + z_{SMF}L_{min}}$$

Equation 3-16

using the obtained values, the beam waist of the propagating beam can be achieved as follows:

$$\omega_0 = \frac{f_L}{\sqrt{(z'-f_L)^2 + z_{SMF}^2}} \omega_{SMF}$$

<div align="right">*Equation 3-17*</div>

Combining Equation 3-14 - Equation 3-17 gives the simplified form:

$$\omega_0 = \frac{f_L}{\sqrt{2}z_{SMF}} \omega_{SMF}$$

<div align="right">*Equation 3-18*</div>

The beam radius on the lens can be obtained from:

$$\omega_L = \sqrt{2\omega_{SMF}^2 + \frac{\lambda L_{min}}{\pi}}$$

The lens with diameter D_L defined by:

$$D_L = 2(1.5\omega_L)$$

<div align="right">*Equation 3-19*</div>

contains 99% of energy of the beam.[3.1]

For the given values of ω_{SMF} and λ, the values of D_L, ω_0 and f_L are plotted as a function

of L_{min} in Figure 3-15, Figure 3-16 and Figure 3-17 respectively:
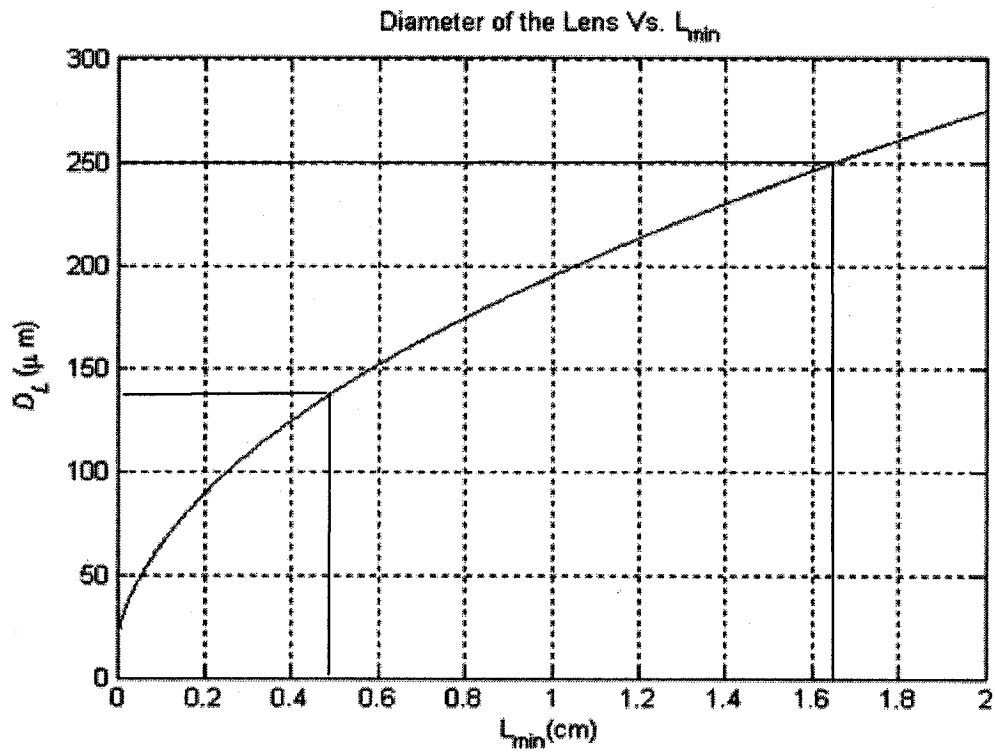
Figure 3-15: Diameter of collimating lens as the distance between two lenses changes.
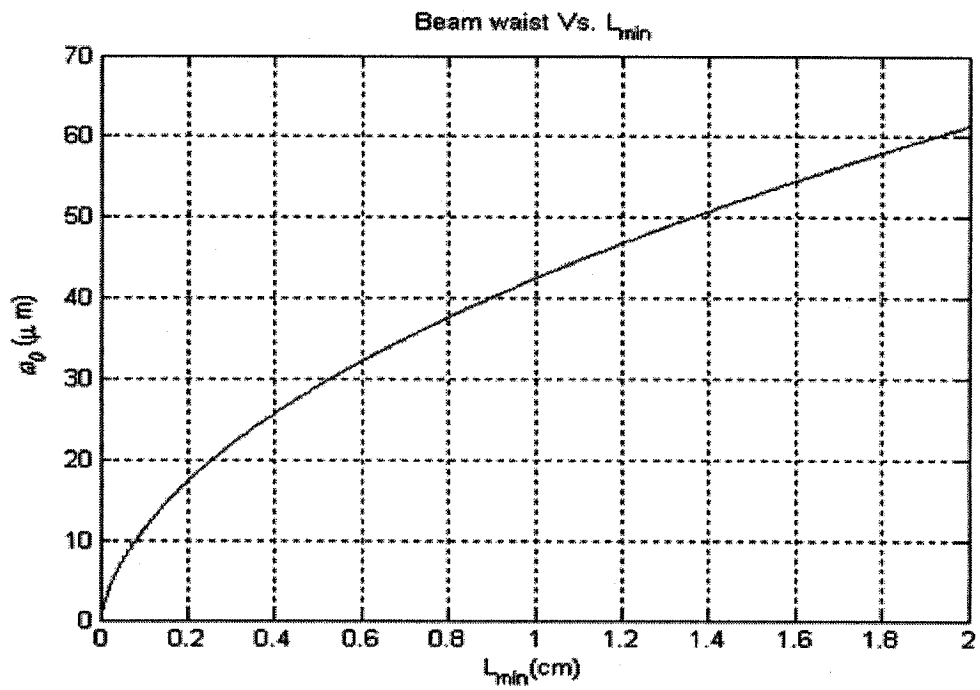
Figure 3-16: Beam-waist size of the beam transmitted through collimating lens.
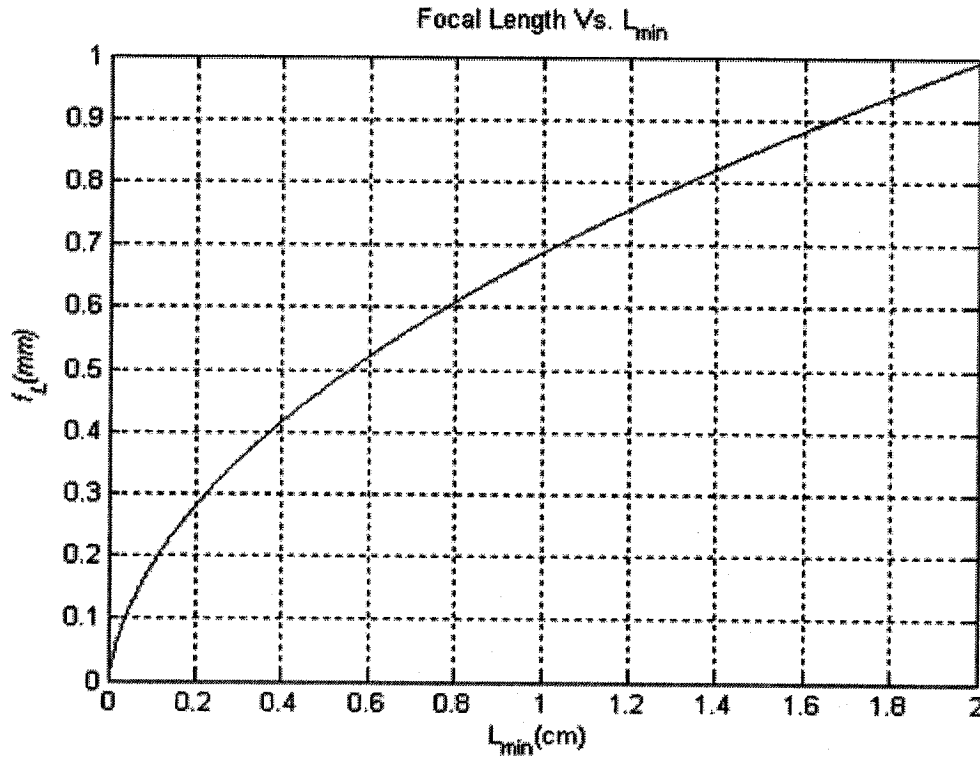
Figure 3-17: Focal length of the lens as a function of L_{min}

3.3.2.2 Design Specification of Collimating Lens

In this section, optimal specification of the focal length and the lens diameter for the collimating lenses are obtained. The first constraint in this process is the size of micro-mirrors which has been established as 250×250 μm^2, in section 3.3.1. In particular, in order to eliminate loss of energy due to aperture of the lens, the beam size should not exceed the mirror and collimating lens dimensions. This imposes the following constraint:

$$D_L \leq 250 \ \mu m$$

Second, the total distance between the two main path collimating lenses must be large enough to fit the twelve micro-mirrors as required by the system. The minimum distance is therefore:

$$min \ (L_{min}) = \ 12(250 \ \sqrt{2} \ )= 4.24 \ mm$$

From Figure 3-15 , which relates L_{min} to D_L, range of acceptable values for these two parameters is obtained based on the above two constraints. L_{min} could vary from 0.424 cm to 1.654 cm, corresponding to values for D_L of 140 μm to 250 μm.

Ideally, the minimum value of L_{min} would be selected since this would result in a smaller device foot print and an even higher percentage of the beam would meet with the mirrors. However, since the results that will be obtained here are to be compared with experiments (to be done in the future), the higher separation distance of 1.4 cm is used to allow for more design flexibility.

From this chosen value for L_{min} ,the parameters D_L, ω_0 and f_L can be obtained from Equation 3-15 and Equation 3-18, respectively:

$$D_L = 229.3 \text{ μm}, \quad \omega_0 = 50.55 \text{ μm}, f_L = 0.8241 \text{ mm}$$

Assuming a minimum lens thickness t=0.5 mm, the above must be adjusted, as shown in Table 3-3:

Table 3-3: Design parameters for collimation system

Parameter	Symbol	Value	Dimension
Minimum Distance (Lens to lens)	L_{min}	1.4	cm
Focal Length of the Lens	f_L	0.832	mm
Beam-waist size	ω_0	51.43	μm
Raleigh range	z_0	6.34	mm
Diameter of the Lens	D_L	229.83	μm
Thickness of the Lens	t	0.5	mm
Distance from the Fiber to the Vertex	z'	0.7	mm
Distance from the Lens to the beam waist	z	7	mm

Figure 3-18, which obtained using MATLAB simulations, shows the evolution of the beam size and radius of curvature as it propagates from input to output power. The location of each mirror is also indicated in this figure.
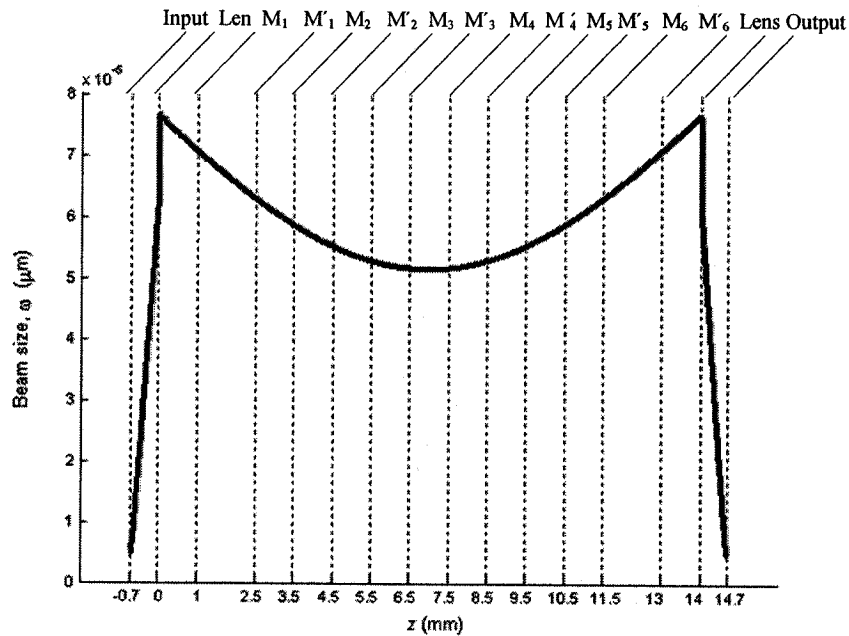

Figure 3-18(a): The propagation of the beam between the two fibers. Locations of the mirrors are shown.
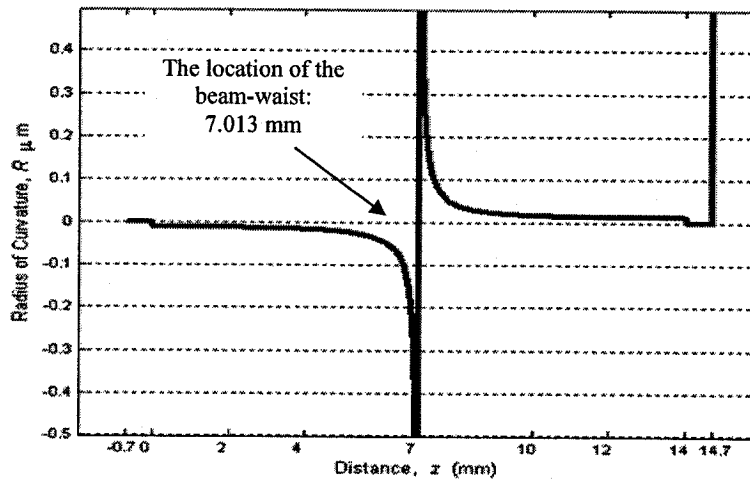

Figure 3-18(b): Location of the beam waist, when no delay is applied.

Table 3-4 gives the beam size at each mirror surface. Due to symmetry, only the values for the first six mirrors are shown:

Table 3-4: Beam-width at the micro-mirror surfaces

Beam-Size	Distance to beam waist(mm)	Value(μm)
ω_{M1}	6	70.79
$\omega_{M'1}$	4.5	63.05
ω_{M2}	3.5	58.74
$\omega_{M'2}$	2.5	55.28
ω_{M3}	1.5	52.84
$\omega_{M'3}$	0.5	51.58

3.3.3 Design of the Delay Block

Given the above-designed collimating system the specifications for the delay block are derived.

3.3.3.1 Theory of Collimated Gaussian beam

As mentioned previously the purpose of the delay segment collimating lenses is to maintain the beam size in the main path unchanged as if the beam did not travel through the delay segment. As the beam hits the mirror M_m in segment m, it is redirected towards the first vertex of delay block. The beam enters the block is reflected twice and exits the block at the second vertex before meeting with mirror M'_m and returning to the main path.

Figure 3-19 shows the unfolded path from mirror M_m to mirror M'_m in the loop number m, Note it gets redirected and keeps on propagating towards the curved surface of the block. Table 3-5 defines each parameter contained in this figure.
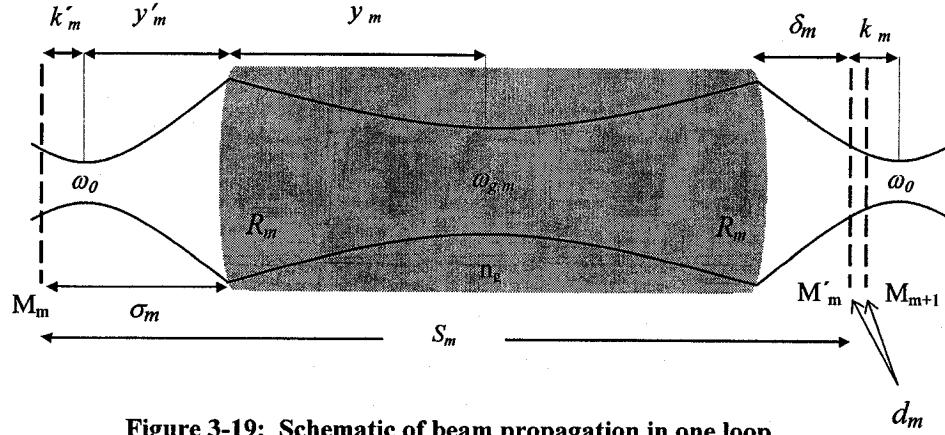
Figure 3-19: Schematic of beam propagation in one loop

Table 3-5: Definition of delay block parameters

Parameters	Definition
R_m	Radius of Curvature
S_m	Length of each delay section
ω_0	Main path beam waist
$\omega_{g,m}$	Beam waist in bulk for each segment
y'_m	Distance from principle beam waist to vertex
y_m	Distance from vertex to $\omega_{g,m}$
σ_m	Distance from first mirror (M_m) to 1st surface
δ_m	Distance from 2nd surface to second mirror (M'_m)
k'_m	Distance from main path beam-waist to M_m
k_m	Distance from main path beam-waist to M'_m
D_m	Diameter of the vertex
n_g	Refractive index of the block
d_m	Separation of the mirrors

Note that the separation of the mirrors, d_m, for the first and last loop is 1.5 mm while the rest is 1 mm.

The aperture diameter of the curved surface is assumed to be three times of the beam size on it (this allows 99% transmittance).

Appendix B relates the parameters R_m, y_m, y'_m and n_g, by applying the matrix method to the thick lens shown in Figure 3-19, yielding Equation 3-20 and Equation 3-21:

$$y_m = \frac{n_g R_m}{n_g - 1} + \frac{n_g R_m^2}{2(n_g - 1)^2 z_0}$$

Equation 3-20

$$y'_m = z_0 + \frac{R_m}{n_g - 1}$$

Equation 3-21

where z_0 is the Raleigh range of main path beam. The magnification in each segment, Mag_m can be obtained from:

$$Mag_m = \frac{\omega_{gm}}{\omega_0} = \sqrt{\frac{z_{gm}}{z_0}} = \frac{R_m}{\sqrt{2}(n_g - 1)z_0}$$

Equation 3-22

The distance that light travels when the mirrors are off is d_m. When they are popped up this distance will increase by S_m, resulting in total delay time τ_m. S_m can be written:

$$S_m = \delta_m + 2n_g y_m + \sigma_m = c\tau_m + d_m$$

Equation 3-23

From Figure 3-19, the distance from M_m to M'_m can be written as:

$$2y'_m + 2n_g y_m + k_m - k'_m = S_m = c\tau_m + d_m$$

Equation 3-24

Since $k_m - k'_m = d_m$; substituting in Equation 3-24 for y_m and y'_m (from Equation 3-20and Equation 3-21, respectively), we obtain:

$$2(z_0 + \frac{R_m}{n_g - 1}) + 2n_g(\frac{n_g R_m}{n_g - 1} + \frac{n_g R_m^2}{2(n_g - 1)^2 z_0}) - c\tau_m = 0$$

or,

$$\frac{n_g^2}{(n_g-1)^2 z_0} R_m^2 + 2\frac{(n_g^2+1)}{n_g-1} R_m + (2z_0 - c\tau_m) = 0$$

<div align="right">*Equation 3-25*</div>

Solving this second order equation for R_m and using Equation 3-20-Equation 3-23 will give all the parameters mentioned in Table 3-5. Note that value of parameter n_g is assumed 1.503.

3.3.3.2 Specification of the Design:

The obtained values are presented in Table 3-6:

<div align="center">**Table 3-6: Designed parameters values for each segment of the block.**</div>

m	τ (ps)	R (mm)	σ (mm)	δ (mm)	z' (mm)	D (mm)	$f/\#$
1	3200	21.741	55.577	45.077	285.88	1.209	5.25
2	1600	14.181	38.047	32.047	136.36	0.850	7.47
3	800	8.891	25.532	23.532	63.519	0.601	10.57
4	400	5.233	16.259	18.259	28.437	0.433	14.67
5	200	2.751	9.3250	1.532	11.760	0.325	19.55
6	100	1.089	4.0215	1.452	3.811	0.257	24.72

Note that $f/\#$ is defined as the focal length of the segment thick lens divided by the lens diameter.

3.4 Review of the Complete Design

This chapter has shown the complete design of a tunable optical delay line, which is able to provide delay times in the range of 100 ps to 6400 ps in increments of 100 ps. It consists of three main components:

1. The MEMS micro-mirrors: the mirrors have the ability to pop-up perpendicularly to the surface of their substrate by the assistant of micro-motors which provide the required torque in order to rotate the mirror. The dimension of each mirror is 250x250 μm^2. The reflectivity of the mirrors is between 0.5 and 0.7 dB. This can be improved further by the use of a gold coating.

2. The main path collimation lenses: these lenses are located following the input and prior the output of the system. Typically, aspheric lenses can be used, but this is not limiting kind of collimation lenses could be used. The focal length is 0.832 mm and the beam-waist is 51.43μm which occurs in 7 mm after the lens.

3. The delay segment: provides the required delay lines. It includes six different segments whose optical lengths increases successively by power of two. In order to maintain the light collimated within each segment, while simplifying implementation, a single piece of material such as glass or plastic was considered. The required collimating lenses could be molded onto this block. The focal length of these lenses and their distances to their corresponding mirrors are determined such that the main path remains the same whether the mirrors are on or off.

REFRENCES:

[3.1] Saleh, " Fundamental of Photonics," New York :Wiley,1991.page 96, 97 Beam Collimation.

[3.2] The Canadian Microelectronics Corporation Web site: **http://www.cmc.ca.**

[3.3] "SUMMiT V Technology ," Sandia National Laboratories, see **http://www.sandia.gov/mems/micromachine/summit5.html.**

[3.4] David A. Koester Ramaswamy Mahadevan Alex Shishkoff and Karen W. Markus, "MUMPs Design Handbook," Revision 4.0, Cronos Integrated Microsystems, 1999

[3.5] Marc Simard, "MEMS micromotors and their application as an optical," Master of Engineering Thesis, McGill University, July 2002.

[3.6] Julliana E. Lin, "Design and Characterization of MEMS micromirror devices," Master of Engineering Thesis, McGill University, 2001.

[3.7] Shi-sheng Lee, Long-sun Huang, Chang-Jin Kim, Ming C. Wu, "Free-space Fiber-optic switches based on MEMS Vertical Torsion Mirrors," Journal of Light-wave Technology Vol. 17 No.1, 1999.

[3.8] Lin L. Y., Goldstein E. L. , Tkack R. W. ,"Free Space Micromachined Optical Switches for Optical Networking," IEEE journal of selected topics in Quantum Electronics,VOL 5, No.1, 1999.

[3.9] J. Zou,Balberg M., Colin Byrne, C. Liu, David J. Brady, "Optical properties of surface micromachined mirrors with Etch Holes," Journal of microelectromechanical systems, Vol. 8, No.4,1999.

[3.10] Gerrard A. "Introduction to Matrix Methods in Optics," 1975, p.77.

[3.11] Wencai Jing, Yimo Zhang, Ge Zhou, "Design of MOEMS adjustable delay line to reduce link set-up time in a tera-bit/s optical interconnection network," Optics Express Vol. 10 No. 14 p.591 July 2002.

[3.12] A. D. Kirk, "Fiber optic switches with digital mirror arrays", 1997 June.

[3.13] Keyun Xue, Quan J. Zhang and Yuanxiang Wang ,"A novel low-cost high performance micro pseudo-spherical lens optimized for fiber collimators," Proceedings of SPIE – Vol. 4906, p. 249-252, August 2002

4 Performance

In this chapter, simulations were performed for the optical delay line module presented in the previous chapter. The results of these simulations are discussed in this chapter and system limitations are identified. In section 4.1, the theory of coupling efficiency and misalignment issues of Gaussian beams are treated. Section 4.2 presents the performance of the module when all the components are ideally aligned. Throughput of the system will be graphed in different of occasions. Finally, in section 4.3, misalignment, which is the most important limitation of free space systems, is discussed.

4.1 Gaussian Beam Coupling Efficiency

The efficiency of optical-power throughput from one optical element to another optical element is usually reduced due to the limitation of alignment accuracy. This limitation is important to consider for evaluating the feasibility of a free space systems. In this section the theory of Gaussian beam coupling efficiency and the formula to calculate it for aligned and misaligned components are reviewed.

To calculate coupling efficiency, one needs to properly understand Gaussian beam propagation characteristics. Once the beam's characteristics are found, insertion loss can be calculated using well-known equations. Other potential sources of power loss, which are not considered in these simulations, are finite aperture size and aberration effects. Aperture size is neglected since the beam's transverse width is small relative to the physical aperture of the elements in this system. Aberration effects have a negligible effect on power loss.

At a specific point in space a Gaussian beam is characterized by its direction, waist size and wave curvature. Since the direction of the beam does not change without outside influence, only the waist size, ω, and radius of curvature, R, are considered. These two parameters can combined into the complex radius of curvature, q, which is calculated using Equation 4.1:

$$\frac{1}{q} = \frac{1}{R} - j\frac{\lambda}{\pi\omega^2}$$

Equation 4.1

where λ is the wavelength of the beam in the medium.

R is given by Equation 4.2 while ω is given by Equation 4.3:

$$R = \frac{1}{\mathrm{Re}(q^{-1})}$$

Equation 4.2

$$\omega = \sqrt{\frac{\lambda}{\pi \, \mathrm{Im}(q^{-1})}}$$

Equation 4.3

The relation of complex radii of curvature of the output compared to the input of an

optical system can be found by the use of matrix method (see Appendix B). Suppose

$q_i(\omega_i, R_i)$ is the complex parameter at the input fiber and $q_f(\omega_f, R_f)$ is complex parameter

at the output fiber, then:[4.1]

$$q_f = \frac{Aq_i + B}{Cq_i + D}$$

Equation 4.4

where A, B, C, D are elements of the system's matrix.

If all the components are perfectly aligned, the coupling efficiency, from free-space to

fiber, is dependant on how well the output beam parameter, q_f matches with the input

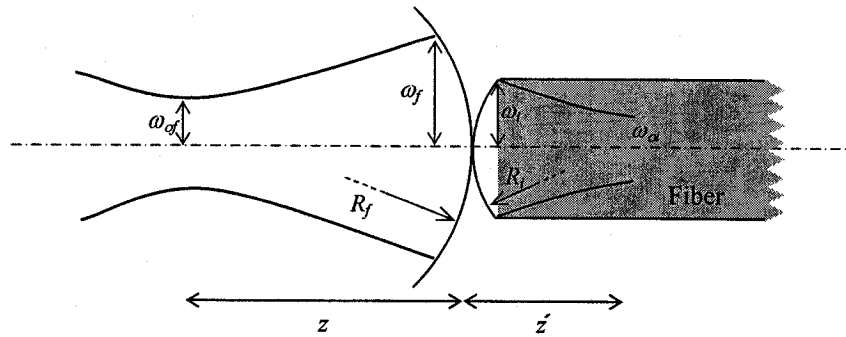beam complex parameter of fiber, q_i, as shown in Figure 4-1.

Figure 4-1: The complex parameters of beam and fiber are mismatched.

The transmission coefficient can be calculated from Equation 4.5: [4.2]

$$t_q = \frac{2}{[(\frac{\omega_f}{\omega_i} + \frac{\omega_i}{\omega_f})^2 + (\frac{k\omega_i\omega_f}{2})^2(\frac{1}{R_f} - \frac{1}{R_i})^2]^{1/2}}$$

Equation 4.5

where $k = \frac{2\pi}{\lambda}$.

t_q is the transmission coefficient due to mismatch in a specific direction, e.g. in the y direction. For the other axis, e.g. in the x direction, the transmission coefficient will be t'_q. Consequently, the complete transmission coefficient is the product of t_q and t'_q .For an aligned system, power coupling efficiency, η_q is:

$$\eta_q = t_q \cdot t'_q$$

Equation 4.6

or, given in decibels:

$$-10\log\eta_q = -10\log t_q - 10\log t'_q$$

Equation 4.7

For the circular beam $t_q=t'_q$, η_q is defined as :

$$\eta_q \text{ (dB)} = -20\log t_q$$

Equation 4.8

This insertion loss is due to the mismatch in the q parameters. An additional source of insertion loss of the Gaussian beam is due to the presence of an undesirable tilt angle,$\Delta\alpha$, and offset ,Δy, between two modes. This is shown in Figure 4-2:
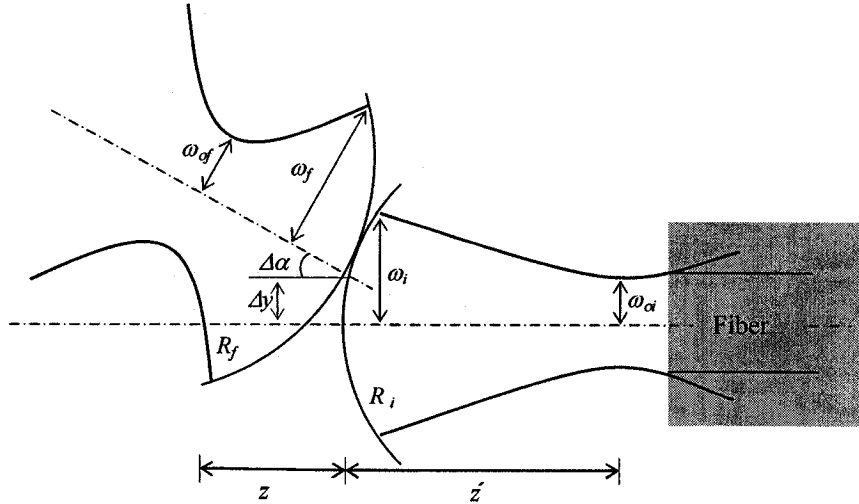

Figure 4-2: Beam offset and tilt angle.

The transmission coefficient due to the beam offset, t_y, and transmission coefficient due to tilt, t_θ, can be calculated using the following equations: [4.3]

$$t_\theta = \sqrt{\exp\left[-(\frac{\Delta\alpha}{\alpha_e})^2\right]}$$

$$t_y = \sqrt{\exp\left[-(\frac{\Delta y}{y_e})^2\right]}$$

$$\alpha_e = \frac{2^{\frac{1}{2}}}{kt_q\sqrt{\omega_o^2 + \omega_i^2}}$$

$$y_e = \frac{2^{\frac{1}{2}}}{t_q[\frac{1}{\omega_o^2} + \frac{1}{\omega_i^2} + (\frac{1}{2}k\omega_o R_o)^2 + (\frac{1}{2}k\omega_i R_i)^2]^{\frac{1}{2}}}$$

Including both complex parameter mismatch and optical component offset/tilt, the transmission coefficient for small displacement along one axis becomes:

$$t_{total} = t_q t_\theta t_y$$

For the circular beam the insertion loss is:

$$\eta_{total} = -20\log(t_{total}) \qquad (\text{dB})$$

Using the above mentioned formula, it is trivial to calculate the insertion loss of the overall system. The required parameters are: q_i, q_o, Δy, and $\Delta\alpha$.

One approach in obtaining these parameters is to use the ray-transfer matrix method. Appendix B showed how to obtain the characteristics of the output beam using the matrix method for 2x2 matrix, however this method is insufficient since it is only valid for optical systems having perfectly aligned components (having no beam offset and tilt). In the 2x2 ray transfer method, the ray parameter vector at the output $\vec{r}_o(y_o, \alpha_o)$, is related

to the input ray parameter vector $\vec{r}_i(y_i, \alpha_i)$, by the system matrix S=$\begin{bmatrix} A & B \\ C & D \end{bmatrix}$:

$$\begin{bmatrix} y_o \\ \alpha_o \end{bmatrix} = \begin{bmatrix} A & B \\ C & D \end{bmatrix}\begin{bmatrix} y_i \\ \alpha_i \end{bmatrix}$$

In order to extend this method to accommodate tilt and offset, we rewrite Equation 4.15

as Equation 4.16.

$$\begin{bmatrix} y_o \\ \alpha_o \end{bmatrix} = \begin{bmatrix} A & B \\ C & D \end{bmatrix} \begin{bmatrix} y_i \\ \alpha_i \end{bmatrix} + \begin{bmatrix} \Delta y \\ \Delta \alpha \end{bmatrix}$$

Equation 4.16

This equation is not in linear form. Since the linear form is more conducive to

computation, the expression in Equation 4.16 is extended to 3x3 matrix form Equation

4.17:

$$\begin{bmatrix} y_o \\ \alpha_o \\ 1 \end{bmatrix} = \begin{bmatrix} A & B & \Delta y \\ C & D & \Delta \alpha \\ 0 & 0 & 1 \end{bmatrix} \begin{bmatrix} y_i \\ \alpha_i \\ 1 \end{bmatrix}$$

Equation 4.17

Note that by setting $\Delta y=0$ and $\Delta \alpha =0$, this new expression reduces to Equation

4.15,since A,B,C and D remain the same.

For example, for a mirror having a nominal angle of 45° to the optical axis, and an

misalignment tilt of $\Delta \theta$ the matrix would be written as:[4.11]

$$T_{mirror} = \begin{bmatrix} 1 & 0 & 0 \\ 0 & 1 & -2\Delta\theta \\ 0 & 0 & 1 \end{bmatrix}$$

In a system containing p elements, p 3x3 matrices denoted, T_1, T_2,..., T_p, could be

required in order to account for offset and tilt in all of these elements. The total matrix for

the system, T_{total}, would then be:

$$T_{total} = T_p...T_2 T_1$$

Equation 4.18

T_{total} contains all the necessary information to calculate the coupling efficiency. q_f can be

calculated, based on Equation 4.4, using known value of q_i and overall A,B,C and D

values which are the elements of $T_{total\ 1x1}$, $T_{total\ 1x2}$,$T_{total\ 2x1}$ and $T_{total\ 2x2}$,respectively.

Elements of $T_{total\ 1x3}$ and $T_{total\ 2x3}$ are exactly representing Δy and $\Delta \alpha$, respectively. Using

q_f, Δy and $\Delta \alpha$, the coupling efficiency from input fiber to output fiber can be obtaining based on Equation 4.5 through Equation 4.14.

Note that this method also accounts for misalignment in the direction of the optical axis, which is referred as displacement. A displacement would be modeled by a simple translation matrix $T_{displacement}$:

$$T_{displacement} = \begin{bmatrix} 1 & \Delta z & 0 \\ 0 & 1 & 0 \\ 0 & 0 & 1 \end{bmatrix}$$

Equation 4.19

or for introducing the curve of the micro-mirror, the concave or convex mirror matrix can be used:

$$T_{Com} = \begin{bmatrix} 1 & 0 & 0 \\ -\dfrac{2}{R_{mirror}} & 1 & 0 \\ 0 & 0 & 1 \end{bmatrix}$$

Equation 4.20

where for concave mirror $R_{mirror} > 0$ and for convex mirror $R_{mirror} < 0$.

Knowing the above mentioned equations, gives the ability to run the simulations for our module using MATLAB software. This will be represented in the next sections. Reference [4.4] and [4.5] are recommended for further information relative on the matrix method.

4.2 Ideally Aligned Module

In this section we evaluate the performance of the system with all the components perfectly aligned. The simulations are performed by unfolding the configuration shown in Figure 3.6 and by using the parameters found in Table 3.5. Note that for all the simulations in this and following section wavelength of light is assumed 1.31 µm .The beam propagation is modeled in Figure 4-3a, and Figure 4-3b shows how the principle

beam-size remains unchanged at the end of each loop (assuming that all mirrors are on). Each delay segment consists of three optical parts: the portion from the first mirror to the vertex of collimating lens, portion traveled in the bulk, which can be considered as a thick lens, and finally the portion from vertex of the collimating lens to the second mirror of the delay segment. The beam propagation in the first and third portions (the propagation in air) is shown in Figure 4-3a. The beam size remains unchanged following its trajectory in the delay segment. Figure 4-3b shows the radius of curvature for these two portions. Note that the distance variable does not account for propagation in the second portion of the optical path(inside the bulk), which is assumed as a thick lens.

Figure 4-4 demonstrates the way beam size within the second portion of a delay segment. One can see the change of beam-size at the beginning and end of each loop is as if there is no delay path. Overall, the principle beam remains unchanged whether the delay segment is on or off. As was mentioned above, this feature provides a roughly zero insertion loss for all range of time delays.

(a)

(b)
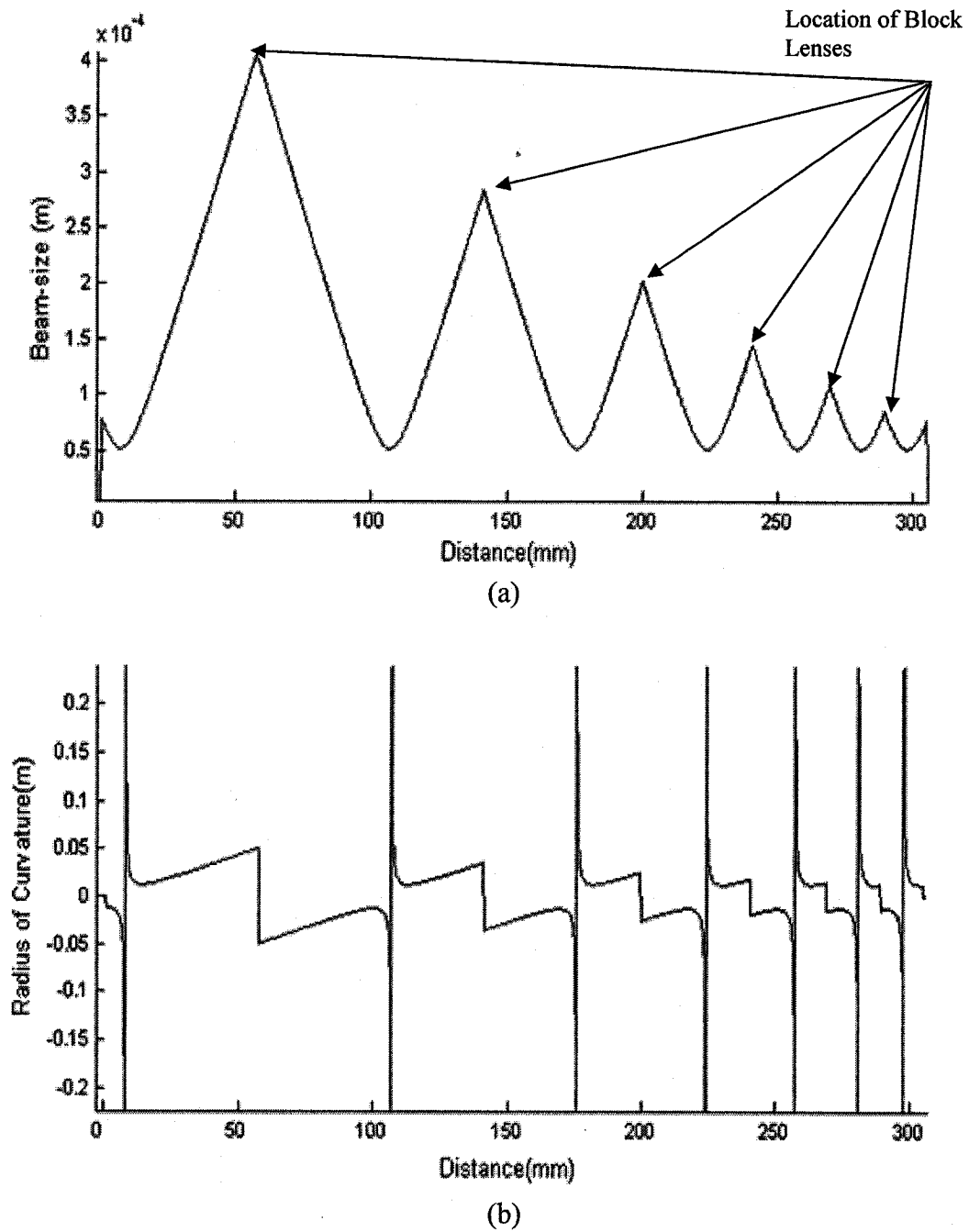
Figure 4-3: (a) Propagation of the beam for maximum delay time. System is assumed unbent. (b) The locations of beam waist can be determined by the variation of beam's radius of curvature.
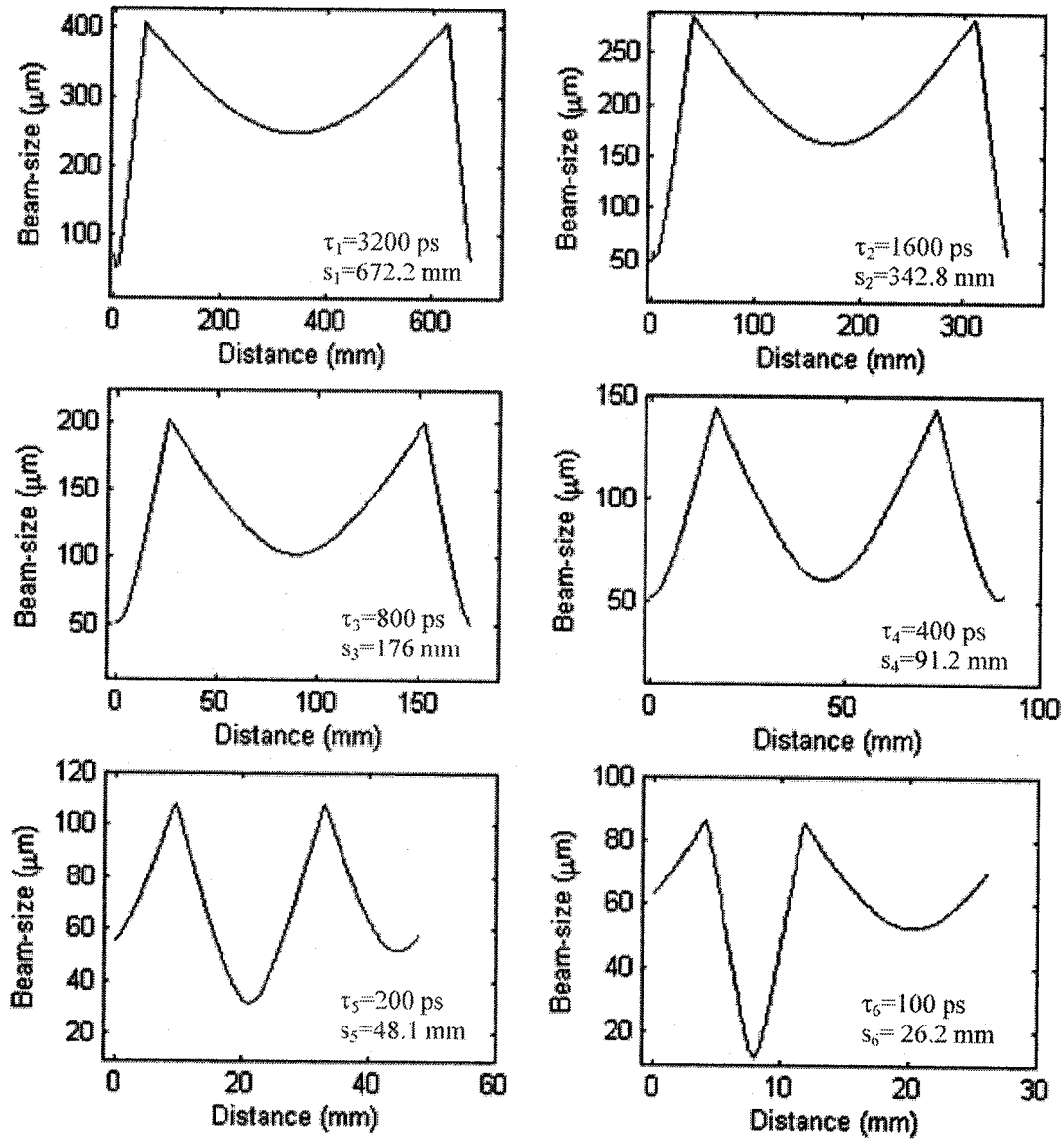
Figure 4-4: The propagation of the collimated beam for each delay segment.

The tolerance tem will be evaluated also for variation of different input parameters. Ideal alignment is still assumed.

Equation 3.26 shows that the value of R depends on the wavelength and the refractive index of the bulk lenses. Therefore, the insertion loss will be affected by variation of these two parameters. Furthermore, the susceptibility of the system to the inaccuracy of

the implementation of parameters such as the focal length of the fiber collimation lens and the curvature of the loop lenses will be investigated.

■ *Coupling Coefficient dependency on Wavelength:*

The parameters have been calculated at a wavelength value of 1.31 μm, variation in the beam's wavelength will change its Gaussian characteristics, resulting in displacement of the beam waist location as well as variation in the beam waist size. This will certainly affect the system insertion loss. Coupling efficiency for different delay times is shown in Figure 4-5 for varying signal wavelength.
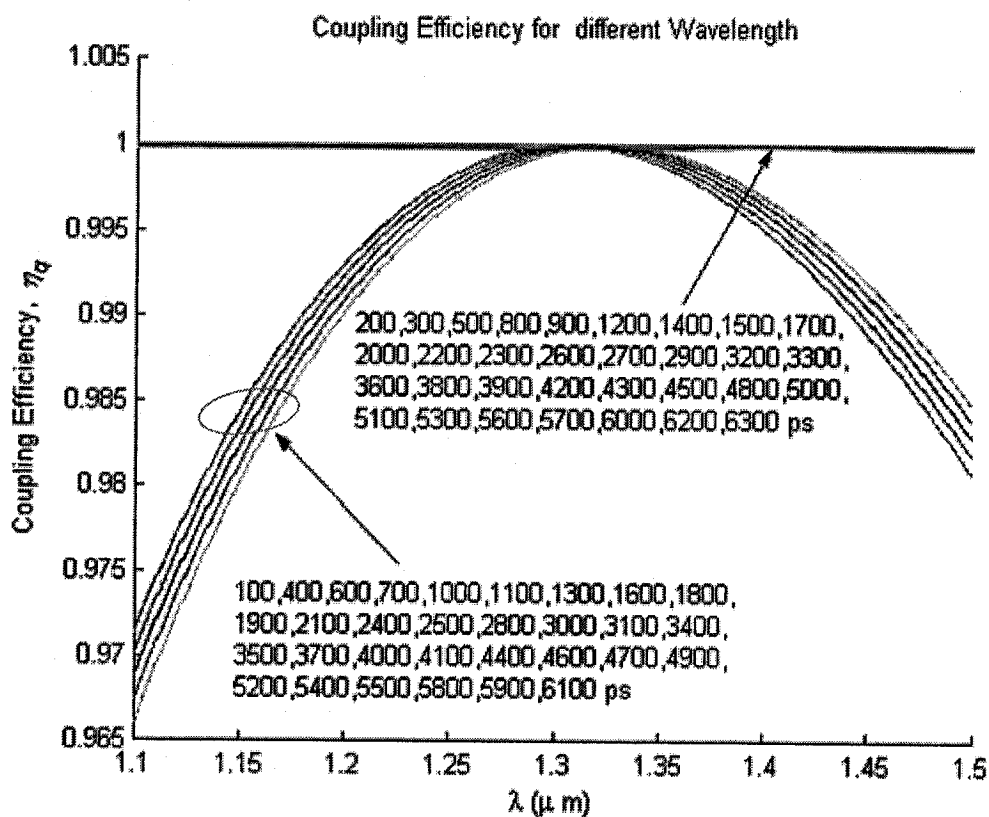
Figure 4-5: Tolerance of coupling efficiency to wavelength for different delays

This figure shows that for different delays, variation of the wavelength of ±200 nm does not increase the insertion loss by more than 0.15 dB.

■ *Insertion loss dependency on the focal length of main path collimation lens:*

The focal length of the fiber collimator determines the location and size of the principle beam-waist. If the focal length varies, both location and size of the principle beam-waist will change and the insertion loss will increase. Note that the design value for the focal length of this lens is 0.832 mm.
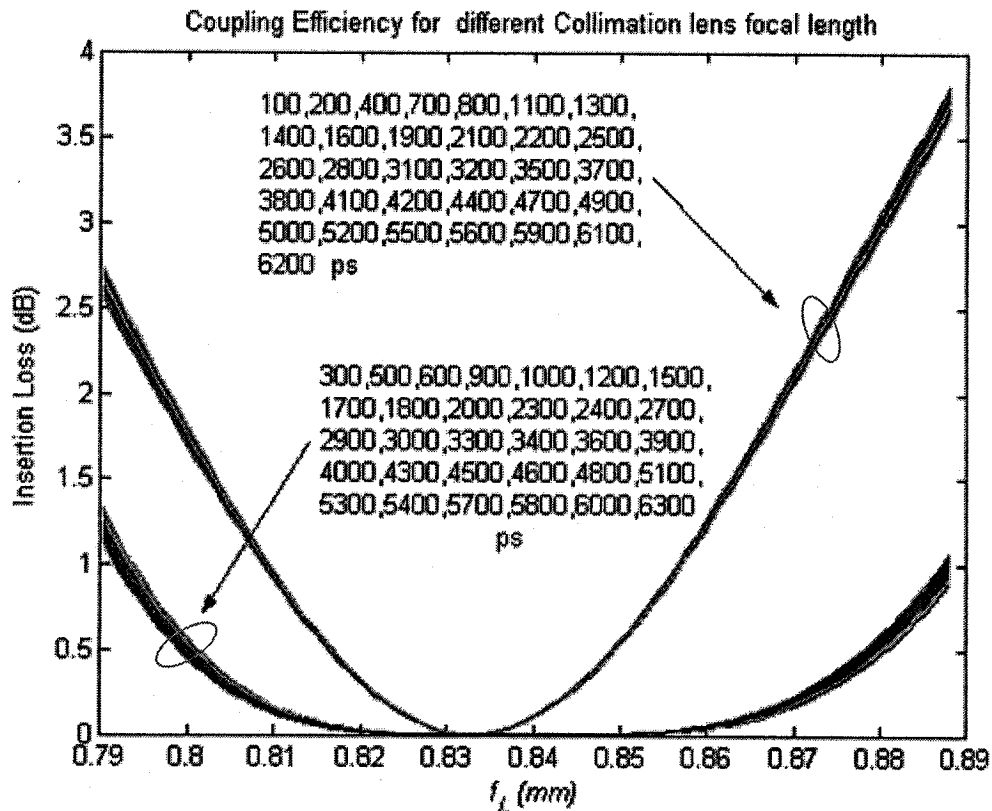

Figure 4-6: Insertion loss of the system vs. focal length of fiber collimation lens for different delays

As can be seen from Figure 4-6 the variations for different delays are mainly divided into two groups of curves. The insertion loss for one group increases more rapidly than for the other group, i.e., it has lower tolerance. This group corresponds to delay times in which an odd number of delay segments are employed. For the system to maintain the insertion loss less than 1 dB, the maximum error in the focal length is 25 μm, which is possible to achieve, since the typical error of implementation is 1%.

■ *Insertion loss dependency on curvature of micro-mirrors:* It was previously assumed that the reflective area of each micro-mirror is flat. The presence of a surface sag or curvature has an effect on collimated beam; hence, this increases the insertion loss of the system. The curvature of the mirror is defined as the inverse of radius of its curvature. In Figure 4-7 the insertion loss for different delay times has been demonstrated for different of mirror curvatures.
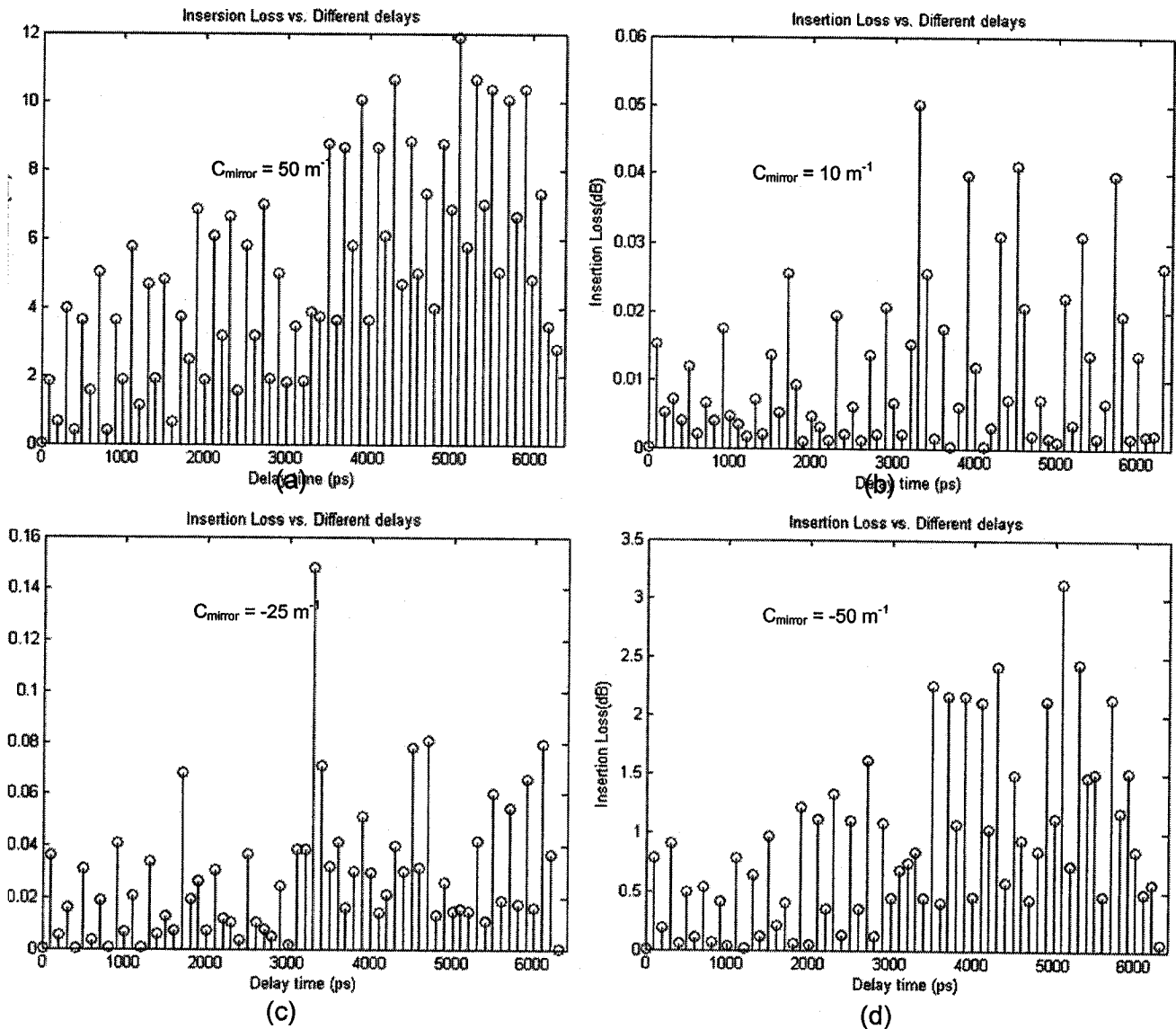
Figure 4-7: Insertion loss vs. delay times for various curvature of micro-mirror: (a) 50 m^{-1} (b) 10 m^{-1} (c) -25 m^{-1}, (d) -50

Figure 4-8 shows the maxima, minima, and mean insertion loss values for all the delay times, for each curvature of micro-mirrors value.
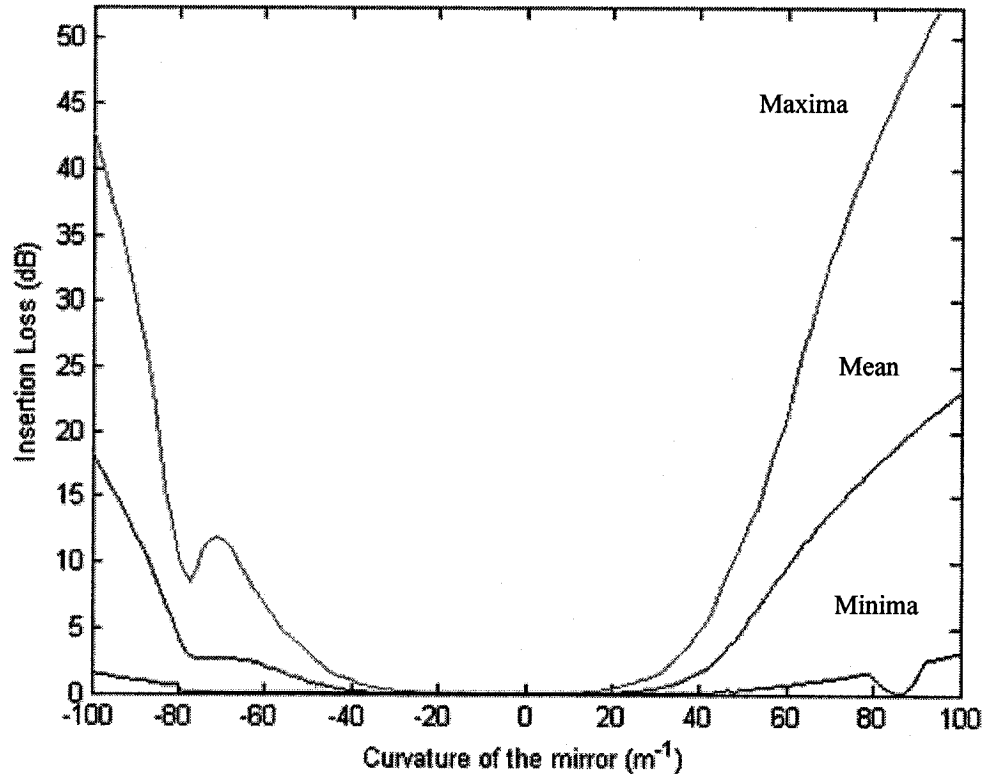
Figure 4-8: Maxima, minima, and the mean of insertion losses vs. curvature of micro-mirrors

Note that the insertion loss remains smaller than 1 dB if curvature is maintained between -40 m^{-1} and 25 m^{-1}.

- *Coupling efficiency dependency on radius of curvature of loop lenses in the delay segments:*

In order to account for variation in the radius of curvature of the delay segment collimation lenses a technique analogous to the Monte-Carlo method has been used[4.7]: assuming a maximum variation, the radius of curvature for each lens is randomly allocated, and the insertion loss is calculated. This is repeated for 1000 iterations and maximum insertion loss is retained. Each of curves has a uniform

distribution and values for maximum variations in radius of curvature are 50 μm, 100 μm and 150 μm. These calculations are repeated for all 64 delay states. Some of results of these simulations are shown in Figure 4-9-Figure 4-11, for some randomly chosen delay times. In each case the distribution of the transmittivity is different. The mean (μ) and standard deviation (STD) values are indicated on the plots.

Note that in order to ensure that the collimating lens is concave the focal length of it must remain positive. The focal length is obtained from Equation 4.21:[4.8]

$$f = [\frac{n_g - 1}{R}(2 - \frac{(n_g - 1)}{n_g}\frac{(2y)}{R})]^{-1}$$

Equation 4.21

this suggests that:

$$2 - \frac{(n_g - 1)}{n_g}\frac{(2y)}{R} \geq 0$$

Or can be written as:

$$R \geq \frac{(n_g - 1)}{n_g}y$$

This implies a restriction on the variation of radius of curvature. This is significant in the sixth delay segment where R_6 =1.09 mm and y_6=3.81 mm, which imposes a maximum inaccuracy of R_6 of 180 μm.
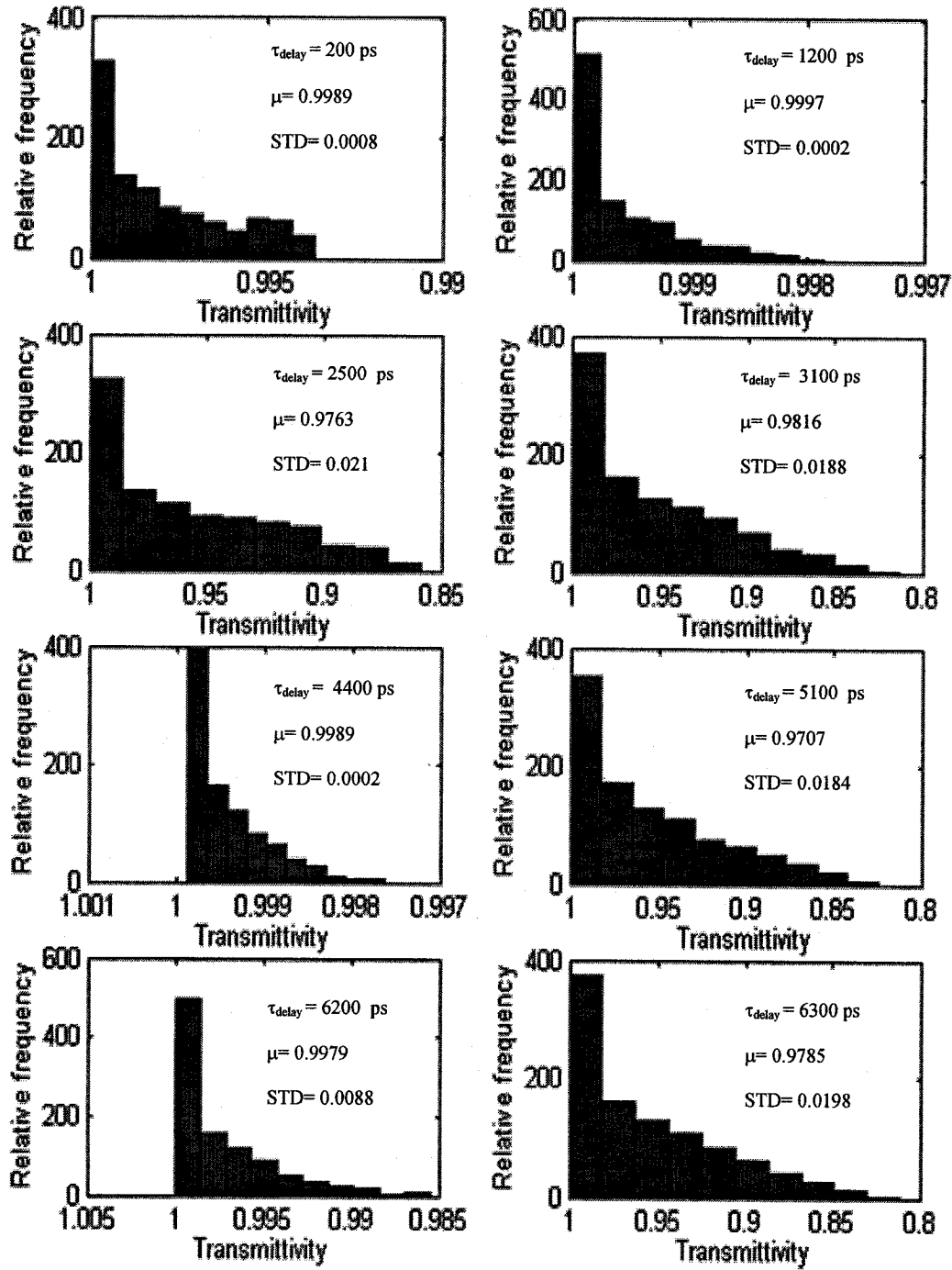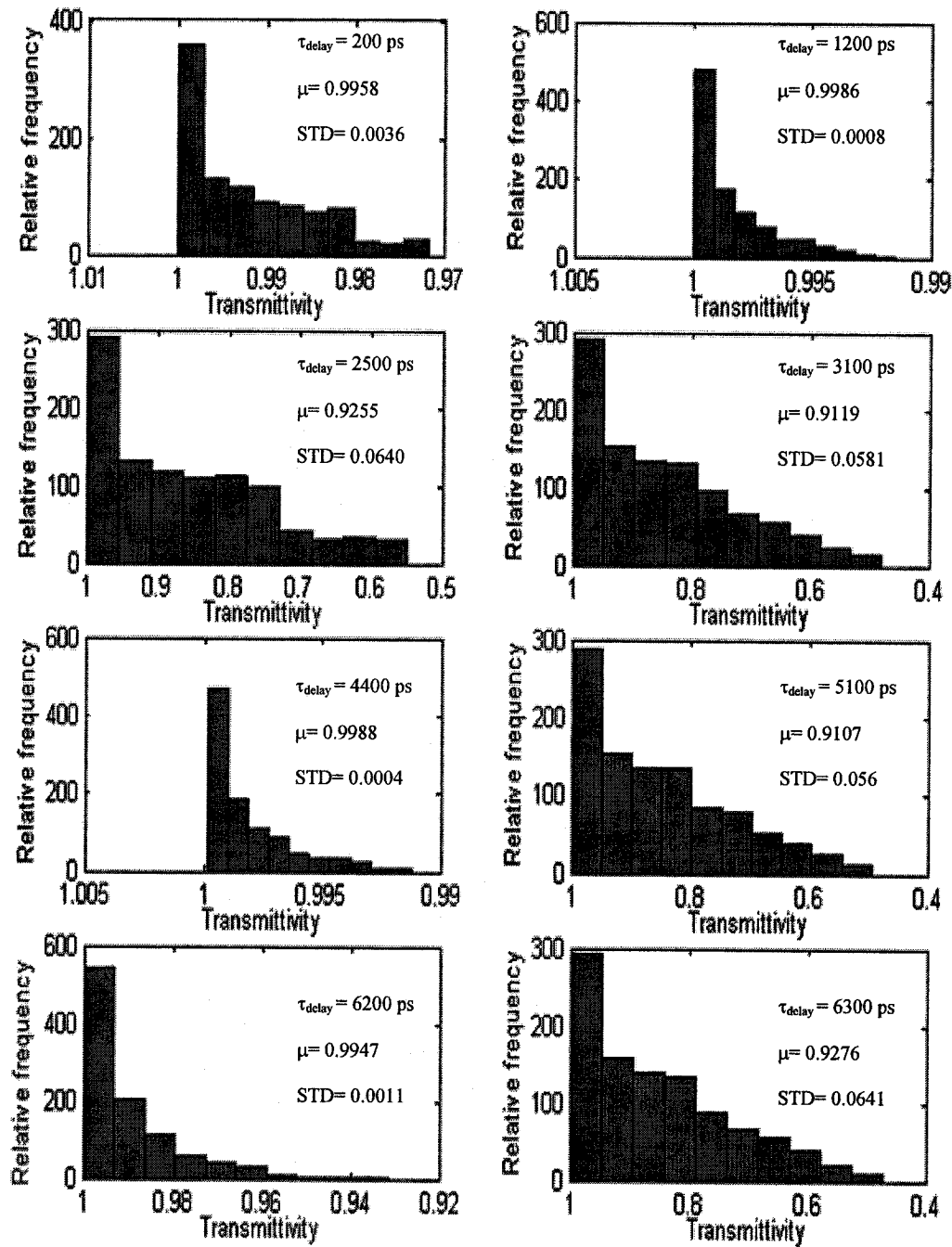
Figure 4-9: Histogram of the transmittivity of the system for different delay times, variation of the bulk curves is: 50 μm. The mean and standard deviation of each case is shown.

Figure 4-10: Histogram of the transmittivity of the system for different delay times, variation of the bulk curves is: <u>100</u> μm. The mean and standard deviation of each case is shown.
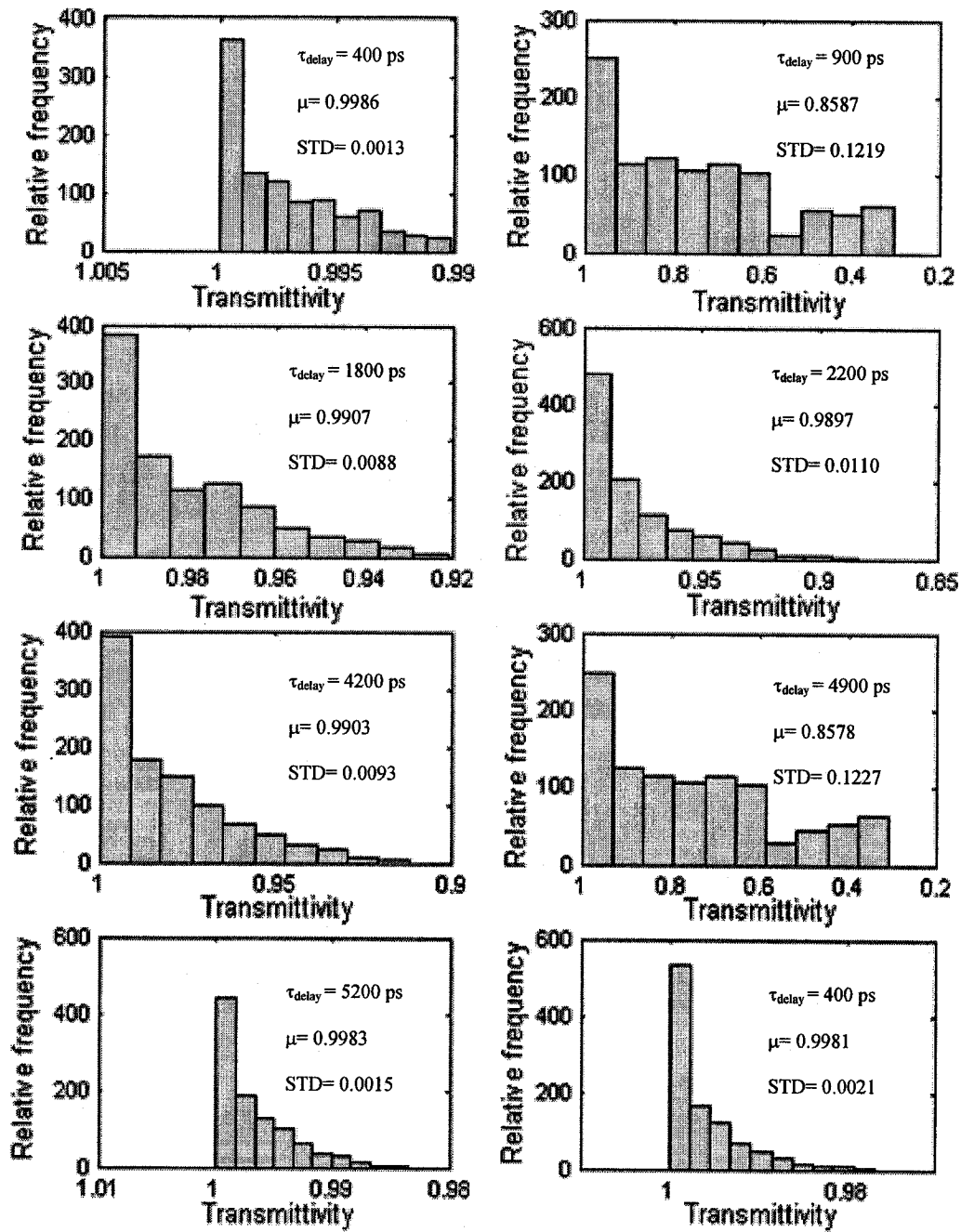
Figure 4-11: Histogram of the transmittivity of the system for different delay times, variation of the bulk curves is: **150** μm. The mean and standard deviation of each case is shown.

4.3 Misalignment of the Components

In the previous section, the performance of a system with a perfect alignment of its components was analyzed. As it is well known, misaligned component in free-space optics has an extreme impact on the system performance.[4.6] Due to current limitations of micromachining technologies, placement errors seem to be inevitable. To calculate the insertion loss in system, both angular and lateral displacement for each components must be considered. In our system there are three main sources of misalignment degradation, which are examined below:

■ *Misalignment in beam collimation module, consisting of the collimation lens and input/output optical fibers.*

Figure 4-12 demonstrates the different types of misalignment and the effect of each at both input and output fiber. The matrix corresponding to the misalignment between input/output fiber and to the main path collimating lens is also shown. of transmitting fiber relative to the collimation lens is also shown. Case (a) is when the fiber and lens are both aligned. In case (b), the collimation lens is displaced from the ideal position along the optical axis. In case (c) collimation lens is displaced laterally with respect to the fiber, and therefore beam sees a change of angle. The matrix for case (c) shows how the beam changes its direction. If the lens is tilted, case (d), the beam will not be displaced but coma effect will be introduced which will slightly reduce coupling efficiency. This effect is not shown in its corresponding matrix. Angular tilt of the fiber, case (e), will introduce the lateral displacement of the beam and lateral displacement of the fiber, case (f), causes tilt to the emerging beam.

Results from different simulations for insertion loss of a system show that axial and lateral displacement of collimation lens cause the highest insertion loss comparing to other type of misalignments.
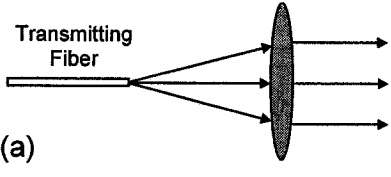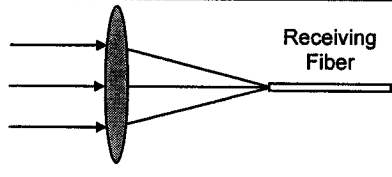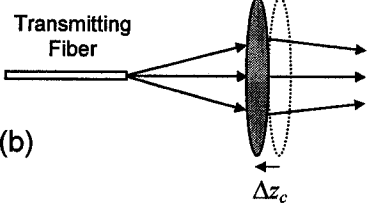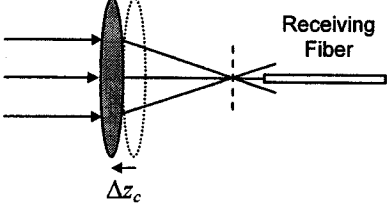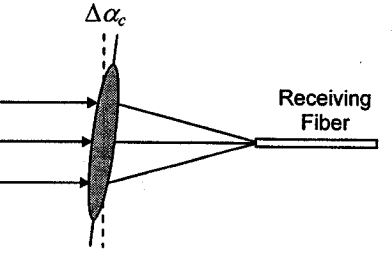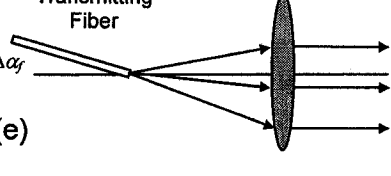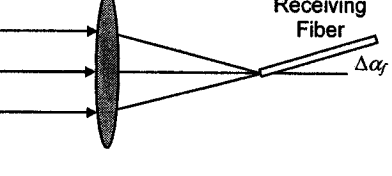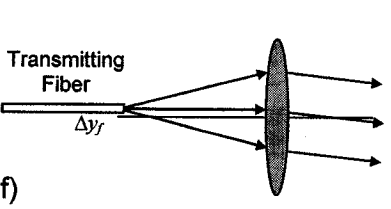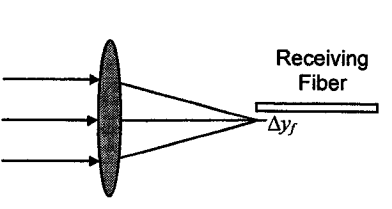
Figure 4-12:Different configuration of misalignment between fiber and collimation lens for Input and out put fiber.

Figure 4-13 shows the contours of insertion loss for variation of lateral and axial displacement both for output and input fibers for four different delay times.

(a) Transmitting fiber τ=2100 ps

(b) Transmitting fiber τ=6200 ps

(c)Receiving fiber τ=1700 ps

(d) Receiving fiber τ=6200 ps
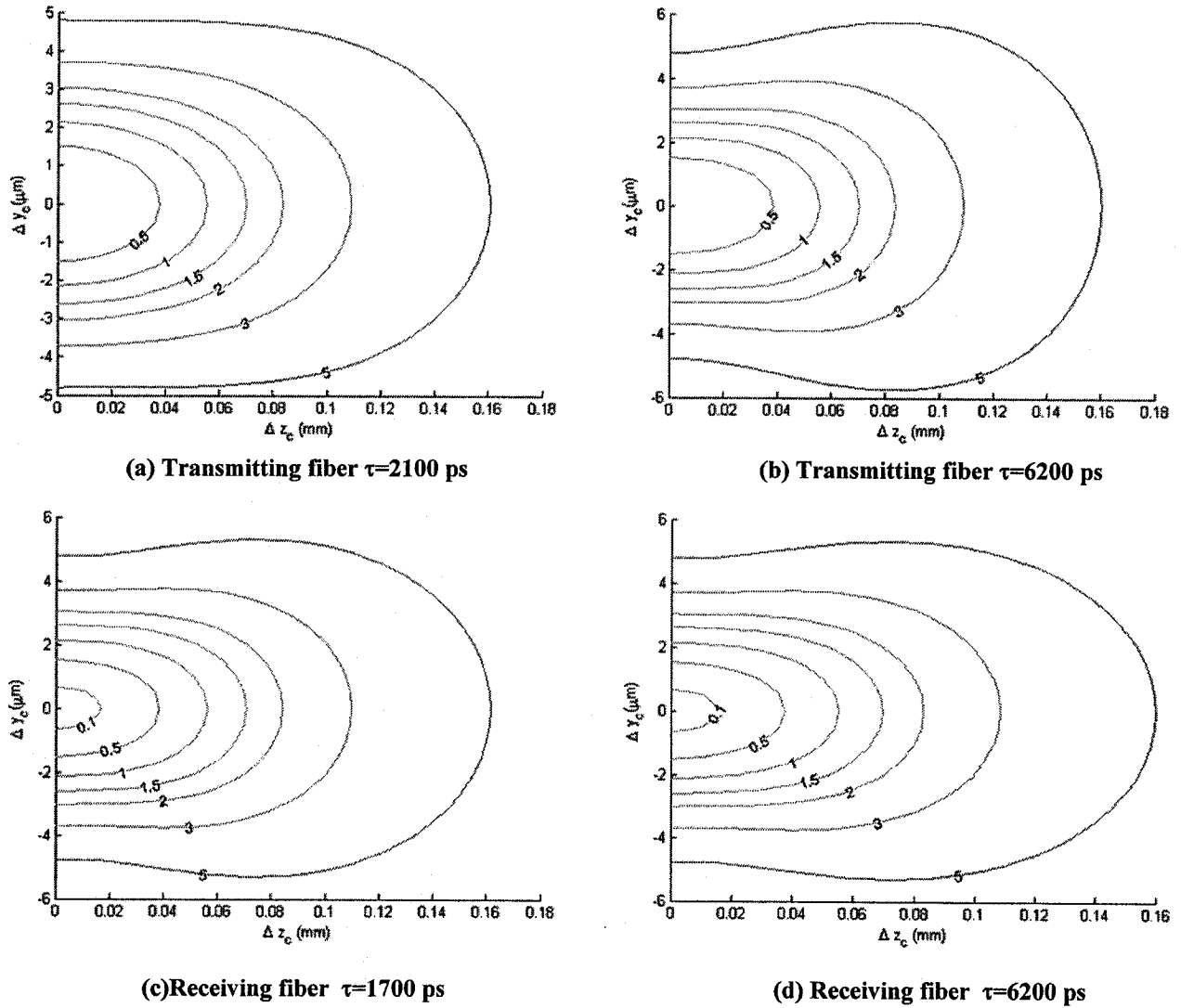
Figure 4-13: Contour of insertion loss as a function of axial and lateral position errors.

■ *Misalignment in micro-mirrors, including tilt and separation distance between them.*

As it was mentioned before due to the limitation at micromachining technology, it is ambitious to expect that each mirror will be popped-up in exactly the desirable position. Unwanted tilt in each mirror will change the direction of the beam, potentially completely redirecting it out of the aperture of the system, thereby completely eliminating the signal.

The accuracy of the mirror angle can not be considered as a constant error. It means each time that micro-mirror is activated it may pop-up at a new tilt angle. Figure 4-14 demonstrates insertion loss of the system, when each mirror pops-up with a random tilt angle (following normal distribution with the mean of 0 and variance of ρ). Note that the insertion loss at each segment will be slightly different. The plots in this figure are for certain delay time. In addition, the mean and standard deviation are provided.
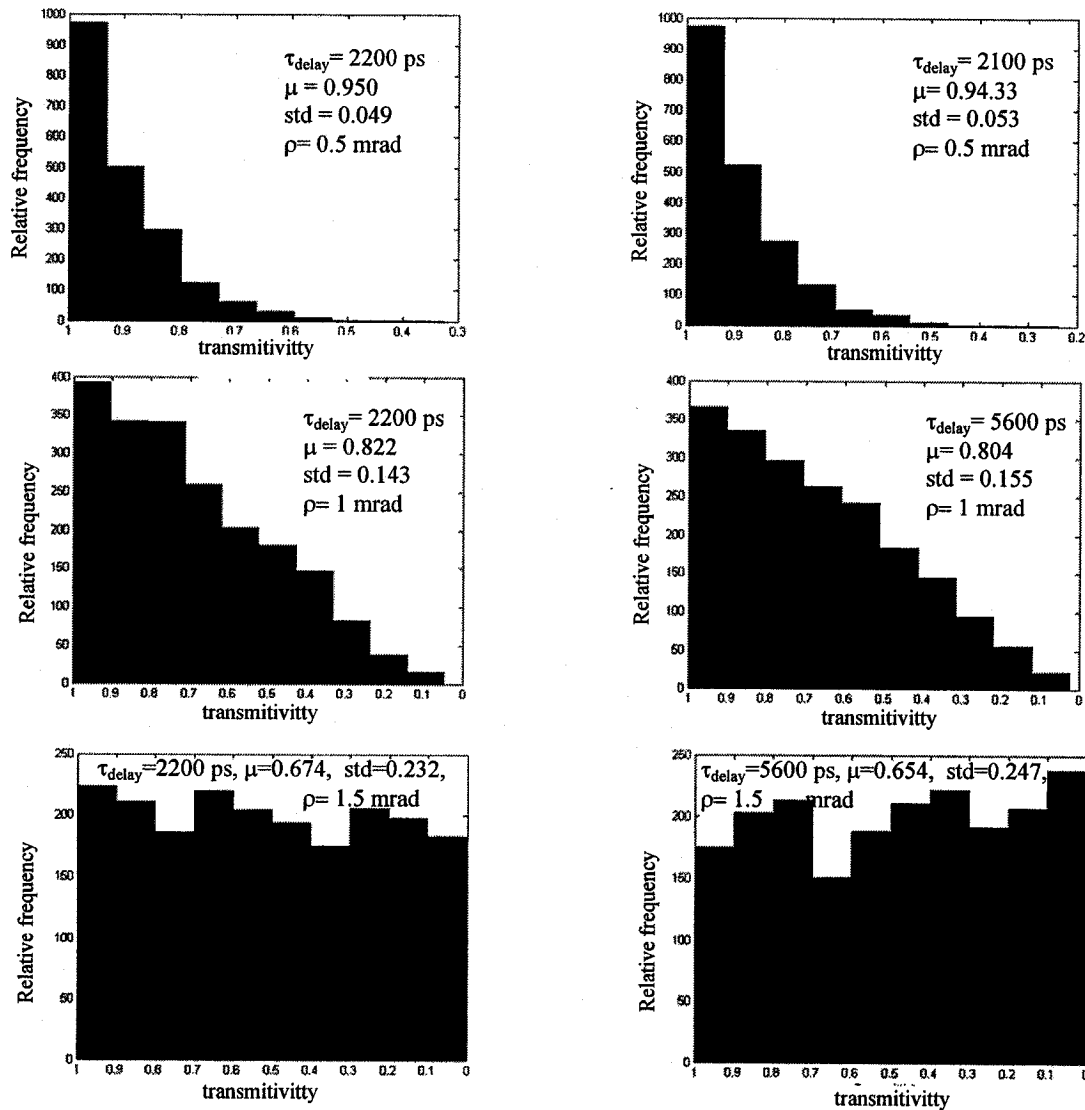

Figure 4-14: Histogram of insertion loss for certain delay times when angular misalignment of micro-mirror is expressed by normal random function with variance of ρ: 0.5, 1, 1.5 mrad.

Figure 4-15 also shows how system loss increases as the variance of assumed tilt angle increases. In this figure mean of insertion loss for all delay times is considered for each value of variance of tilt.
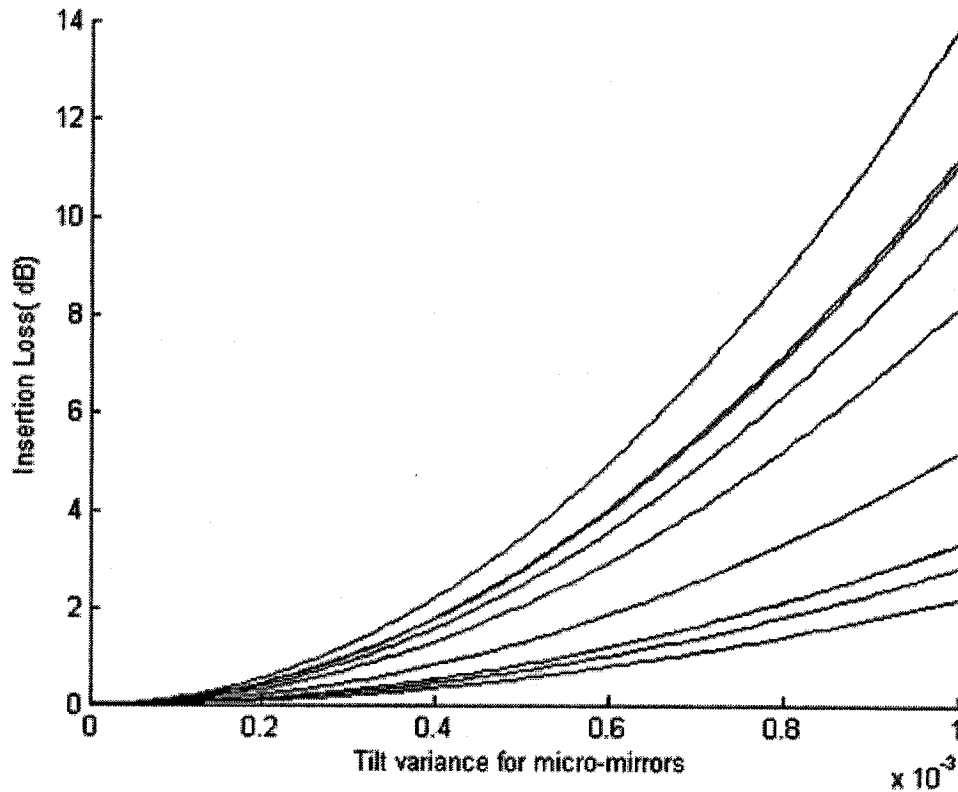
Figure 4-15: Insertion loss of the system for different values of tilt variance of micro-mirrors (note that different curves are achieved due to the random tilt.)

From this figure, it can be estimated that insertion loss of the system maintains below and acceptable loss of 1 dB if the variance of tilt does not surpass 0.5 mrad.

■ *Insertion Loss versus variation of relative distance of the bulk and micro-mirrors:*

Another part of our system which could lead to misalignment is the delay block located above the micro-mirrors. It is difficult to locate the block at the exact desirable position relative to the micro-mirror surfaces. It can be laterally shifted and/or tilted (the axis of tilt can be any point and this makes the problem even more challenging). As it is shown

in Figure 4-16 the tilt $\Delta\alpha_b$ of this component occurs along the left side of the bulk and the

block is shifted by amount of Δl.
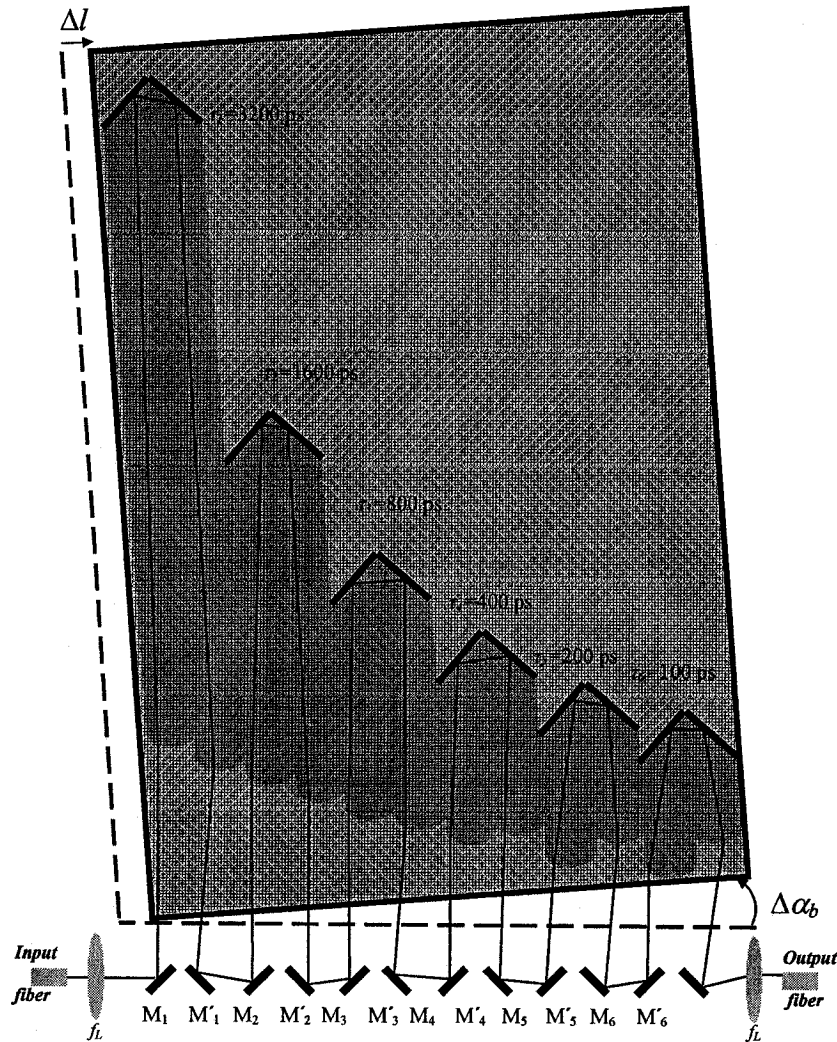
Figure 4-16: The misalignment of bulk relative to micro-mirrors

Contours of insertion loss for certain delay times are illustrated in Figure 4-17.
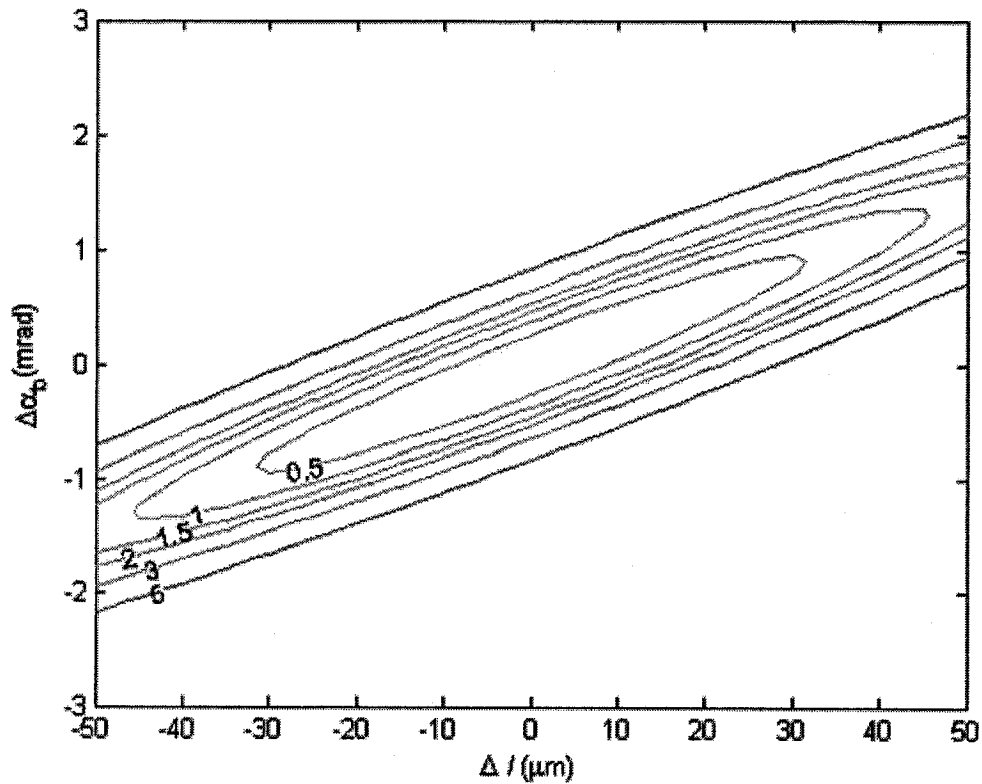
Figure 4-17: Contours of insertion loss for tilt and shift of the block. τ=6300 ps

4.4 Review of performance

In two previous sections, the performance of our module has been investigated in light of today's fabrication limitations. In addition to what was discussed in the section 4.1, other sources of performance degradation are aperture limits and less-than-perfect reflectivity of micro-mirrors. Table 4-1 shows inaccuracy tolerances for different components which would maintain the insertion loss under 1 dB and 2 dB. These values are assumed the mean of insertion losses of all delay times. The effect of limited aperture is considered in these values. It should be stated that the tolerances provided in this table refer to the situation where each misalignment is treated separately.

Table 4-1: Required tolerance for system components

Parameter	Symbol	Tolerance for insertion loss < 1 dB	Tolerance for insertion loss < 2 dB
Collimation lenses focal length	Δf_L	±25 µm	±30 µm
Curvature of micro-mirrors	C_{mirror}	±20 m^{-1}	±40 m^{-1}
Radius of curvature of loop lenses	ΔR	50 µm	100 µm
Axial displacement of transmitter collimation lens	Δz_c	±50 µm	±80 µm
Lateral displacement of transmitter collimation lens	Δy_{cT}	±2 µm	±3 µm
Axial displacement of transmitter collimation lens	Δz_{cF}	±50 µm	±80 µm
Lateral displacement of transmitter collimation lens	Δy_{cF}	±2 µm	±3 µm
Angular tilt of each mirror	$\Delta \alpha_{mirror}$	±0.3 mrad	±0.5 mrad
Angular tilt of the block relative to micro-mirrors	$\Delta \alpha_b$	±.4mrad	±.8 mrad
Lateral shift of the block relative to micro-mirrors	Δl	±15 µm	23 µm
Axial displacement of bulk relative to micro-mirrors	Δh	±4 mm	8 mm
Reflectivity of micro-mirrors	r_f	>99%	>98%

Yet another source of potential system degradation, which in not treated here, are aberrations produced by optical elements. These could cause collimated beam depart from the ideal Gaussian behavior.

As it has been seen, the different kinds of misalignment can significantly limit the performance of the system. In order to improve the effect of misaligned elements the use of two controllable mirrors is suggested. These mirrors are located after the input collimation lens and before output collimation lens. The idea is to tilt these mirrors to return the beam to its principle path. The first mirror can alleviate the height error and second one is to improve the angle error of the beam. As it can be seen in Figure 4-18, dashed line shows the light path when mirrors are at 45°. The height and angle of beam on second mirror have been changed due to the misalignment of the system. Hence the coupling efficiency will reduce. In order to improve it, we use first mirror to correct the height and second mirror is used to divert the light into its main path.
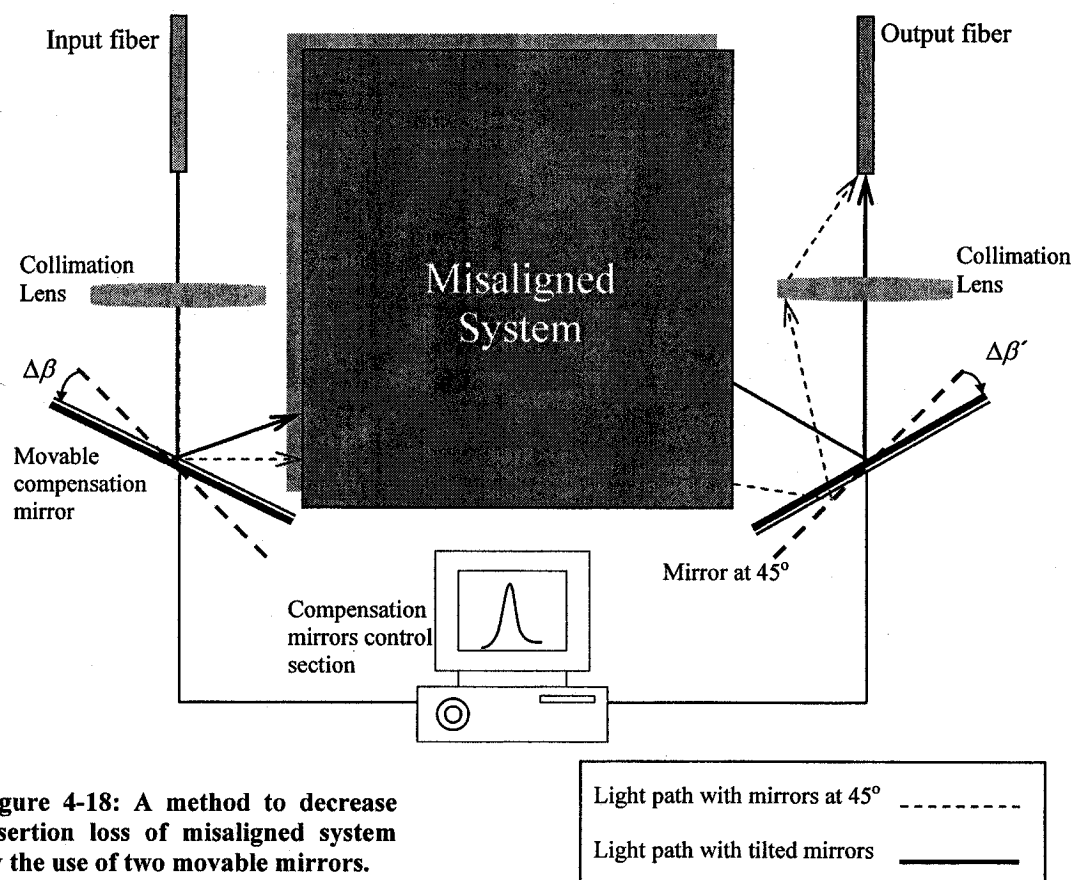

Figure 4-18: A method to decrease insertion loss of misaligned system by the use of two movable mirrors.

Light path with mirrors at 45° _ _ _ _ _ _ _ _ _

Light path with tilted mirrors _____

These compensation mirrors can be controlled by a computer and light detector as it tilts both mirror until the peak efficiency be obtained. If both mirrors can be tilted in the range from -50 mrad to 50 mrad (This is the value which meets the aperture limitation of micro-mirrors) and each step would be 2 mrad then for different delays, light can be compensated by the use of two mirrors. Figure 4.19 shows how the peak of 0.94 occurs in appropriate angles. The tilt of each micro-mirrors changes randomly for each delay. The variance of these changes is assumed 11 mrad.
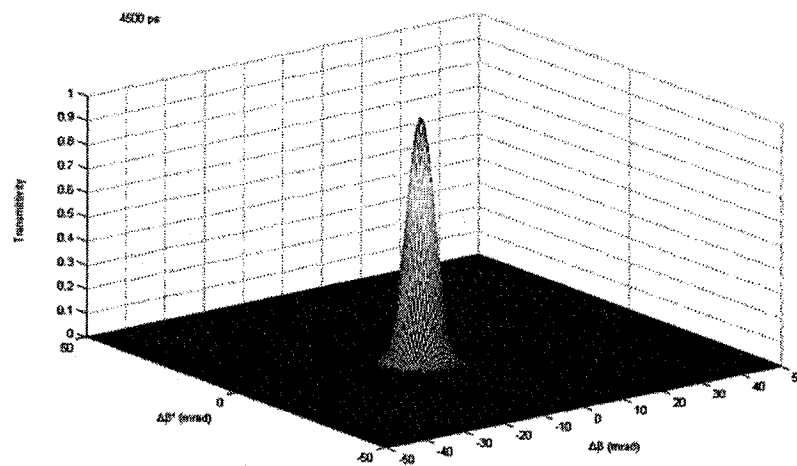
(a)
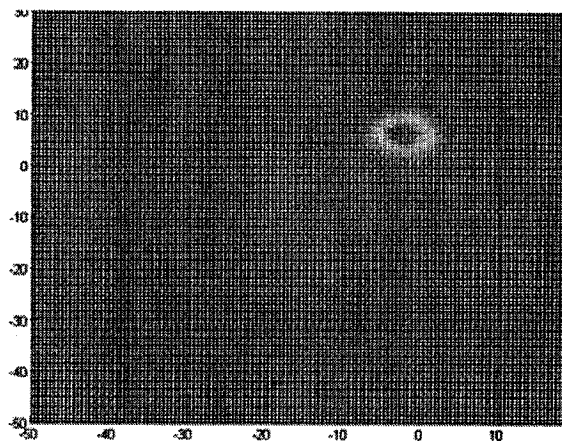
(b)

Figure 4-19:Compensation of misalignment by the use of two tilting mirrors. (a) for 4800 ps delay time. (b) for 6000 ps. Mirrors are tilted -4 mrad and 6.7 mrad

References:

[4.1]   Saleh, " Fundamental of Photonics," New York :Wiley, p. 82, 1991.

[4.2]   Yariv, "Optical Electronics," Fourth Edition , p/ 50-52

[4.3]   W.B. Joyce and B. C. DeLoach, Alignment of Gaussian beam , Applied Optics vol. 23, , p. 4187-4196,1984

[4.4]   R. W. Johnstone, M. Parameswaran, Determination of optical alignment in free- space micro-optical-bench systems using paraxial ray-transfer matrice

[4.5]   Gerrard A., Burch J. M." Introduction of Matrix Method in Optics." chapter 2 and 3, John Wiley and Sons, 1975.

[4.6]   Tovar A. A., Caperson L.W. , "Generalized beam matrices: Gaussian beam propagation in misaligned complex optical system, J. Opt. Soc. Am. A, Vol. 12, No. 17, 1995.

[4.7]   David T. Neilson, "Tolerance of optical interconnections to misalignment," Applied Optics, Vol. 38, No. 11, 1999.

[4.8]   Dubi A., Monte-Carlo method in systems engineering , 2000

[4.9]   Hecht, Optics, 3rd Edition,1998 by Addison Wesley Longman ,Inc. Page 248

[4.10] Sjojiro Nemoto, "Transformation of waist parameters of a Gaussian beam by thick lens," Applied Optics Vol.29, No. 6, February 1990

[4.11] Andrew Kirk, "Fiber optic switches with digital mirror arrays: Alignment and tolerancing issues," Report prepared for Texas Instruments, Materials and Control Group, June 1997

[4.12] Zhao D., Wang S., "The ray transfer matrices for a tilted flat reflector,"Optik, Vol. 98, No. 4, 1995

5 Conclusion:

In this chapter, a review of design and analysis of a tunable optical delay line module will be shown. Advantages and disadvantages of this design will be discussed based on the performance results simulated in chapter 4. Challenging problems and issues with experiments will be discussed in section 6.2.

5.1 Review of design:

In this thesis, a 6-bit tunable optical delay line module has been designed and analyzed. This device is able to provide a delay time in range of 100 ps to 6300 ps with the time resolution of 100 ps.

The design consists of three main parts, 1) collimation lenses, which is to prevent light diffraction from fiber to fiber. Aspheric lenses with thickness of 0.5 mm and focal length of 0.832 mm have been used. 2) delay-paths, which provide the desired delay time. Each delay path consists of two media; free space and bulk material.

Both ends of bulk material is molded out to form a collimating lens for delay path. Lenght of these paths are chosen to be in binary fashion and each provides a delay time of 100 ps , 200 ps , 400 ps, 800 ps, 1600 ps , 3200 ps respectively. 3) MEMS mirrors, which are operating as switches to redirect the light into different delay paths to obtain a desired delay time. For 6 delay paths, 12 MEMS mirrors are needed. These mirrors have been designed at McGill University and fabricated by CMC. The effective area of these mirrors is 250 x 250 mm and the speed of switching is about order of ms.

some of the advantages of this system is listed below:

- Precise delay time: Since all the delay paths is precisely designed and there is no moving part in delay paths , one can expect an accurate delay times for all the range of 100 ps to 6300 ps.

- Uniform insertion loss: the distance from each mirror to bulk material in delay path and focal length of delay path collimating lenses are calculated in the way that insertion loss for all delay times would be the same.

- Polarization sensitivity: all components in this design are not polarization sensitive so the systems loss is not related to polarization state of incident beam.

There are also some disadvantages in this system. Since the design is based on free-space optics, there would be misalignments issues which can affect the efficiency of the overall system. There are also some problems regarding the accuracy of implementation of elements which can be seen in section 4.2.

In order to add another delay path, for example 6400 ps, one should note that pair of extra MEMS mirrors is needed. This will increase the length of overall system. The beam size on the first mirror of first loop should not exceed than size of the micro-mirror. So in order to add another delay path, beam size on the first mirror should be calculated and if it exceeds than micro-mirror size, larger mirrors should be applied.

For shorter delay lines for example order of 10 ps, there are some implementation issues since the shortest delay path would be only 2mm and it is difficult to achieve this length accurately.

5.2 Future work

One of the most important works for future is to improve the quality of micro-mirrors. Larger aperture size of MEMS mirrors results less optical power loss due to the misalignment, and also angular misalignment of the micro-mirrors which can destroy all the power as shown in 4.2.2, should be alleviated by the improvement of implementation. As suggested in section 4.3 using two correction mirrors seem to be necessary as it is difficult to maintain the power loss less than 1 dB with normal setup. Implementation issues of these two mirrors and control methods of these elements should be investigated in future research.

Micro mirror chips fabricated by CMC have been received recently and need to be characterized for misalignment issues. It is also suggested that the design with use of Grin colliamting lenses will be investigated.

Appendix A: Coupling efficiency for the variable distance collimating system

Suppose we are asked to design the collimation system for the system such as the delay line illustrated in Figure 3.4.

If there is no delay applied, light will travel the minimum length of L_{min} between to collimating lenses. Now if we consider the delay segments are all on, the maximum distance that light travels between two lenses is:

$$L_{max} = L_{min} + c\tau_{max}$$

where c is the speed of light in free-space and τ_{max} can be obtained from: $\tau_{max} = (2^m - 1)\tau_0$

Now suppose the collimation system has been designed based on the maximum distance, as the length between two lenses varies from L_{max} to L_{min}, insertion loss between two fibers have been will change.
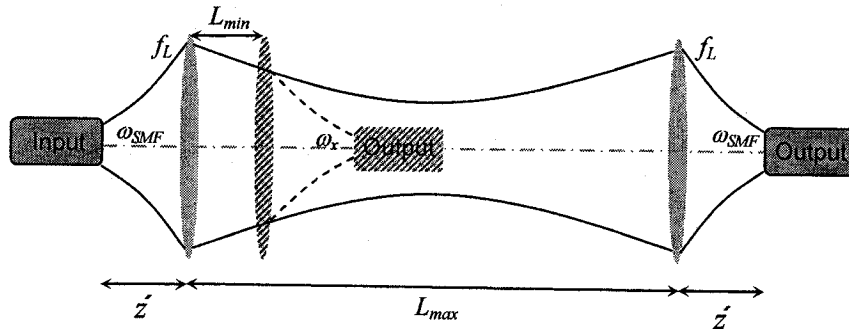

Figure 1-A: Schematic of a collimation system with variable distance

Table 1.A represents the parameter for the maximum length:

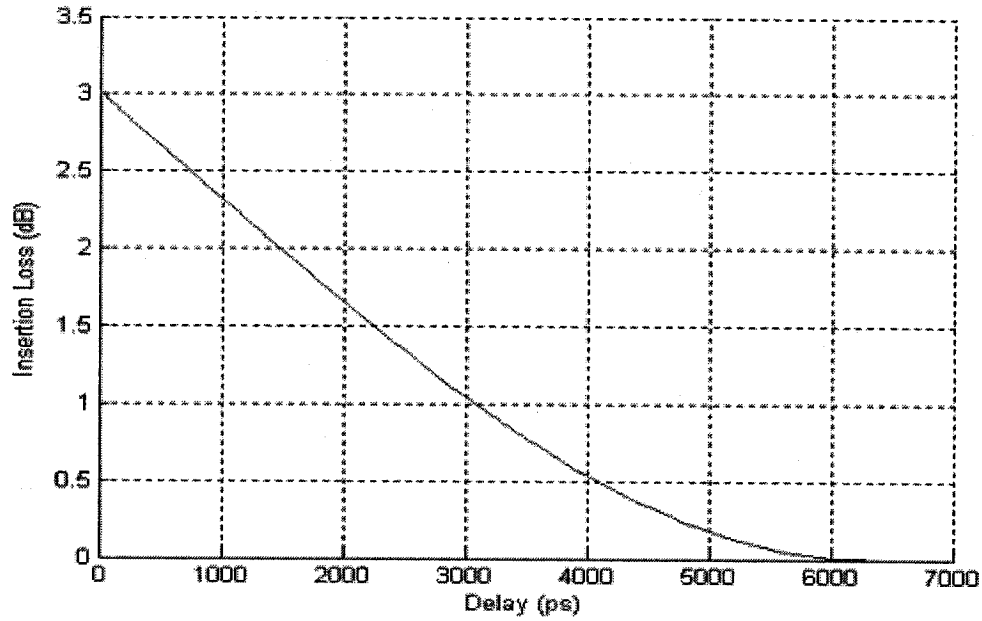| Parameter	Symbol	Value
Beam-wais of fiber	ω_{smf}	4.77 μm
Wavelength	λ	1.31 μm
Maximum Length between lenses	L_{max}	1.8904 m
Minimum distance between lenses	L_{min}	14 mm
Fiber to lens distance	z'	0.311 mm
Focal length of the lenses	$f_{L,max}$	0.26 mm

Figure 2-A: Insertion Loss changes as distance varies for different delay times

Appendix B: General formula for beam collimation

Assume we have the Gaussian beam whose beam-waist, ω_i , is located in the distance

of z form an optical system. For paraxial ray tracing this optical system is recognized by

the matrix called ABCD-Matrix. As it is demonstrated in Figure 1-B, the beam passes by

the optical system and continues propagating towards new beam-waist at distance z'

from the optical system.

Characteristic of Gaussian beam at each point is determined by the beam-width and the
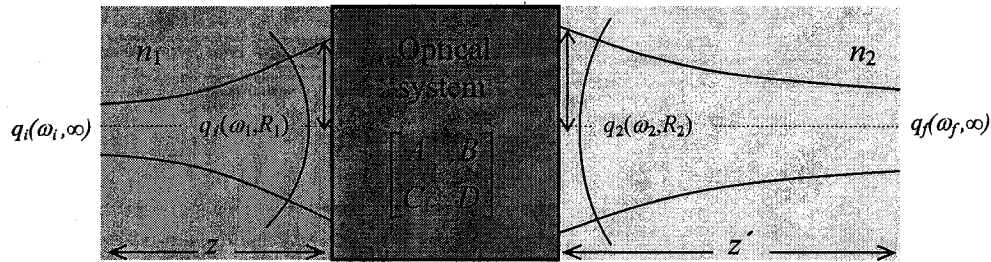
radius of curvature at that point.

Figure 1-B: Diagram of an propagation of light through an optical system

These two parameters form the q parameter which can be obtained:

$$\frac{1}{q} = \frac{1}{R} - j\frac{\lambda}{\pi n \omega^2}$$

<div align="right">*Equation 1.B*</div>

For the first beam-wais $R_i = \infty$ and we can simply write:

$$q_0 = jz_R$$

<div align="right">*Equation 2.B*</div>

where z_R is the Raleigh range for this beam.

After traveling the distance of z:

$$q_1 = q_0 + z$$

<div align="right">*Equation 3.B*</div>

It is shown at [3-1] that the q parameter of the output beam of this optical system can be

shown as:

$$q_2 = \frac{Aq_1 + B}{Cq_1 + D}$$

Equation 4.B

if z' is a distance that beam propagates towards its beam-waist then:

$$q_f = q_2 + z'$$

Equation 5.B

with,

$$q_f = j z_f$$

Equation 6.B

so if we combine Equation (1.B) and eq(6.B) we can write:

$$q_f = \frac{A(q_0 + z) + B}{C(q_0 + z) + D} + z'$$

Equation 6.B

or,

$$jz_f - z' = \frac{A(jz_R) + (Az + B)}{C(jz_R) + (Cz + D)}$$

Equation 7.B

if we separate the real and imaginary part of equation above, then:

$$z_f = \frac{\det(Matrix)}{(Cz + D)^2 + (Cz_R)^2} z_R$$

Equation 8.B

$$z' = -\frac{(Az + B)(Cz + D) + ACz_R^2}{(Cz + D)^2 + (Cz_R)^2}$$

Equation 9.B

where: $det(Matrix) = AD - BC = \dfrac{n_1}{n_2}$

To calculate the maximum distance of the beam-waist to lens we can simply get derivative of z' as a function of z and let it equal to zero. And after the calculation we see the condition to have the maximum distance from lens to beam waist is;

$$(Cz_{max} + D)^2 = (Cz_R)^2$$

Equation 10.B

or

$$z_{max} = z_R - \frac{D}{C}$$

Substituting this equation in Equation 8-B and Equation 9-B we find the magnification and the distance when the beam-waist is located as distant as possible to the lens.

$$M^2 = \frac{z_f}{z_R} = \frac{\det(Matrix)}{2(Cz_R)^2}$$

Equation 11.B

$$z'_{max} = -\frac{A}{C} + \frac{\det(Matrix)}{2C^2 z_R}$$

Equation 12.B

These formulas give the information about the collimated light passing through the optical system with ABCD matrix.